Functional aspects of phosphorylation of the oncogenic transcription factor Ecotropic Viral Integration site 1 (EVI1)

A thesis submitted to the University of Manchester for the degree of Doctor of Philosophy in the Faculty of Biology, Medicine and Health

2020

James Kelly

School of Medical Sciences

Division of Cancer Sciences

Table of Contents

Final word count: 30,629

List of Figures

List of Tables

List of Publications

Publications and manuscripts in preparation:

Paredes R, Schneider M, Stevens A, White DJ, Williamson AJK, Muter J, Pearson S, **Kelly JR**, Connors K, Wiseman DH, Chadwick JA, Loffler H, Ying Teng H, Lovell S, Unwin R, van de Vrugt HJ, Smith H, Kustikova O, Schambach A, Somervaille TCP, Pierce A, Whetton AD, Meyer S (2018) EVI1 carboxy-terminal phosphorylation is ATM-mediated and sustains transcriptional modulation and self-renewal via enhanced CtBP1 association. Nucleic Acids Research. doi:10.1093/nar/gky536.

Paredes R, **Kelly JR**, Geary B, Almarzouq B, Schneider M, Pearson S, Narayanan P, Williamson A, Lovell SC, Wiseman DH, Chadwick JA, Jones NJ, Kustikova O, Schambach A, Garner T, Amaral FMR, Pierce A, Stevens A, Somervaille TCP, Whetton AD, Meyer S (2020) EVI1-phosphorylation at S436 regulates interactions with CtBP1 and DNMT3A and promotes self-renewal. In submission.

Abbreviations

5mC	5-methylcytosine
AD	Acidic domain
ADE	Cytarabine, Daunorubicin and Etoposide regime
ALL	Acute lymphoblastic leukaemia
AME	AML1/EVI1 fusion protein
AML	Acute myeloid leukaemia
APL	Acute promyelocytic leukaemia
ATM	Ataxia telangiectasia mutant
ATPases	Adenosine triphosphatases
ATR	ATM and Rad3-related protein
ATRA	All-trans-retinoic acid
BLAST	Basic local alignment search tool
BM	Bone marrow
BMF	BM failure
BSA	Bovine serum albumin
Cdk2	Cyclin-dependent kinase 2
CFU	Colony forming unit
CLP	Common lymphoid progenitors
CMP	Common myeloid progenitors
CMV	Cytomegalovirus
CtBP1	C-terminal binding protein 1
CtBP2	C-terminal binding protein 2
Cytarabine	Cytosine-arabinoside
dCK	Cytarabine-5′-monophosphate by deoxycytidine kinase
DMEM	Dulbecco’s modified eagle medium
DMSO	Dimethyl sulfoxide
DNMT	DNA methyltransferase
EDTA	Ethylenediaminetetraacetic acid
ETV6	Ets variant 6
EVI1	Ecotropic viral integration site 1
FA	Fanconi anaemia
FAB	French-American-British
FACS	Fluorescence activated cell sorting
FBS	Fetal Bovine Serum
FDR	False discovery rate
FPKM	Fragments per kilobase million
FSC	Forward scatter
GAPDH	Glyceraldehyde-3-phosphate-dehydrogenase
GFP	Green fluorescent protein
GM-SCF	Granulocyte-macrophage colony-stimulating factor
H2AX	Histone 2AX

H_2O_2	Hydrogen peroxide
hENT1	Nucleoside transporter 1
HEPES	N-(2-Hydroxyethyl)piperazine-N′-(2-ethanesulfonic acid)
HSC	Haematopoietic stem cell
HSCT	Haematopoietic stem cell transplantation
HSPC	Haematopoietic stem and progenitor cell
IB	Immunoprecipitation buffer
IBMF	Inherited BMF
IC50	Half maximal inhibitory concentration
IL	Interleukin
IP	Immunoprecipitation
IR	Intervening region
IRES	Internal ribosomal entry site
ITASSER	Iterative threading assembly refinement
Kit	CD117
LAR II	Luciferase assay reagent II
LDS	Lithium dodecyl sulphate
L-G	L-Glutamine solution
Lin	Negative for lineage markers
LSD1	Lysine demethylase 1A
LT-HSC	Long-term repopulating HSC
LUT	Look up table
MACS	Magnetic activated cell sorting
MD	Molecular dynamics
MDS	Myelodysplastic syndrome
MDS1	Myelodysplasia syndrome associated protein 1
MECOM	MDS-EVI1 Complex
MEF	Mouse embryonic fibroblasts
MEM	Minimal essential medium
MIDAS	Multiple reaction monitoring-initiated detection and sequencing
MLL	Mixed lineage leukaemia
MPP	Multipotent progenitor
MTOB	4-methylthio-2-oxobutyric acid
MS	Mass spectrometry
NDPK	Nucleoside diphosphate kinase
NLS	Nuclear localisation site
PBS	Phosphate buffered saline
PCR	Polymerase chain reaction
PFA	Paraformaldehyde
Plat-E	Platinum-E
PLB	Passive lysis buffer
PMBMP	Primary murine bone marrow progenitors
PME	Particle mesh Ewald
PMSF	Phenylmethylsulfonyl fluoride

PR	Proline-rich domain
P/S	Penicillin-Streptomycin
P-Sp	Para-aortic splanchnopleural region
RMSF	Root mean square fluctuation
RNA*seq*	RNA-sequencing
ROI	Regions of interest
ROS	Reactive oxygen species
RPMI1640	Roswell park memorial institute 1640 medium
RT-qPCR	Quantitative real-time PCR
RUNX1	Runt-Related transcription factor 1
RUSAT	Radioulnar synostosis with amegakaryocytic thrombocytopenia
RUVBL1	RuvB-like 1 protein
RUVBL2	RuvB-like 2 protein
Sca1	Stem cell antigen 1
SCF	Stem cell factor
shRNA	Short hairpin RNA
SILAC	Stable isotope labelling of amino acids in cell culture
SSC	Side scatter
ST-HSC	Short-term repopulating HSC
TAE	Tris-acetate-EDTA
TCEP	Tris(2-Carboxyethyl)Phosphine
Tie2	Tyrosine kinase with immunoglobulin-like and EGF-like domains 1
Top2cc	DNA-Top2 cleavage complex
TU	Transforming units
WHO	World Health Organisation

Abstract

The University of Manchester

James Russell Kelly

Degree: Doctor of Philosophy

Thesis Title: Functional aspects of phosphorylation of the oncogenic transcription factor Ecotropic Viral Integration site 1 (EVI1)

Date: June 2020

Ecotropic viral integration site 1 (EVI1) is a transcriptional regulator essential for haematopoiesis. Mutations affecting *EVI1* can result in bone marrow failure, whereas aberrantly high expression is commonly seen in in acute myeloid leukaemia (AML) with 3q chromosomal aberrations, where *EVI1* is encoded at the *MECOM* locus. High *EVI1* expression is associated with poor prognosis and chemo-resistance. Dynamic protein interactions with transcriptional co-repressors, such as CTBP, have been shown to mediate the transcriptional regulation of EVI1 target genes and in modulating EVI1 oncogenic function. Dynamic phosphorylation of EVI1 at serine 858/860 (S858/860) and serine 436 (S436) were discovered in the AML SB1690CB cell line and have subsequently been identified in numerous other cell types and clinical samples. These phosphorylation sites and their role for EVI1 function are investigated within this thesis.

In order to investigate the function of phosphorylation of EVI1, site-directed mutagenesis was used to generate non-phosphorylated and non-phosphorylatable EVI1 at S858/860 and S436 respectively and used for colony and re-plating assays, drug titration assays, RNA-sequencing (RNA*seq*), RT-qPCR, immunoprecipitations and immunofluorescence.

S858/860 phosphorylation was shown to be mediated by ATM in response to genotoxic stress. Phosphorylation of S858/860 proved essential to EVI1-mediated haematopoietic self-renewal. Inhibition of ATM was efficacious in reducing EVI1-mediated transformation of Rat1 fibroblast when used in combination with hydrogen peroxide and chemotherapy agents Etoposide, Daunorubicin and Cytarabine. The phosphorylatability of EVI1 at S436 proved critical to EVI1-mediated re-plating of transduced Kit+ HSPCs. RNA*seq* analysis confirmed EVI1-target genes, such as *ALDHA1A* and *CEPBA* that are essential to haematopoietic self-renewal. Immunoprecipitation confirmed complimentary computational modelling prediction that phosphorylation of EVI1 at S436 negatively affect interaction with CtBP1. Collaborative mass spectrometry analysis revealed preferential interaction of phosphorylatable EVI1 at S436 with DNMT3a. Analysis of methylation by 5mC immunofluorescence staining suggested an interference of EVI1 with *de-novo* methylation.

This study suggests a new therapeutic avenue in EVI1-expressing leukaemia, using ATM inhibitors in combination with chemotherapy treatment in EVI1 overexpressing leukaemia. Inhibition of kinases targeting S436 will be important for further understanding of the role of this phosphorylation site, also with respect to EVI1-mediated methylation patterns.

Declaration and Copyright Statement

I declare that no portion of the work referred to in the thesis has been submitted in support of an application for another degree or qualification of this or any other university or other institute of learning.

i. The author of this thesis (including any appendices and/or schedules to this thesis) owns certain copyright or related rights in it (the "Copyright") and s/he has given The University of Manchester certain rights to use such Copyright, including for administrative purposes.

ii. Copies of this thesis, either in full or in extracts and whether in hard or electronic copy, may be made only in accordance with the Copyright, Designs and Patents Act 1988 (as amended) and regulations issued under it or, where appropriate, in accordance with licensing agreements which the University has from time to time. This page must form part of any such copies made.

iii. The ownership of certain Copyright, patents, designs, trademarks and other intellectual property (the "Intellectual Property") and any reproductions of copyright works in the thesis, for example graphs and tables ("Reproductions"), which may be described in this thesis, may not be owned by the author and may be owned by third parties. Such Intellectual Property and Reproductions cannot and must not be made available for use without the prior written permission of the owner(s) of the relevant Intellectual Property and/or Reproductions.

iv. Further information on the conditions under which disclosure, publication and commercialisation of this thesis, the Copyright and any Intellectual Property and/or Reproductions described in it may take place is available in the University IP Policy (see http://documents.manchester.ac.uk/DocuInfo.aspx?DocID=24420), in any relevant Thesis restriction declarations deposited in the University Library, The University Library's regulations (see http://www.library.manchester.ac.uk/about/regulations/) and in The University's policy on Presentation of Theses

Acknowledgements

First and foremost I would like to thank my supervisor Dr Stefan Meyer for the opportunity to complete my PhD in his research group. His continued enthusiasm for the project and honest tutorage has been a constant motivation. I am also appreciative of the guidance of both my co-supervisor Professor Anthony Whetton and Dr Tim Somervaille throughout the project.

Thank you to the members of the SCALPL group that I have worked with over the last three years that have made working at the WMIC gratifying experience. A special thank you must go to Dr Roberto Paredes who has been a mentor, collaborator and friend throughout my PhD. Further thanks must go to Dr Andrew Pierce, Stella Pearson, Dr Bethany Geary and Dr Liqun Zhang for always offering advice and guidance whenever possible. I am also thankful to the CRUK core facility, specifically Dr Adam Stevens, Terence Garner, Dr Fabio MR Amaral and Dr Batool Almarzouq for their data analysis support and training offered to me.

A huge thank you must go to the Toti Worboys family, for without their spirit to make a difference and without their fundraising efforts this project would not have existed. I will be eternally grateful to them for making this opportunity possible. Additionally I would also like to thank Children's Cancer and Leukaemia Group for funding the project.

Lastly I would like to thank the support provided by my wonderful family and friends. Thanks to my mum, dad, brother and niece who have always been there when needed. Thanks to my kooky friends that have offered a constant balance. Most importantly, thank you to my partner for their fortitude. Without these people this project would not have been possible.

Chapter 1 Introduction

1.1 Haematopoiesis

Haematopoiesis is the process in which bloods cells are formed. Multipotent stem cells arise during embryonic development and finally reside within the bone marrow to maintain haematopoiesis throughout a human life. Defects in haematopoiesis can lead to a range of diseases such as bone marrow failure or leukaemia.

In the traditional model of haematopoiesis all haematological cells are derived from a haematopoietic stem cell (HSC) (*Figure 1.1)*. The HSCs reside in the bone marrow and are believed to be the only population that can self-renew and also undergo multilineage differentiation. HSCs can be subcategorised into those that renew for the life of the host, long-term repopulating HSC (LT-HSC), and short-term repopulating HSC (ST-HSC) that renew for a defined time period before differentiating further. During normal haematopoiesis ST-HSC differentiate into a multipotent progenitor (MPP) that can irreversibly mature/differentiate into oligolineage-restricted progenitors, common myeloid progenitors (CMP) or common lymphoid progenitors (CLP). It is at this stage where the progenitors are committed to their specific lineage and will differentiate into a number of specialised haematopoietic cells such as lymphocytes, macrophages or dendritic cells[1–6]. Maturation of blood cells correlates with the expression of specific surface markers. LT-HSC and ST-HSC express CD117 (Kit+) and stem cell antigen 1 (Sca1+) cell surface markers and are negative for lineage markers (Lin-) such as CD3 and CD20 to name a few. As the cell differentiates to MPP, the surface marker CD34+ will start to be expressed. Upon myeloid lineage commitment, cells will lose the Sca1 and CD34 cell surface markers[7–9]. Detection of cell surface markers by fluorescence activated cell sorting (FACS) has enabled isolation of specific cell populations which has revolutionised the study of haematopoiesis.

Haematopoiesis is maintained by a complex coordinated transcriptional programme mediated by a network of transcription factors with an essential role

within this process. These transcription factors ensure the dynamic differentiation and maturation of HSCs according to requirements of lifelong maintenance of LT-HSCs. Wilson *et al* highlighted ten transcription factors governing a complex regulatory network maintaining transcriptional program of HSC[10]. These include the well-studied transcriptional regulators GATA2[11] and RUNX1[12], and a number of other transcription factors of which recent data implicate that these also have an essential role in haematopoiesis, such as the *MECOM and ETV6* encoded proteins[13]. This essential role is evident as inherited disruption in these genes cause perturbed or inefficient haematopoiesis.

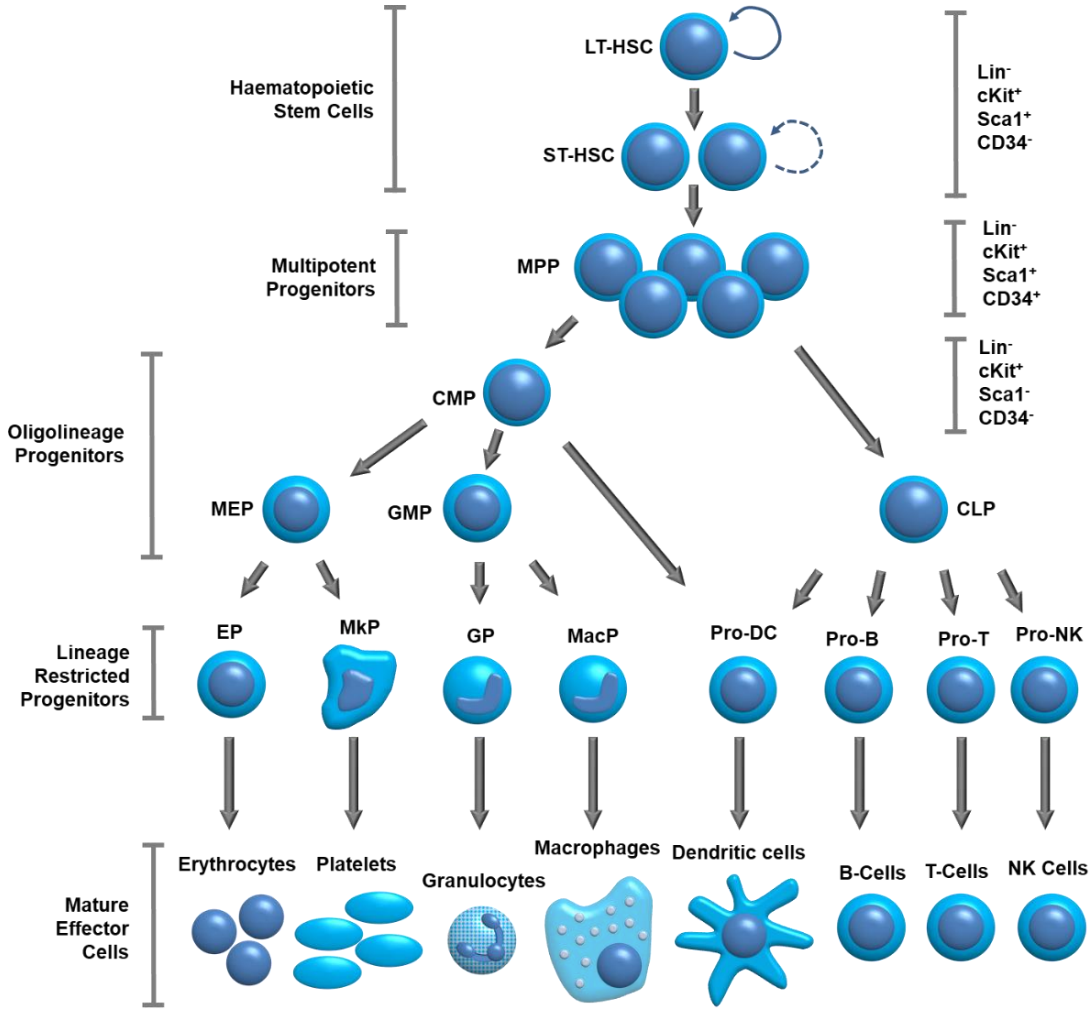

Figure 1.1: Schematic representation of the classical hierarchy of haematopoiesis.
(Adapted from Seita et al.[6])

1.2 Bone Marrow Failure

Bone marrow (BM) failure (BMF) is a haematological disorder that manifests by the inability to maintain the production of blood cells, presenting as either single- or multi-lineage cytopenias. BMF can either be acquired or inherited (IBMF). Acquired causes of BMF include toxic or infectious causes and will not be discussed in the context of this thesis. IBFM can be caused by inherited disruption of genes essential to haematopoiesis, such as *GATA2*, *RUNX1* and *MECOM*. Mutations in *RUNX1* result in single-lineage cytopenia with abnormal platelet number and/or functionality[14], whereas *GATA2* mutations typically result in multi-lineage cytopenia[15]. Patients with pathogenic variants in these genes have a higher susceptibility to develop myelodysplastic syndrome (MDS) or acute myeloid leukaemia (AML)[16–18].

Similar to *GATA2* and *RUNX1*, *MECOM* (MDS1-EVI1 Complex) germline mutations have been found to cause haematopoietic failure. There are several transcripts from the *MECOM* locus, which will be discussed in detail later. Pathogenic variants in *MECOM* have been identified with a variable phenotype. Of so far less than thirty described cases with *MECOM* mutations, two patients with interstitial microdeletions within *MECOM* have resulted in congenital thrombocytopenia[19,20]. One patient developed aplastic anaemia and underwent successful bone marrow transplantation[19]. The other patient died soon after birth from congenital abnormlities[20]. Three patients with missense mutations within *MECOM* have radioulnar synostosis with amegakaryocytic thrombocytopenia (RUSAT)[21]. RUSAT has been also linked with *Hoxa11* mutations and presents with skeletal abnormalities as well as thrombocytopenia which progresses to panocytopenia[22]. The three patients all underwent haematopoietic stem cell transplantation (HSCT), highlighting the importance of *MECOM* for normal haematopoiesis[21]. More recently, Bluteau *et al* found six patients with *de novo* missense mutations in the *MECOM* gene that led to severe aplastic anaemia within the first few months after birth[23]. A recent study by Ripperger *et al* identified the first case of familial germline mutations in *MECOM* associated with familial AML[24]. All four patients displayed skeletal abnormalities; one had congenital thrombocytopenia with two patients

displaying myeloid malignancies[24]. In the largest cohort to date, Germeshausen *et al* identified 12 patients with 10 novel germline mutations in *MECOM*[25]. Family analysis of 11 patients revealed *de novo* mutations in four patients, three mutations that also presented with phenotype in other family members and four mutations that were familial but family members were unaffected at the time of reporting[25]. Of the 12 patients, five presented with RUSAT, and the other seven patients presenting with severe pancytopenia without RUS[25]. All but two patient underwent successful HSCT[25].

The most common IBMF syndrome is Fanconi anaemia (FA)[23,26]. FA is caused by a disruption of *FANC* genes, which encode for proteins involved in the DNA damage response[27]. Clonal chromosomal aberrations in the bone marrow of FA patients develop frequently and are associated with MDS and the transformation to AML[28–30]. The most common chromosomal aberrations are gains of 1q and 3q, which are often seen with either partial or complete monosomy 7[31–33]. The 3q gains in FA intriguingly result in the aberrant expression of *EVI1*, encoded at the *MECOM* locus[34]. The high *EVI1* expression has been shown to be a critical event in leukemic transformation in children with FA[34,35] , the relevance of which will be discussed later.

1.3 Leukaemia

Leukaemia is a disease of uncontrolled proliferation of immature haematopoietic progenitor cells. Genetic aberrations in haematopoietic progenitor cells lead to the abnormal proliferation of blasts, disrupting normal haematopoiesis. These cells have a proliferative advantage and fail to differentiate and/or undergo apoptosis. The genetic aberrations can involve aberrantly expressed kinases (such as *BCR/ABL*) or aberrantly expressed transcriptional regulators (such as *EVI1*) that perturb normal haematopoiesis. Development of leukaemia is not driven by a single genetic aberration, rather an accumulation of collaborative mutations. The initial pre-leukemic chromosomal aberration or mutation of a single gene in an early HSC can lead to clonal expansion but not development of the disease. This increased clonal expansion can result in a higher mutation rate, increasing the chances of a mutation in a collaborative gene that can enhance proliferation or prevent differentiation and/or apoptosis, eventually resulting in emergence of the disease[36–38].

1.3.1 Acute Leukaemia sub-classification

The historical French-American-British (FAB) classification system based classification upon the morphology of leukaemia cells. Since the establishment of the FAB system the understanding of leukaemia has advanced. Since the 1970s, recurrent non-random chromosomal changes in leukaemia have been observed. The World Health Organisation (WHO) implemented a prognostic model that takes into account the cytogenetic aberrations and specific mutations that occur in leukaemia. The cytogenetic findings are common non-random chromosomal aberrations with balanced translocations or inversions, leading to a chimeric fusion gene. These genes are often epigenetic regulators, signalling pathway components, cell-cycle regulators and transcription factors. There are also patients that appear cytogenetically normal, but harbour mutations in specific genes[36]. The most recent WHO classification of AML and ALL can be seen below (*Table 1.1*).

Table 1.1: The WHO classification of acute leukaemia. *(Adapted from Arber et al.[18])*

Acute Myeloid Leukaemia (AML)
AML with recurrent genetic abnormalities
AML with t(8;21)(q22;q22.1);RUNX1-RUNX1T1
AML with inv(16)(p13.1q22) or t(16;16)(p13.1;q22);CBFB-MYH11
APL with PML-RARA
AML with t(9;11)(p21.3;q23.3);MLLT3-KMT2A
AML with t(6;9)(p23;q34.1);DEK-NUP214
AML with inv(3)(q21.3q26.2) or t(3;3)(q21.3;q26.2); GATA2, MECOM
AML (megakaryoblastic) with t(1;22)(p13.3;q13.3);RBM15-MKL1
AML with BCR-ABL1
AML with mutated NPM1
AML with biallelic mutations of CEBPA
AML with mutated RUNX1
AML with myelodysplasia-related changes
Therapy-related myeloid neoplasms
AML, NOS
AML with minimal differentiation
AML without maturation
AML with maturation
Acute myelomonocytic leukaemia
Acute monoblastic/monocytic leukaemia
Pure erythroid leukaemia
Acute megakaryoblastic leukaemia
Acute basophilic leukaemia
Acute panmyelosis with myelofibrosis
Myeloid sarcoma
Myeloid proliferations related to Down syndrome
Transient abnormal myelopoiesis (TAM)
Myeloid leukaemia associated with Down syndrome
Acute Lymphoblastic Leukaemia (ALL)
B-lymphoblastic leukaemia / lymphoma
B-lymphoblastic leukaemia/lymphoma, NOS
B-lymphoblastic leukaemia/lymphoma with recurrent genetic abnormalities
B-lymphoblastic leukaemia/lymphoma with t(9;22)(q34.1;q11.2);BCR-ABL1
B-lymphoblastic leukaemia/lymphoma with t(v;11q23.3);KMT2A rearranged
B-lymphoblastic leukaemia/lymphoma with t(12;21)(p13.2;q22.1); ETV6-RUNX1
B-lymphoblastic leukaemia/lymphoma with hyperdiploidy
B-lymphoblastic leukaemia/lymphoma with hypodiploidy
B-lymphoblastic leukaemia/lymphoma with t(5;14)(q31.1;q32.3) IL3-IGH
B-lymphoblastic leukaemia/lymphoma with t(1;19)(q23;p13.3);TCF3-PBX1
B-lymphoblastic leukaemia/lymphoma, BCR-ABL1–like
B-lymphoblastic leukaemia/lymphoma with iAMP21
T-lymphoblastic leukaemia / lymphoma
Early T-cell precursor lymphoblastic leukaemia
Natural killer (NK) cell lymphoblastic leukaemia/lymphoma

1.3.2 Acquired chromosomal changes in Acute Lymphoblastic Leukaemia

Acute lymphoblastic leukaemia is associated with a distinct spectrum of cytogenetic changes. These include hyperdiploidy and several others. Relevant for this study is the rarity of genetic changes involving the 3q segment and disruption of the *MECOM* locus. One study identified two patients with lymphoid malignancies that harbour 3q26 aberrations, leading to aberrant expression of *MECOM*[39]. One patient with B-acute lymphoblastic leukaemia harboured a t(2;3)(p12;q26) translocation and the other patient diagnosed with T-cell non-Hodgkin lymphoma harboured a t(3;9)(q26;p23) translocation[39]. However, ALL can also uncommonly show *MECOM* overexpression without 3q aberrations[40]. Typically, transcriptional alteration of *MECOM* leading to aberrant expression of *MECOM* in ALL is a secondary event as a result of chromosomal aberrations in other genes[41–44].

1.3.3 Acquired chromosomal changes in Acute Myeloid Leukaemia

Several acute myeloid leukaemia specific chromosomal changes have been identified and their prognosis implications became clear over the years. The most common recurrent genetic abnormalities seen in AML include mutations of the nuclear chaperone *NPM1*, the epigenetic regulator *DNMT3a*, and the transcription factors *RUNX1* and *CEBPα*. Frequently seen chromosomal aberrations include t(15;17)(q22;21), t(8;21)(q22;q22), inv(16)(p13q22) and those involving 11q23, which lead to the chimeric oncoproteins PML-RARA, RUNX1-RUNX1T1, CBFB-MYH11 and MLL-x respectively. Of these translocations, those involving *MLL* have an adverse prognosis [36,45]. Changes involving 3q segment and subsequent disruption of the *MECOM* locus, which is seen in a small but very important group of AML will be the focus of this study.

In AML, 4-5% of cases display rearrangements in 3q[46]. Aberrations involving chromosome 3q26, translocations in t(3;3)(q21;q26) and inv3(q21;q26) being

most common, can lead to abnormal expression of *EVI1*[47–49]. Of all AML patients, 2-2.5% display aberrations in inv(3)/t(3;3), of these patients displaying this aberration, all have aberrant *EVI1* expression[50,51].

In addition to the chromosomal aberrations seen solely in 3q, dysregulation of *EVI1*, can also result from translocations of chromosome 3 and other chromosomes such as t(2;3)(p15-22;26), t(3;7)(q26;q21), t(3;6)(q26;q25) and t(3;17)(q26;q22)[47]. These translocations can result in EVI1 fusion proteins and lead to *EVI1* overexpression[52]. EVI1 fusion proteins can also occur in t(3;21) and t(3;12) aberrations that result in a chimeric transcription factor of *EVI1*- and Runt-Related Transcription Factor 1 (*RUNX1*) or Ets Variant 6 (*ETV6*) respectively[52].

EVI1 overexpression is not solely dependent on 3q aberrations, as 3q aberrations are rare in paediatric patients yet *EVI1* overexpression occurs in up to 28% of paediatric AML patients[53–56]. In non-3q AML, *EVI1* overexpression occurs at a high frequency in patients harbouring 11q23 aberrations and is associated with monosomy 7[50,54–63]. In a large AML cohort carrying 11q23, *EVI1* expression was seen in ~43% of cases[64]. Of AML with MLL rearrangements, high expression of *EVI1* is seen in *MLL-AF6*, *-AF9*, *-AF10*, *-ENL* and *–ELL* fusion genes[64]. It has been suggested that AML cases that display *EVI1* overexpression but no 3q aberrations may harbour a cryptic translocation involving 3q26 that is responsible for *EVI1* overexpression[59,65,66].

1.3.4 Biological and clinical implications of 3q aberrations in AML

Treatment of AML is usually through combination chemotherapy, involving combination treatment with cytosine-arabinoside (Cytarabine), Daunorubicin and Etoposide (ADE)[67–69]. The majority of chemotherapy compounds mechanisms of action is the prevention of DNA replication. Both Etoposide and Daunorubicin are topoisomerase II inhibitors that prevent the relaxing of positive or negative supercoiling of DNA, preventing re-ligation and causing double-strand breaks[70]. Cytarabine is classified as an anti-metabolite that inhibits DNA

replication through three proposed mechanisms: prevention of normal pyrimidine synthesis, inhibition of DNA polymerases and miscoding by incorporation into DNA and RNA[71].

Response to chemotherapy treatment is typically dependent on the genetic aberrations seen in the leukaemia. In a cohort of 534 AML patients, *EVI1*-overexpression was found in 41 patients[59]. Patients with *EVI1*-overexpression less frequently attained complete remission and had an impaired 5-year overall survival in comparison to AML without *EVI1*-overexpression[59]. Gene expression analysis allows the delineation of patterns determined by *EVI1* overexpression that is associated with poor outlook in both adult and paediatric AML[56–58].

The poor prognosis of *EVI1*-expressing leukaemia has been linked with chemotherapy resistance. In a human myeloid leukaemia cell line, overexpression of *EVI1* protected against the cytotoxic effects of Daunorubicin and Etoposide but not Cytarabine[72]. However, in the human AML cell line UCSD/AML1, which has t(3;3)(q21;q26.2) that leads to overexpression of *EVI1*[73], knockdown of EVI1 with short hairpin RNA (shRNA) caused sensitivity to Cytarabine[74]. The association of aberrant expression of *EVI1* with chemotherapy resistance is not limited to leukaemia. In stage III ovarian carcinomas, overexpression of *EVI1* has been found to correlate with resistance to combination chemotherapy paclitaxel/carboplatin[75]. Nasopharyngeal carcinoma cell lines that have high expression of *EVI1* also exhibit resistance to the chemotherapy compound Fluorouracil[76]. Knockdown of *EVI1* expression by siRNA in these cell lines results in an increase in sensitivity to Fluorouracil treatment[76].

Several therapeutic strategies have been studied to target the chemotherapy resistance associated seen in *EVI1*-overexpressing leukaemia in order to improve treatment response. Recently, a small study adding treatment with all-trans-retinoic acid (ATRA) to chemotherapy has shown a higher remission rate in *EVI1*-overexpressing AML[77]. Originally purposed for acute promyelocytic leukaemia (APL)[78], combination of ATRA with chemotherapy in patients with AML had poor results in clinical trials[79,80]. However, in AML with *EVI1*-overexpression, ATRA in combination chemotherapy may have efficacious *in*

vivo[81]. In AML that fails to respond to ATRA treatment, inhibition of the histone demethylase LSD1 has been investigated[82], and a number of small molecule inhibitors are currently in clinical trial[83]. Additionally the hypomethylating agent Decitabine has proved efficacious in AML cell lines with high *EVI1* expression and in patient derived xenograft models of *EVI1*-overexpressing AML[84]. Alternatively targeting the mitochondrial creatine kinase CKMT1 with cyclocreatine has also proved successful in *EVI1*-postive AML cell lines and in xenograft mouse models[85].

Given the current lack of therapeutic perspectives for EVI1 overexpressing novel therapeutic perspectives targeting EVI1 are desperately needed.

1.4 EVI1

1.4.1 MECOM Genes, Transcripts and Proteins

EVI1 is encoded at the *MECOM* (*MDS1* and *EVI1* complex) locus on chromosome 3q26. The human *MECOM* locus is approximately 580Kb long and also encodes the myelodysplasia syndrome associated protein 1 (*MDS1*) gene. The initial 520Kb contain 4 exons that encode *MDS1*. The downstream 60Kb containing 16 exons, of which 14 are expressed that encode *EVI1*[86]. In human tissue a number of transcripts generated from the *MECOM* locus were detected[87]. There is a transcriptional start site within exon 1 of the *MDS1* gene, exon 3 of the *EVI1* gene and multiple within exon 1 of the *EVI1* gene. Transcription from exon 1 of the *MDS1* gene leads to a *MDS1-EVI1* fusion transcript as a result of alternative splicing of *MDS1* exon 2 to *EVI1* exon 2. The different transcriptional start sites within exon 1 of the *EVI1* gene generate EVI1 transcripts with variable 5'-ends (1A, 1B, 1C and 1D). The transcriptional start site within exon 3 of the *EVI1* gene results in the canonical EVI1 transcript (3L).

From the main transcript, 3L, the full length EVI1 protein is translated (1051 amino acids) (123kDa). For the EVI1 protein several functionally important domains have been identified (*Figure 1.2*). There are two zinc finger domains: ZF1-7 (21-239aa), which consists of seven zinc finger motifs at the N-terminus and ZF8-10 (733-812aa) that are three motifs at the C-terminus[88]. Both ZF domains are responsible for EVI1 binding to DNA. The N-terminal ZF1-7 domain binds to specific (C/T)AAGA(T/C)AAGATAA sequences of DNA via the ZF4-7 motifs. The ZF1-3 motifs are not involved in direct binding but have been suggested to have an auxiliary function by influencing specificity for GACAA sequences[89]. The C-terminal ZF8-10 domain binds specifically to GAAGATGAG and GACAA DNA sequences[90,91]. The binding of EVI1 to DNA via the ZF domains has been attributed to EVI1-mediated transcriptional regulation[92]. Between the ZF domains there is a repressor domain (RD) (514-724aa) that contains two C-terminal binding protein (CtBP)-interacting motifs, PFDLT (553-557aa) and PLDLS (584-588aa), that are essential to binding CtBP1 and CtBP2 (CtBP)[93–95]. In addition to the CTBP binding motifs, the ZF1-7 domain has been

shown to be integral to CtBP1 binding[96]. In the intervening region (IR) (240-513aa) between the RD domain and the ZF1-7 domain a putative nuclear localisation site (NLS) (421-434aa), which might be mediating the localisation of EVI1 in the nucleus[88,96]. Additionally there is an acidic domain (AD) (886-937aa) at the C-terminus of EVI1[97]. This 1051 KD EVI1 protein isoform will be the focus of this study.

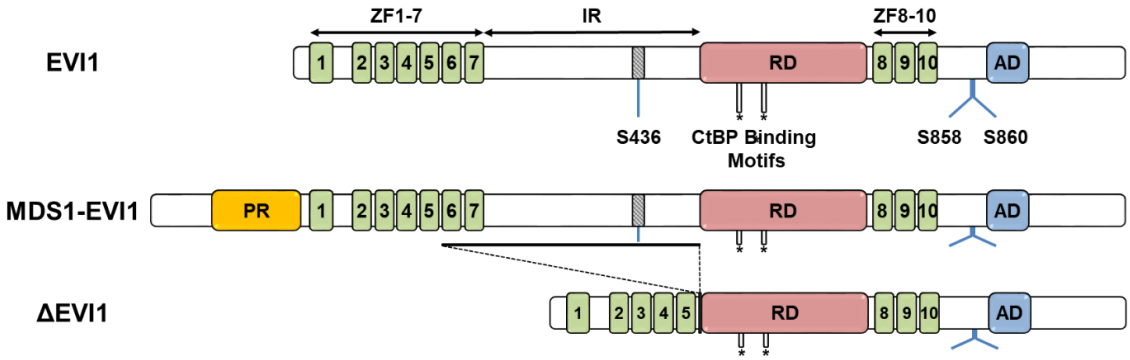

Figure 1.2: Schematic representation of the MECOM proteins. *The main protein isoforms translated from the MECOM locus. Dotted lines represent sections of the protein missing in the isoform ΔEVI1. Shaded grey box indicates the putative nuclear localisation site. Stars indicate CtBP interacting motifs, PFDLT and PLDLS. PR=Positive-regulatory domain. Green boxes=Zinc-finger motifs. RD=Repressor domain. AD=Acidic domain. IR=Intervening region.*

From the *MDS1-EVI1* transcript a MDS1-EVI1 fusion protein is translated (1230 amino acids) (135kDa). The MDS1-EVI1 has a proline-rich domain (PR) at the N-terminus that has methyltransferase activity[98,99]. The PR domain has also been shown to be responsible for positive transcriptional regulation of MDS1-EVI1 which has led to suggestions that MDS1-EVI1 might have an antagonistic role to EVI1[47,100,101]. An additional protein isoform is generated from the *MECOM* locus: ΔEVI1 (727 amino acids,103kDa)[102]. This isoform is generated as a result of splicing from a splice donor site in exon 6 to an alternative splice acceptor site in exon 7[96]. This splicing results in the loss of the majority of the ZF6 motif, the whole ZF7 motif and the whole IR between ZF1-7 and the RD (*Figure 1.2*). As a result of the loss of these regions, ΔEVI1 is unable to bind DNA via the ZF1-7 domain but it retains the function to bind ETS DNA motifs as

ZF8-10 are intact[102,103]. Further, ΔEVI1 has a different nuclear localisation patterns to the other EVI1 protein isoforms[96].

1.4.2 The Role of MECOM in Haematopoiesis

Initial *in vivo* studies using *EVI1* knockout mice resulted in a phenotype that suggested that EVI1 was essential in haematopoiesis. Loss of *EVI1* in these studies lead to bone marrow failure. The first knockout mouse model involved deletion of *EVI1* exon 7 (*EVI1*$^{d7/d7}$), which resulted in impaired expression of *MDS1-EVI1* and *EVI1* but *ΔEVI1* expression was unaffected. In this model *EVI1*$^{d7/d7}$ embryos did not survive beyond 10.5 days due to numerous developmental defects[104]. Embryo models also use cells from the para-aortic splanchnopleural (P-Sp) region, the site of definitive haematopoiesis with cells that have high levels of *EVI1* expression[105]. Deletion of *EVI1*$^{d7/d7}$ in cells from the P-Sp region results in diminished numbers of HSC cells[106]. Transduction of *EVI1*$^{d7/d7}$ cells with *EVI1* rescues the haematopoiesis[107], which was shown to be dependent on EVI1-mediated regulation of *GATA2* expression[106]. This model first suggested that EVI1 was important for haematopoiesis by *GATA2* regulation.

An alternative *EVI1* knockout model was developed which targeted exon 4 of *EVI1* (*EVI1*$^{d4/d4}$), which resulted in impaired expression of *MDS1-EVI1*, *EVI1* and *ΔEVI1*. Embryos with *EVI1*$^{d4/d4}$ survived longer in comparison to *EVI1*$^{d7/d7}$ embryos. The different genetic background or the lack of *ΔEVI1* expression is likely to explain the difference in survival between the two deletion models. In agreement with the *EVI1*$^{d7/d7}$ model, the P-Sp region from *EVI1*$^{d4/d4}$ embryos have significantly fewer HSCs compared to wild-type controls. In the reconstitution of the haematopoietic system in embryos and adult BM, heterozygous *EVI1*$^{+/d4}$ cells showed greater repopulating activity and had a greater number of HSC compared to reconstitution with *EVI1*$^{d4/d4}$ cells. EVI1 has an essential dose dependent role in HSCs as knockout leads to reduced HSC number and functionality and heterozygous *EVI1* mutants display an

intermediate phenotype in regards to number of HSCs and reconstitution activity[13].

Another study developed two models to study EVI1 in haematopoiesis[108]. The first model possessing an inducible knockdown of *EVI1* exon 3 (*EVI1*$^{t3/t3}$), which results in the impairment of all three EVI1 isoforms. The second model that targets the *MDS1* exon 1 (*ME*$^{d1/d1}$) that only results in the loss of *MDS1-EVI1* expression. In concordance with the *EVI1*$^{d7/d7}$ model, *EVI1*$^{t3/t3}$ results in impaired HSC function. In the *ME*$^{d1/d1}$ model, the reduction of *MDS-EVI1* expression results in decreased number of HSC cells. Furthermore, *ME*$^{d1/d1}$ cells fail to repopulate the bone marrow of irradiated mice. This study further confirmed the essential role of EVI1 in HSC s but also suggested an important role for MDS1-EVI1.

An additional model was generated that used an internal ribosomal entry site (IRES) with a green fluorescent protein (GFP) reporter (EVI1-IRES-GFP) to monitor *EVI1* expression within adult BM haematopoiesis. Expression of *EVI1* is exclusive to HSCs and is specifically enriched in the LT-HSC. Within LT-HSCs, cells which express *EVI1* have greater repopulating potential compared to cells that do not express *EVI1*. Only *EVI1* positive LT-HSCs able to repopulate the BM of irradiated mice. EVI1 also had a dose-dependent role within this model as heterozygous mice had a reduced proportion of LT-HSCs compared to EVI1-GFP mice. The reduced number of LT-HSCs could be rescued by transduction with EVI1[108,109]. In summary, the EVI1 mouse models outline an essential role of EVI1 in haematopoiesis and for the maintenance of HSC. Knockout of EVI1 leads to defective haematopoiesis and bone marrow failure, whereas overexpression of *EVI1* leads to enhanced proliferation and self-renewal.

1.4.3 MECOM Transcriptional Regulation

The aberrant expression of *EVI1* in HSCs transforms the haematopoietic transcriptional programme by directing transcriptional regulation of key genes critical to normal haematopoiesis. Direct targets for EVI1-mediated

transcriptional regulation include *GATA2*, *PTEN*[110] and *PBX1*[111]. However, to further define a transcriptional programme directed by EVI1 in HSC, numerous groups have performed transcriptomic studies.

In order define the early transcriptional programme engaged by *EVI1* expression, Kustikova *et al* performed a gene expression microarray on EVI1-transduced Lin- negative cells from C57BL/6J mice[112]. This study defined a stemness transcriptional programme in which important haematopoietic markers, such as *Aldh1a1*, *Sca1 and Pbx1*, are regulated by EVI1 overexpression. Fenouille *et al* further refined the dataset in human leukaemia, confirming the enrichment of genes involved in cellular proliferation and differentiation, such as *PTEN*, that are suppressed by *EVI1* expression, but finding *EVI1* overexpression modulated genes from the cellular energy-related pathways[85]. From both microarray data and CHIP-qPCR generated, the group suggests that EVI1 modulates metabolism in AML by repression of myeloid differentiation regulator *RUNX1* and subsequent upregulation of the creatine kinase CKMT1a[85].

A global CHIP-sequencing analysis and RNA*seq* aimed to identify EVI1 target genes found that EVI1 binds directly to the master myeloid differentiation gene *CEBPE*, mediating its downregulation[113]. The study also confirmed other EVI1 target genes, such as *GATA2*, *PBX1* and *PTEN*. An additional study focussing on both EVI1 and ΔEVI1 found a high degree of overlap of isoform-specific binding sites[103]. The exact binding sites between the isoforms differs because of the truncated ZF1-7 domain of ΔEVI1[103]. This study further confirmed that bound genes by both EVI1 and ΔEVI1 play a role in the regulation of transcription, cellular differentiation and intracellular signalling cascades[103].

1.4.4 MECOM Oncogenic Potential

Expression of *EVI1* is critical to early embryonic development and haematopoiesis. However, aberrantly high expression detected in AML and

other cancers is clinically recognised as an important oncogenic event associated with poor prognosis.

The first model used to study oncogenic features of EVI1 was the Rat1 fibroblast model[97,114]. Transduction of Rat1 fibroblast with EVI1 results in an increase in anchorage independent growth [97]. Both ZF1-7 and ZF8-10 domains, the IR region and the RD domain have been implicated to have an important role in EVI1-mediated anchorage-independent growth of Rat1 fibroblast[97,114,115]. The EVI1-mediated transformation of Rat1 fibroblasts is suggested to be a at least partly a result of dysregulation of cyclin-dependent kinase (Cdk) 2 kinase activity[116]. To further define the specific regions of EVI1 that are responsible for EVI1-mediated transformation of Rat1 fibroblasts, site directed mutagenesis has been used. Mutagenesis of the CtBP binding sites of EVI1 reduces the transformation of Rat1 fibroblasts, indicating an important role for EVI1-CtBP protein interaction[94].

The study of EVI1 in Rat1 fibroblast is limited as it does not replicate haematopoiesis. An alternative model to study the oncogenic role of aberrantly high EVI1 within the haematopoietic environment is primary murine bone marrow progenitors (PMBMP). A re-plating assay was first established to assess whether transduction of PMBMP with fusion oncogenes perturbed normal self-renewal or differentiation potential[117].

Initial studies of EVI1 in the PMBMP re-plating assay investigated the fusion protein AML1/EVI1 (AME)[118–120]. These studies found that in both Thy-1^{lo}Sca-1^{+}H-2K^{hi} cells and Kit+ cells from C57BL/J6 mice, transduction with AME resulted in sustained re-plating potential compared with non-transduced cells[118–120]. The sustained re-plating potential is mediated by the ability to bind CtBP, both ZF1-7 and ZF8-10 domains, the RD domain and the AD domain of EVI1[120].

Basic colony assays that have no re-plating, have shown that transduction with EVI1 causes a significant increase in the colony forming potential of numerous primary murine haematopoietic stem cell populations. These include Thy-1^{lo}Sca-1^{+}H-2K^{hi} [121,122], Lin-[123] and Lin− Sca-1+ kit+ cell populations[108]. The first

study to perform re-plating of PMBMP found that transduction with EVI1 doubled the self-renewal potential of Lin- cells from C57BL/J6 mice[124]. More recently it was confirmed that EVI1 confers re-plating potential of Kit+ cells, selecting for a broad population of HSC, from C57BL/J6 mice[125]. Another study found contradictory results in PMBMP with MLL-fusion proteins[126]. The study found that in either *ME*$^{d1/d1}$ or *EVI1*$^{t4/t4}$ cells (previously described in *Section 1.4.3*) that are transduced with either *MLL-AF9* or *MLL-EN*L fusion transcripts, MDS1-EVI1, and not EVI1, is able to rescue re-plating capability[126]. MDS1-EVI1 may be important for the self-renewal of PMBMP in the context of MLL-fusions, however MDS1-EVI1 alone cannot sustain colony forming potential[123].

1.4.5 EVI1 Protein Post-Translational Modifications

The EVI1 protein is subject to post-translational modifications. Many of them might regulate the function of the protein and interactions with other proteins. The majority of EVI1 posttranslational modifications have been discovered in studies addressing global changes of the proteome. Few functional studies have been conducted to investigate these posttranslational modification[125,127–129]. Post-translational modifications of EVI1 include sumoylation, acetylation, ubiquitination and phosphorylation.

1.4.5.1 Phosphorylation

While the functional analysis of EVI1 posttranslational modifications is so far only very limited, some progress has been made towards understanding of EVI1 phosphorylation. As with the other posttranslational modifications, the discovery of the phosphorylation sites has been through mass spectrometry[95,125,130–139]. The identification of phosphorylation sites of EVI1 has largely been a consequence of studies investigating the phosphoproteomic profile of specific cancer tissues or cell lines.

The most detailed characterised phosphorylation site of EVI1 is the phosphorylation at serine 196 (S196), which is located in ZF6, which has been identified in the Fanconi Anaemia derived AML cell line SB1690CB[125]. This study used site-directed mutagenesis to generated a non-phosphorylatable and non-phosphorylated mutant (S196A), which results in the substitution of serine to alanine, and a phosphomimetic mutant (S196D), which changes serine to aspartic acid[125]. This study found that mimicking the phosphorylation was detrimental to EVI1 DNA binding and EVI1-mediated transformation of Rat1 fibroblasts[125].

Our group has performed mass spectrometry and identified several phosphorylation sites of EVI1 in SB1690CB cells (*Appendix Figures 7.1 and 7.2*). This experimental work confirmed phosphorylation at serine 858/860 (S858/860). Phosphorylation at S860 was first identified in a screen for ATM substrates in response to irradiation[133]. The S858/860 phosphorylation site was also confirmed to be an ATM- SQSP target motif[133]. The phosphorylation of serine 436 was also confirmed in the SB1690CB cells, which has previously been reported in HeLa cells[136–138], breast cancer[132,134,135], ovarian cancer[134], NSCLC[132,139] and colorectal cancer[130]. The results of this experiment are discussed in greater detail later in this report. Given that phosphorylation is important to EVI1 function as evident by the results published regarding S196, the phosphorylation sites S858/860 and S436, which have not been functionally investigated, are the focus of this study.

1.4.6 EVI1 Protein Interactions

EVI1 has been shown to interact with proteins involved in transcriptional and epigenetic regulation, which play an essential role in EVI1 oncogenic function. Protein interactions are modulated by the formation of dynamic tertiary complexes and are regulated by post-translational modifications. Mass spectrometry (MS) experiments have detected a large number of proteins that interact with EVI1 (*Appendix Table 7.1*). The first mass spectrometry study of EVI1-interacting proteins was performed in the ovarian cancer cell line SKOV3,

and found a total of 73 interacting proteins[95]. Of the high confidence interacting proteins identified by stable isotope labelling of amino acids in cell culture (SILAC)-based MS, 30 were confirmed to interact with EVI1 by co-immunoprecipitation. This study found an enrichment in EVI1 interacting partners that play a role in the DNA damage response, and proteins involved in regulation of transcription and signal transduction. The study does also report the interaction of EVI1 with RuvB-like 1 (RUVBL1) and RuvB-like 2 (RUVBL2), DNA helicases and adenosine triphosphatases (ATPases), that can enhance oncogenic function of transcription factors such as c-MYB in AML[140]. RUVBL1 and RUVBL2 can also associate with chromatin-remodelling complexes to regulate DNA damage repair and transcription[141].

More recently, Ivanochko *et al* found a total of 115 high confidence EVI1 interacting proteins in the transduced human breast carcinoma cell line, T-47D. This study focussed on comparing the different interacting partners between EVI1 and the MDS1-EVI1 protein isoforms. MDS1-EVI1, but not EVI1, was able to interact with the NuRD complex, an epigenetic regulatory complex essential for the proliferation and differentiation of haematopoietic stem cells[142], by binding of the N-terminal PR domain to RBBP4, which the study modelled *in silico*. The study also confirmed the interaction of EVI1 with C-terminal binding protein 1 (CtBP1), which has been shown to be important for EVI1 oncogenic potential by promoting leukaemogenesis[131,143]. Although direct interaction of EVI1 with all the proteins detected within these studies is unlikely, it does suggest that EVI1 dynamically interacts with large protein complexes.

1.4.6.1 CtBP

The interaction of EVI1 with the transcriptional co-repressors CtBP1 and CtBP2 is well established[93–95,131,144–146]. The two CtBP-binding motifs, PFDLT (553-557aa) and PLDLS (584-588aa), within the RD domain of EVI1 facilitate EVI1 binding to CtBP. Of the two motifs, the PLDLS motif is essential to the interaction, whereas the PFDLT motif is not[93]. CtBP contains two PLDLS-

binding cleft (27-121aa and 327-352aa) that facilitates binding to PLDLS motifs (*Figure 1.3*)[147]. CtBP1 and EVI1 co-localise within the nucleus[118,131], where the CtBP-EVI1 binding is requiring the whole CtBP protein[93]. The dimerisation of EVI1 has been shown to be important for the CtBP-EVI1 interaction, but MDS1-EVI1, which only forms monomer is less efficient in binding CtBP despite containing the binding motifs[148].

The CtBP-EVI1 interaction has been shown to be essential for EVI1-mediated transformation of Rat1 fibroblast[94], and EVI1-mediated transcriptional repression[93,118,149]. CtBP has been implicated to be involved in repressing the DNA damage response in breast cancer by targeting promoters of *FANC* genes[150,151]. It has recently been shown that CtBP-EVI1 interaction increases in response to genotoxic stress in EVI1 over-expressing AML cells and this is mediated by the EVI1 carboxy-terminal phosphorylation[131]. CtBP has further been implicated in leukemia by the interaction with MLL[152].

CtBP has been shown to be essential to normal embryonic development. Knockout of CtBP results in early embryonic lethality[153]. CtBP is functional active as a transcriptional repressor in conditions with high levels of NADH, such as hypoxia in haematological malignancies[154], where CtBP binds to NADH and the putative substrate MTOB (4-methylthio-2-oxobutyric acid) to form functionally active dimers[155]. CtBP dimers form a co-repressor complex that contains a number of epigenetic regulatory elements that govern function of the complex in epigenetic regulation (*Figure 1.3*)[147]. The complex contains the DNA binding factors, such as ZEB1/2[156] and Znf217[157], which bind to CtBP1 or CtBP2 through the PLDLS/RRT motifs[147]. The complex also contains the epigenetic regulators HDAC1/2, the HMTs G9a and GLP and the histone lysine-specific demethylase LSD1[147]. These epigenetic regulators associate with the complex through binding to co-repressors that bind to CtBP such as CoREST[158], CDYL[159], LCoR[160] and Wiz. Both HDAC1/2 acetylate multiple lysine residues of histones whereas the HMTs G9a and GLP seem to specifically target H3K9 for methylation leading to consequential transcriptional repression[147,161]. LSD1 function in regulating transcription with CtBP is cofactor- and promoter dependent, as demethylation of H3K4 results in transcriptional

repression whereas demethylation of H3K9 causes transcriptional activation[147,162,163]. Recent developments into small molecule inhibitors that compete with MTOB have proven successful in reversing CtBP mediated transcriptional repression[155]. The interaction with CtBP is critical to EVI1 oncogenic function, therefore potential targeting of CtBP through small molecule inhibitors might prove successful in EVI1-driven leukemia.

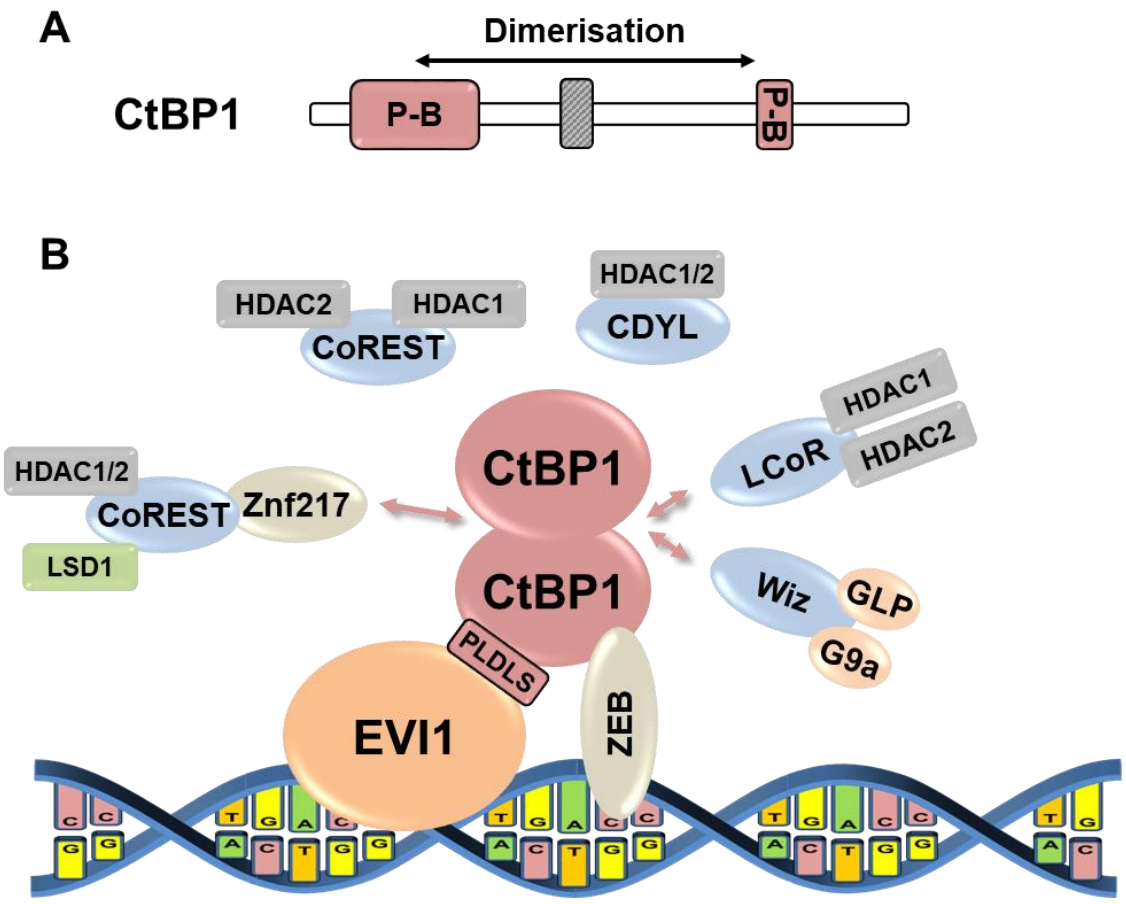

Figure 1.3: The CtBP1 protein and the CtBP1-interacting complex. (A) *Schematic representation of the CtBP1 protein. Shaded grey box indicates NAD(H) binding domain. P-B=PLDLS-binding domain. Dimerisation=Region of the protein responsible for forming the dimerization interface.* ***(B)*** *EVI1 binds to CtBP, which binds to DNA via Znf217 or ZEB. CtBP forms complexes with epigenetic regulators via binding of co-repressors (light blue). (Adapted from Chinnadurai 2007[147], Ginder 2011[164])*

1.4.6.2 DNMT3a

EVI1 has also been shown to interact with the DNA methyltransferases DNMT3a and DNMT3b, which has been linked with a role of EVI1 in DNA methylation processes[165]. DMT3a and b perform *de novo* cytosine DNA methylation at CpG sites by formation of homotetramers or heterotetramers with DNMT3L or other transcription factors (*Figure 1.4*)[164,166]. Tetramerisation occurs through binding of residues (729-774aa) within the catalytic domain (627-912aa) (*Figure 1.4*). Mutations in these residues lead to the impaired dimerization and lack of methylation at clustered CpG sites[166]. DNMT3a specifically has been shown to be essential in HSC function: Loss of DNMT3a function impairs differentiation and is promoting self-renewal[167,168]. Mutations within the catalytic domain of DNMT3a, common in AML, prevents tetramer formation and leads to disrupted methylation patterns and potential leukaemogenesis[166,169–171]. In non-leukemic HSC, disruption of *DNMT3a* results in focal hypomethylation[172].

Altered methylation patterns have been associated with silencing of tumour suppressor genes in cancer[173]. In a genome wide DNA methylation profiling study of 344 AML patients, methylation patterns characterised 16 biologically and clinically distinct groups[174]. Patients categorised into poor prognosis groups had DNA methylation patterns that were significantly enriched in CpG dinucleotide regions in specific sets of genes[174]. Lugthart *et al* investigated DNA methylation in EVI1 overexpressing AML cells and found an abnormal DNA methylation signature at CpG enriched promoters in comparison to normal HSCs and other EVI1 negative AML cells[165]. Within the abnormally methylated CpG rich promoters, the majority of genes were hypermethylated with an overrepresentation of EVI1 binding sites[165]. Within the hypermethylated promoter signature in EVI1-expressing AML cells, EVI1 bound *in vivo* to the promoters[165]. The study also demonstrated that EVI1 interacts with DNMT3a; also Senyuk *et al* detailing this interaction is through the catalytic domain of DNMT3a and is dependent on the ZF1-7 domain of EVI1[175].

It has been shown that EVI1 mediates repression of critical genes in haematopoiesis by methylation of CpG islands within promoters regions of specific genes[84,165,176,177]. Methylation of CpG islands within the *CADM1* gene, a tumour suppressor gene which is methylated in poor prognosis subset of AML[178,179], is enhanced by *EVI1* overexpression and frequently seen associated with 3q26 rearrangements[176]. Additionally, the tumour suppressor genes *TOPORS*, *PCDH16* and *CTCFL* have aberrant CpG island methylation with *EVI1* overexpression[165]. More recently, EVI1 has been shown to methylate the promoters of microRNAs. In the leukaemia cell lines AML-1 and Kasumi-3 that have aberrant *EVI1* expression, the promoter of miR-9 has significantly higher CpG island methylation compared to EVI1 negative lines[84]. Additionally, EVI1 induces the methylation of CpG islands within the promoter of miRNA-124[177]. Given that high expression of miR-9 is associated with poor prognosis in AML[180], understanding EVI1-mediated methylation is important to refining treatment of AML. Interaction of EVI1 with DNMT3a mediates the hypermethylation of CpG islands within EVI1 specific target genes that are essential in haematopoiesis.

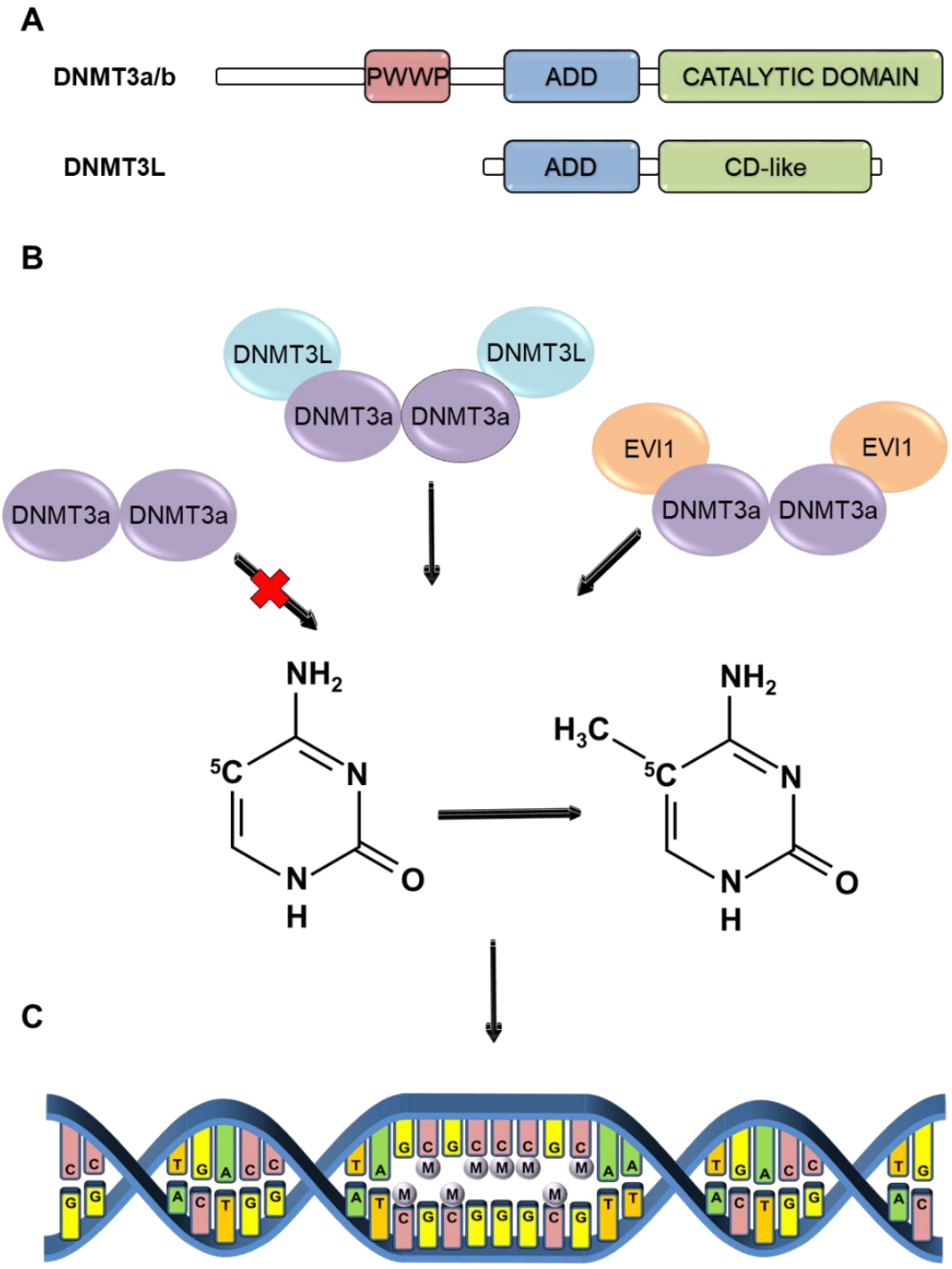

Figure 1.4: Schematic Representation of the DNMT3 proteins, protein interaction and functional output. ***(A)*** *The structure of DNMT3a/b and DNMT3L. PWWP: proline-tryptophan-tryptophan-proline domain. ADD: ATRX-DNMT3-DNMT3L-type zinc finger domain. CD: catalytic domain.* ***(B)*** *The tetramerisation of DNMT3a to either DNMT3L or EVI1 and the resulting the addition of a methyl group to a cytosine base.* ***(C)*** *The hypermethylation of CpG islands. (Adapted from Guo et al*[181]*, Holz-Schietinger et al*[166] *and Wong et al*[182]*)*

1.5 Hypothesis and Aims

EVI1 is subject to dynamic phosphorylation events that mediate protein function. Here it is hypothesised that the phosphorylation events at the serine 436, and the double phosphorylation at serine 858/860, mediate EVI1 function by modulating protein interactions. These differential protein interactions result in divergent downstream signal events that are essential to EVI1 oncogenic function.

This study aims to:

- Investigate how EVI1 is dynamically phosphorylated at the carboxy-terminal sites 858 and 860.
- Investigate the functional and therapeutic consequences of carboxy-terminal EVI1 phosphorylation
- Investigate the functional and therapeutic consequences of serine 436 EVI1 phosphorylation

Chapter 2 Materials and Methods

2.1 Cells Culture

2.1.1 Cell Lines and Culture Conditions

Established cell lines used within this study are listed in *Table 2.1*. The medium used for the respective cell line is outlined in *Table 2.2*. Typical cell culture conditions were as follows:

Cell lines were maintained in either T25 or T75 flasks (Corning) in the required volume of the respective medium. Cells were split every 3-4 days to ensure confluency did not exceed 90%. Adherent cells were washed with phosphate buffered saline (PBS) prior to trypsinisation. Trypsinisation involved the addition of 3ml of TrypLE Express Enzyme (Life Technologies) and incubation for 2-10 minutes at 37ºC in the incubator. Cells were then washed with the respective medium, centrifuged at 400xg for 5 minutes and re-suspended in the appropriate volume of medium to ensure an efficient split. Cell cultures were maintained at 37ºC with 5% CO_2 within a HERAcell 240i incubator (Thermo Scientific).

Table 2.1: Cell lines used in this study. *(*=Acronym for media used found in Table 2.2)*

Cell Line	Cell Type	Media*	Source / Reference
HEK293FT	Human Embryonal Kidney	D10	Lab collection
Rat1 Fibroblasts	Rodent Fibroblasts	D10	Lab collection
Platinum-E (Plat-E)	Human Embryonal Kidney Retroviral Packaging Cells	D10	Lab collection
Mouse Embryonic Fibroblasts (MEFs)	Murine Embryonic Fibroblasts	D10	Lab collection
5637	Human Bladder Carcinoma	R20	Lab collection
SB1690CB	Human Acute Myeloid Leukaemia	R20 (SB)	Generated by Meyer *et al* [183]

Table 2.2: Cell culture media.

Medium	Composition
D10	440mL Dulbecco's Modified Eagle Medium (DMEM) 1x (Sigma).
	50mL (10%) Fetal Bovine Serum (FBS) (Sigma).
	5mL 200mM L-Glutamine solution (L-G) (Sigma).
	5mL 10,000U/ml-10mg/ml Penicillin-Streptomycin (P/S) (Sigma-Aldrich).
R20	390ml Roswell Park Memorial Institute 1640 Medium (RPMI1640) (Lonza)
	100mL (10%) FBS (Sigma).
	5mL L-G (Sigma).
	5mL P/S (Sigma-Aldrich).
R20 (SB)	345ml RPMI1640 (Lonza)
	100mL (20%) FBS (Invitrogen).
	50mL Conditioned medium obtained from 5637 bladder carcinoma cell line
	5mL L-G (Sigma).
	5mL P/S (Sigma-Aldrich).
	10ng/ml rIL3 (R&D Systems) (added fresh to each culture)
M20	440ml Minimal Essential Medium (MEM) (Gibco)
	50mL (20%) FBS (Sigma).
	5mL L-G (Sigma).
	5mL P/S (Sigma-Aldrich).
SM	131ml RPMI1640 (Lonza)
	15mL (10%) FBS (Sigma).
	4mL 0.5M EDTA (Invitrogen)
XVIVO	X-VIVO10 Medium (Lonza)
XVIVO (Kit)	X-VIVO10 Medium (Lonza)
	Stem cell factor 20ng/mL (Peprotech)
	GM-CSF 10ng/mL (Peprotech)
	Interleukin 6 10ng/mL (Peprotech)
	Interleukin 3 10ng/mL (Peprotech)
OptiMEM	Opti-MEM Reduced Serum Medium (Gibco)
OptiMEM GlutaMax	Opti-MEM Reduced Serum Medium, GlutaMAX Supplement (Gibco)
Freezing Medium (cell lines) (CL)	Respective Medium
	10% dimethyl sulphoxide (DMSO) (AppliChem Panreac).
Freezing Medium (sensitive lines) (SL)	90 % FBS (Sigma).
	10% DMSO (AppliChem Panreac).

2.1.2 Cryopreservation

Cells were centrifuged at 400xg for 5 minutes. Cells were then re-suspended in their respective freezing medium at a density of 1-5x10^6 cells in 1ml in a Nunc cryo-tube (Thermo Fisher Scientific). To achieve slow freezing by Δ1^{o}C/minute, cells were then stored overnight at -80^{o}C using a Mr Frosty Freezing Container (Thermo Scientific). For long term storage cells were transferred to liquid nitrogen or -150^{o}C deep freezing capacity. To thaw cells cryo-tubes (Nunc) were incubated in a 37^{o}C water bath until fully thawed and immediately re-suspended in 5ml of the respective medium pre-warmed in a 15ml Falcon tube. Cells were centrifuged at 400xg for 5 minutes at room temperature and re-suspended in 5ml of the respective medium in a Falcon T25cm^3 flask.

2.1.3 Cell Counting

Cells were homogenised via pipetting prior to counting. 15µl of cell suspension was diluted 1:1 with Trypan Blue 0.4% (Sigma) and pipetted into a haemocytometer (Hawksley) to perform a cell count. Using a DMIL microscope (Leica) cells were counted at 10x magnification. Four quadrants were counted, and the following equation used to calculate cells per ml:

Equation 2.1: *Calculation of cell number using a haemocytometer*

$$Cells\ per\ ml = \frac{number\ of\ cells\ counted}{number\ of\ quadrants\ counted}\ x\ dilution\ factor\ x\ 10^4$$

2.1.4 Microscopy

Cell culture microscopy was performed using a DMIL microscope (Leica) unless stated otherwise. Photography was performed with the same microscope along with a MC170 HD camera (Leica).

2.1.5 Generation of Stable Transduced Cell Lines

2.1.5.1 Lentiviral Production for Rat1 Fibroblast and Mouse Embryonic Fibroblasts Transduction

HEK293FT cells were used to produce lentivirus. Cells were seeded in a T75 plate at 50% confluency in D10 medium the day before transfection. On the day of transfection, 25µg of plasmid DNA in combination with 3.7µg pHCMVG, 5µg pMDLg/pRRE, 3.1µg pRSV-Rev and 37µl FUGENEHD (Promega) was incubated at room temperature for 15minutes in 5ml OptiMEM GlutaMax medium and added dropwise to cells. Further details regarding the plasmids used are outlined below (*Methods 2.2.1*). Cells were incubated overnight at 37ºC. The following day the medium was removed and OptiMEM GlutaMax added with cells incubated at 37ºC overnight. An initial batch of virus was harvested with medium collected, passed through a 0.45µm filter and concentrated by centrifugation using Vivaspin 20 tubes (Sigma-Aldrich). OptiMEM GlutaMax medium was added to the cells, incubated for 24 hours and a second batch of virus harvested as described.

2.1.5.2 Lentiviral Transduction of Rat1 Fibroblast and Mouse Embryonic Fibroblasts

On the day prior to transduction, Rat1 fibroblast or mouse embryonic fibroblasts (MEF) cells were seeded in Opti-MEM medium in a T75 (Corning) to achieve 50% confluency at transduction. On the day of transduction, concentrated lentiviral supernatant was added to the cells in a dropwise manner. Cells were allowed to expand for 4 days prior to FACS GFP+ selection.

2.1.5.3 Selection of GFP+ Rat1 Fibroblasts and Mouse Embryonic Fibroblasts

Transduced cells were sorted by their GFP expression using either the BD FACSAria III or BD Influx (Becton Dickinson) machines with assistance from the

CRUK Manchester centre core facility staff. Prior to sorting, cells were trypsinised, centrifuged at 400xg for 5 minutes and re-suspended in 1ml FACS buffer in 5ml polystyrene tubes (Corning). During the cell sort, cells were first gated on the Forward Scatter (FSC) against Side Scatter (SSC) to select for live cells. Cells were then assessed for GFP expression by excitation with a 488nm laser and measuring emission at 500-20nm. GFP expression at these wavelengths was plotted against emission at 610/20nm to account for any auto-fluorescence. Un-transduced cells were gated as a negative control for GFP expression and transduced cells selected outside this gating. Cells were sorted into 1ml PBS and cultured as normal. Cells were sorted at regular intervals to select for stable transduced cells (*Figure 2.1*). Flow cytometry data was analysed with FlowJo (BD) software.

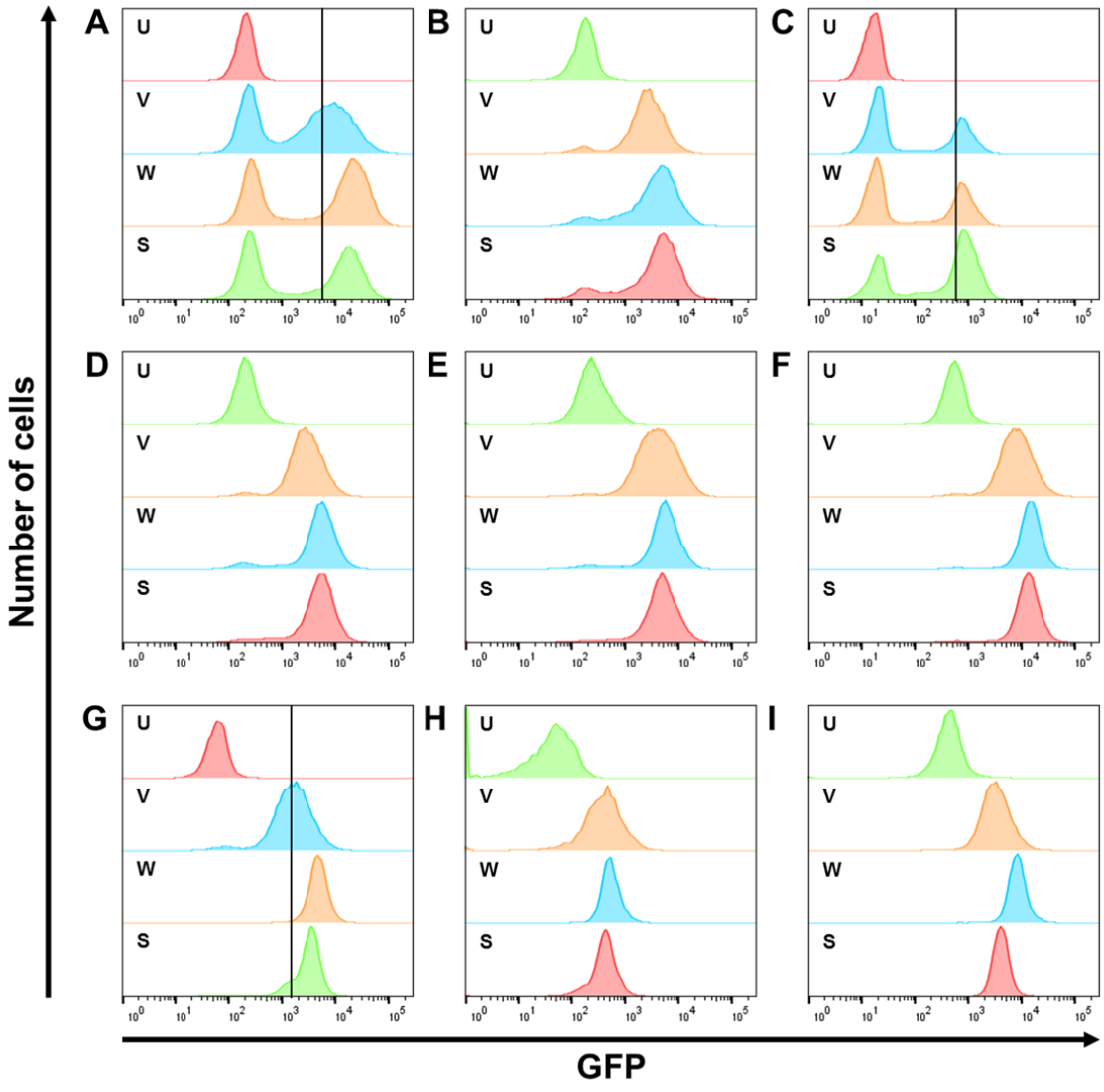

Figure 2.1: Generation of stable transduced Rat1 fibroblast using lentivirus. *Each plot contains four histograms in the order of un-transduced (U), vector (V), EVI1-WT (W) and EVI1-S436A (S) transduced cells (see section 2.2.1)* ***(A)*** *GFP expression during FACS sorting of Rat1 fibroblast transduced with lentivirus.* ***(B)*** *Assessment of GFP expression one week after the initial sort.* ***(C)*** *GFP expression during a second sort two weeks after the initial sort.* ***(D)*** *Assessment of GFP expression two days or* ***(E)*** *one week or* ***(F)*** *two weeks after the second sort.* ***(G)*** *GFP expression during a final sort four weeks after the second sort.* ***(H)*** *Assessment of GFP expression one week or* ***(I)*** *one year after the final sort. The black line through all four histograms indicates gating strategy.*

2.1.5.4 Titration of Lentivirus

Lentiviral supernatant was serially diluted and used to infect Rat1 fibroblast to estimate the number of viral particles per ml of medium (transforming units per ml = TU/ml). Cells were harvested, counted and plated at 25,000 cells per well in a 24-well plate. A total of 250µl of diluted lentivirus was added to 250µl of cells and cells underwent spinoculation at 1250xg for 60 minutes at 32^{o}C. After 24 hours, fresh medium was added to cells. After an additional 24 hours, cells were washed twice with PBS, underwent trypsinisation and re-suspended in 500µl into a 5ml FACS tube. GFP was assessed using a LSRII flow cytometer (BD Biosciences) as described above (*Methods 2.1.5.3*). Viral titre was calculated using the equation below (*Equation 2.2*) with viral titres plotted using GraphPad Prism (*Figure 2.2*).

Equation 2.2: *Calculation of Viral Titre (N = number of cells plated, P = proportion of GFP positive cells, V = volume/concentration of viral supernatant).*

$$\text{Viral titre } ({}^{TU}/_{ml}) = \frac{N \times P}{V}$$

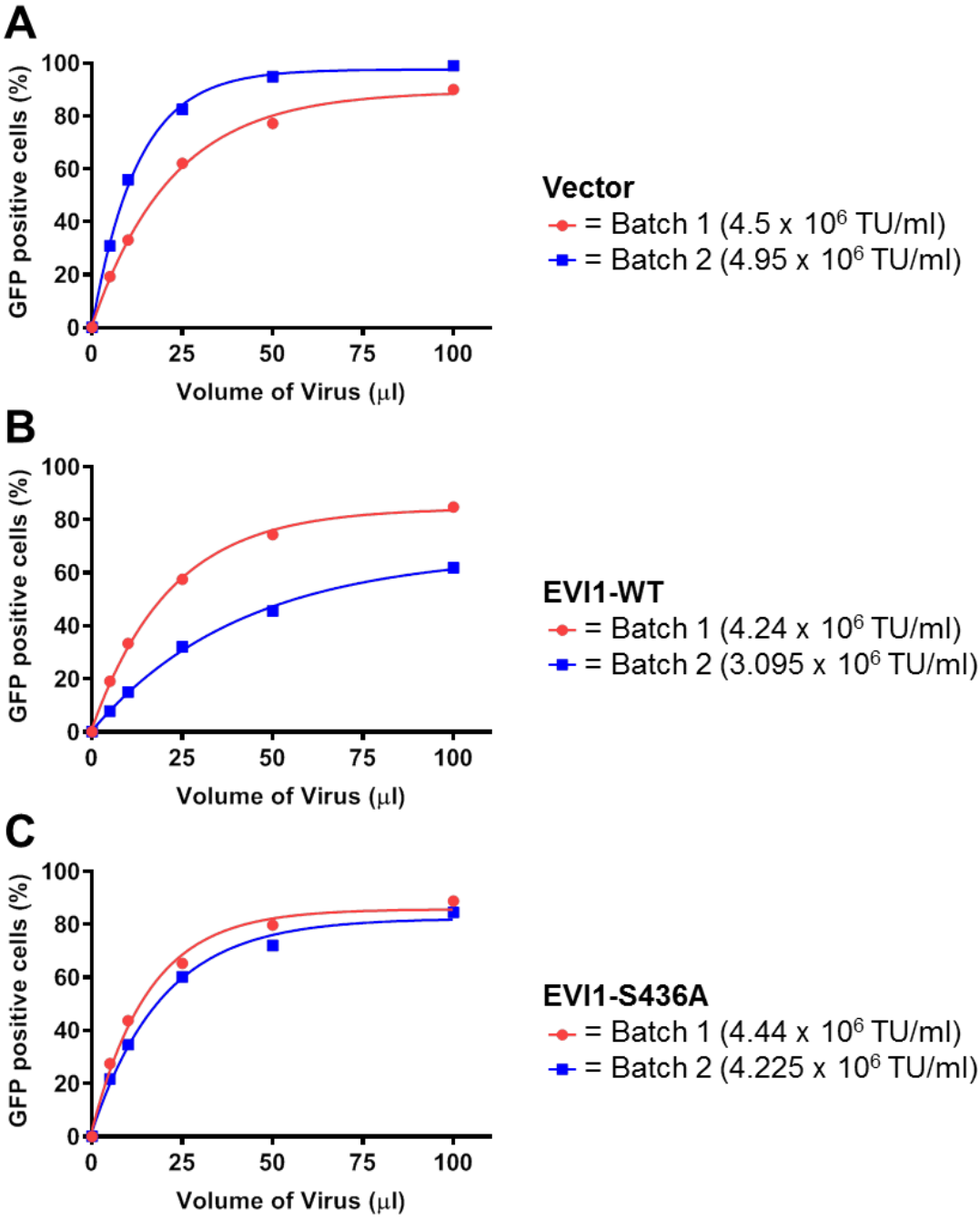

Figure 2.2: Viral titre in Rat1 fibroblast transduced with lentivirus. *The lentivirus from the viral titre was also used to transduce primary murine bone marrow progenitors in the re-plating assay. (**A**) Un-transduced Rat1 fibroblast transduced with lentivirus either batch 1 or two containing pLenti-GFP or (**B**) pLenti-EVI1-WT-GFP or (**C**) pLenti-EVI1-S436A-GFP. Details regarding the plasmids used are outlined in Methods 2.2.1.*

2.1.6 Treatment of Cells

Cells were treated with the compounds listed below (*Table 2.3*). Dilutions were prepared fresh for each experiment.

Table 2.3: Compounds used in the treatment of cells.

Source	Mechanism	[Stock]	Dose / Concentration	Company
Radiation	Generation of Reactive Oxygen Species (ROS)[184]	-	0.5Gy-4Gy	Gulmay Medical Ltd. (320kV x-ray system)
Hydrogen Peroxide	Reactive Oxygen Species (ROS)[185]	30% soln.	10mM-0.1μM	Sigma
Etoposide	DNA Topoisomerase II Inhibitor[70]	10mM	0.1mM-1nM	Selleckchem
Daunorubicin	DNA Topoisomerase II Inhibitor[70]	10mM	0.1mM-1nM	Selleckchem
Cytarabine	Anti-metabolite[71]	150mM	1mM-1nM	Selleckchem
KU-55933	ATM inhibitor[186]	10mM	10μM	Selleckchem
AZD0156	ATM inhibitor[187]	10mM	100μM-1nM	AstraZeneca
AZD1390	ATM inhibitor[188]	10mM	100μM-1nM	AstraZeneca

2.1.7 Drug Titration Assays

Cells were plated in a 96-well plate (Corning) at a density of 1000 cells per 90μl per well. 100μl serum free medium was added to outside wells and plates were incubated overnight at 37ºC. The compound of interest (*Table 2.3*) was diluted in the appropriate solvent to generate a dose response curve. Cells were then diluted in serum free medium and 10μl added to the cells previously plated. Plates were incubated at 37ºC for 72 hours. 10μl of cell proliferation reagent WST-1 (Roche) was added to each well. After 4 hours incubation with wst-1, absorbance was measured on an 800TS microplate reader (BioTek) at 450nm. Wst-1 was used as a marker for cellular proliferation by metabolic activity. Wst-

1 is cleaved to formazan by mitochondrial dehydrogenases. The amount of formazan generated is proportional to the number of metabolically active cells. Formazan has a significantly higher absorbance at 450nm wavelength compared to Wst-1. Therefore, if cells are proliferating, more formazan is generated and there is more absorbance at 450nm.

2.1.8 Analysis of Proliferation by WST-1

The background absorbance was measured at 450nm for subtraction from measurements of samples. Sample values were then normalised to the untreated control (*Equation 2.3*). Molar concentrations were expressed in a log scale. Data was plotted in GraphPad Prism as normalised absorbance value against log concentration of compound. A non-linear progression curve was fit using the log(inhibitor) vs response – Variable slope (four parameters) (*Equation 2.4*). From the non-linear progression curve the half maximal inhibitory concentration (IC50) was derived.

Equation 2.3: *Calculation for the normalisation of 450nm absorbance values.*

$$X = \frac{X - AVERAGE(Plate\ Background)}{AVERAGE(Control - Plate\ Background)} * 100$$

Equation 2.4: *Calculation for IC50 using the log(inhibitor) vs response – Variable slope (four parameters) equation.*

$$Y = \frac{Y(MIN) + (Y(MAX) - Y(MIN))}{1 + 10^{((logIC50 - X) * Hill\ Slope)}}$$

2.1.9 Rat1 Fibroblast and Mouse Embryonic Fibroblast Colony Forming Assay

Cells were trypsinised, counted and re-suspended in D10 medium to prepare a concentration of $1x10^4$ cells per 100µl medium. A total of 100µl cell suspension

was added to a 5ml polystyrene tube (Falcon). Where required, treatment was added as a drop to the other side of the tube. Using a 1mL syringe with a 21G needle (Appleton Woods), 900µl of pre-warmed semi-solid medium Methocult M3231(Stem Cell Technologies) was added to the tube and homogenised with the cell suspension and treatment. The mixture was left to settle until all bubbles had risen. The total volume (1ml) was then divided equally between 3 wells of a 24-well plate (Corning). Cells were incubated for 14 days and number of colonies formed was recorded.

2.1.10 Generation of Transduced Murine Primary Cells

2.1.10.1 Isolation of Primary Murine Bone Marrow Progenitor Cells

Mouse femurs and tibias were cut from 8-10 week old C57/BL6 mice, and excess tissue removed. The femurs and tibias were crushed using a mortar and pestle with 5ml SM Buffer to extract bone marrow cells. Cells were collected with a 19G needle and passed through a 70µm cell strainer to disaggregate cells. Cells were immediately selected for the CD117 (Kit+) marker.

2.1.10.2 Kit+ Selection

Following isolation from the bone, primary murine bone marrow cells were centrifuged at 400xg for 5 minutes then re-suspended in CD117 MicroBeads (mouse) (MACS – Miltenyi Biotec) (diluted 1:5 in SM buffer) and incubated on ice for 15 minutes. Cells were then washed with 1ml SM buffer and filtered using a 0.5µm cell strainer. Cells were again centrifuged at 400xg for 5 minutes and re-suspended 500µL SM buffer in a 5mL polystyrene Falcon tube (Corning). Selection of Kit+ cells was performed on an AutoMACS (Miltenyi Biotec) system using a 4^{o}C pre-cooled filter sterile running buffer (PBS with 2mM EDTA and 0.5%BSA). After selection the cells were centrifuged for a final

time at 400xg for 5 minutes and re-suspended in 4ml XVIVO (Kit) medium and plated into a 6-well plate (Corning).

2.1.10.3 Efficiency of Kit+ Cell Isolation

For quantification of Kit+ cells from bone marrow harvests, cells were centrifuged at 400xg for 5 minutes. Cell were washed in 1ml SM buffer and transferred to a 5ml polystyrene tube. Cells were centrifuged again and re-suspended in 100µl mix of SM buffer and the APC labelled CD117 antibody (Biolegend). Cells were incubated for 30 minutes in the dark prior to flow analysis to allow for antibody binding. Cells were assessed for the Kit marker using a LSRII flow cytometer. Emission was measured at 650-670nm after excitation with a 640nm laser.

2.1.10.4 Lentivirus Production for Transduction of Kit+ cells

HEK293FT cells were used to produce lentivirus. Cells were seeded in a T175 plate at 50% confluency in Opti-MEM medium the day before transfection. On the day of transfection, a mixture of 25µg of plasmid DNA in combination with 3.7µg pHCMVG, 5µg pMDLg/pRRE, 3.1µg pRSV-Rev and 37µl FUGENEHD (Promega) was incubated at room temperature for 15 minutes and added dropwise onto cells. Cells were incubated overnight at 37^{o}C. The following day the medium was removed and XVIVO medium added with cells again incubated at 37^{o}C overnight. The first batch of viral medium was then collected, passed through a 0.45µm filter and concentrated by centrifugation using Vivaspin 20 tubes (Sigma-Aldrich). Medium was added to the cells, incubated for 24 hours and the second batch of virus harvested as described. The lentivirus was produced and used fresh for each transduction.

2.1.10.5 Lentiviral Transduction of Kit+ cells

Harvested Kit+ cells were seeded at $2x10^6$ in 4ml XVIVO (Kit) medium in a 6-well plate (Corning) and incubated for 24 hours. Transduction was performed using 250µl of the first batch of concentrated lentiviral supernatant, 4µg/ml protamine (Sigma) and $5x10^5$ Kit+ cells in 250µl XVIVO (Kit) medium. Cells were infected by spinoculation (1250xg for 60 minutes at 32^{o}C) and incubated overnight at 37^{o}C. The procedure was repeated with the second batch of concentrated lentiviral supernatant and again incubated overnight. Viral supernatant was removed and cells were cultured for an additional 24 hours in X-VIVO (Kit) medium prior to FACS selection of GFP+ cells.

2.1.10.6 Selection of Transduced Kit+ cells

Transduced Kit+ cells were sorted by their GFP expression using either the BD FACSAria III or BD Influx (Becton Dickinson) machines with aid from the CRUK Manchester centre core facility staff. Before selection, transduced Kit+ cells were centrifuged at 400xg for 5 minutes, re-suspended in 500µl XVIVO medium and transferred to 5ml polystyrene tubes (Corning). Cells were then sorted as described above (*Methods 2.1.5.3*) with graphs showing transduction efficiency below (*Figure 2.3*). Cells were sorted into 500µl XVIVO medium.

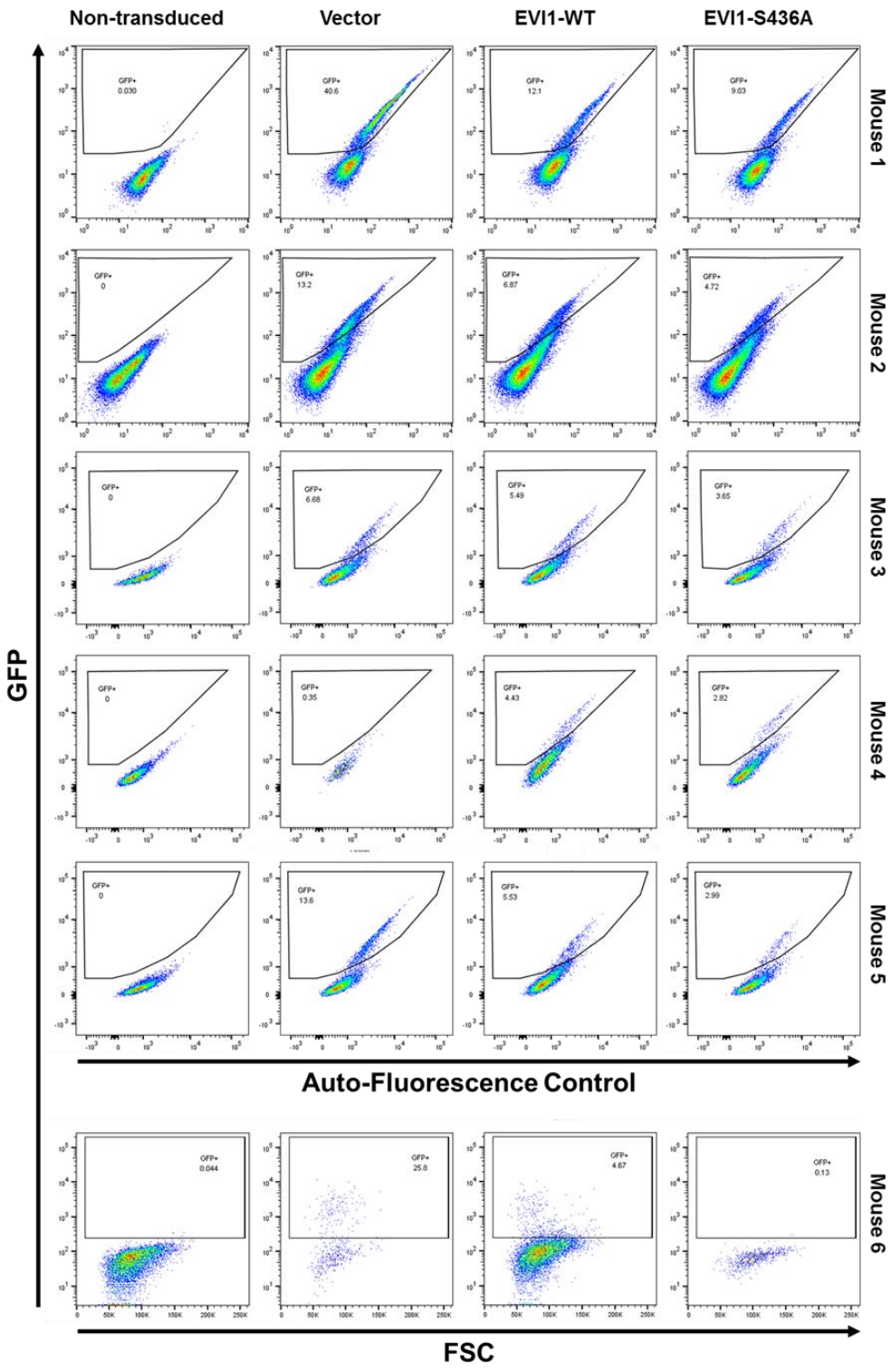

Figure 2.3: Flow-cytometric analysis of EVI1-transduced Kit+ cells. *Representative FACS plots of the gating strategy and GFP positive cells during FACS sorting. Each column of plots represents a transduction status from left to right: Un-transduced, Vector, EVI1-WT and EVI1-S436A transduced cells (See Methods 2.2.1 and Chapter 3.3). The rows represent different mice the Kit+ cells were isolated from. For the majority of mice the GFP was measured against a nearby channel on the FACS sorter to account for any auto-fluorescence of the cells.*

2.1.11 Kit+ Serial Re-Plating Assay

Post GFP+ selection, Kit+ cells were centrifuged at 400xg for 5 minutes, counted and re-suspended in XVIVO medium to give $2x10^4$ cells per 100µl medium. The cell suspension (100µl) was added to a 5ml polystyrene tube (Falcon) with cytokines (*Table 2.2*) added as a droplet to the side of the tube. Where required 1µl of H_2O_2, to a final concentration of 30µM, was added to the other side of the tube (*Figure 2.4*). Using a 1mL syringe with a 21G needle (Appleton Woods), 900µl of pre-warmed semi-solid medium Methocult M3231 (Stem Cell Technologies) was added to the tube and triturated to homogenise the solution. The mixture was left to settle until all bubbles had risen. The volume (1ml) was then divided equally between 3 wells of a 24-well plate (Corning). The remaining wells were filled with 1ml PBS. Plates were incubated for 7 days at 37ºC, after which colonies were counted. Cells were then recovered by addition of 2ml ice cold PBS to each well and the 3 wells per condition were added to a 15ml Falcon tube (Corning). Cells were centrifuged at 400xg for 5 minutes and re-suspended in XVIVO (Kit) medium. Cells were then counted and $2x10^4$ cells were then re-plated. H_2O_2 treated cells were either treated again with H_2O_2 (30µm) for the next re-plating round or left untreated. After the final round of re-plating number of colonies were counted.

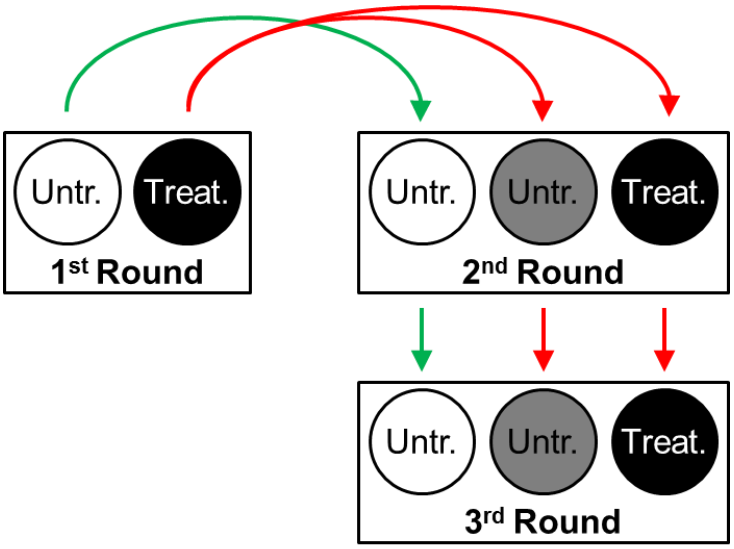

Figure 2.4: Schematic representation of the Kit+ re-plating assay. *Cells that were untreated in round 1 continued to be left untreated for the remainder of the assay. Cells that were treated in round 1 of the assay were then split into two groups for the remainder of the assay: untreated or treated again.*

2.1.12 Cytospin

A total of $2x10^4$ cells were re-suspended in 200µl PBS. These cells were then added to 76x26mm microscopy slides (Academy) with filter paper and a cytospin funnel. These were centrifuged at 800rpm for 5 minutes on a Cytospin 2 (Shandon) machine. Cells were left to air dry and stored until the staining process.

2.1.13 Giemsa Stain

Cytospin slides were fixed in May- Grünwald Q Path (VWR) for 2 minutes and then washed in water. Slides were then stained in Giemsa staining solution (BDH) for 15 minutes and rinsed with water. Cells were then analysed by their morphology according to characteristic features[189–191].

2.1.14 Luciferase Assay

Minimal promoter affinity of EVI1 and EVI1-mutant proteins was assessed by a dual-luciferase reporter assay on the known EVI1 target *PLZF* and *FOS* promoters[192,193]. The vector containing the firefly luciferase (pPLZF-luc or pFOS-luc) is under the control of the *PLZF* or FOS promoter respectively with the vector containing the Renilla luciferase (pRenilla-luc) used as a reference[192,193].

The Dual-Luciferase Reporter Assay System (Promega) was used for this assay. Rat1 fibroblasts were plated in 24-well plate at 50,000 cells per well prior to transfection. The following day, cells were transfected with 100ng pPLZF-luc or pFOS-luc and 10ng pRenilla-luc with FugeneHD in OptiMEM. Cells were incubated for 48 hours. After incubation, medium was removed and cells were washed with x1PBS. Cells were then lysed with 100µl 1x Passive lysis Buffer (PLB) for 15 minutes at room temperature. Once lysed, 20µl PLB was plated per well in triplicate in a 96-well white plate (Greiner-Bio). 100µl of Luciferase assay reagent II (LAR II) was added to each well and the luminescence was measured using a Victor plate reader (Perkin Elmer). Immediately after luminescence was measured, 100µl of Stop and Glo Reagent was added to each well, and plates were again measured for luminescence. To assess promoter repression, the pPLZF-luc or pFOS-luc luminescence measurement was calculated as a ratio to the control pRenilla-luc luminescence measurement with values normalised to the vector control.

2.1.15 Immunofluorescence

Individual methods of mounting were used for different cells. Kit+ cells were isolated and transduced as described above (*Methods 2.1.10.1-5*). Once transduced, cells were incubated for 24 hours at 37^{o}C. After 24 hours incubation, 2.5x10^{4} cells per stain were washed once with phosphate-buffered saline (1x PBS) and re-suspended in X-VIVO medium at 2.5x10^{4} cells per

200µl. Cells were then added to 76x26mm microscopy slides (Academy) with filter paper and a cytospin funnel and spun at 200rpm for 1 minute on a Cytospin 2 (Shandon) machine. Using a PAP pen (Sigma-Aldrich), cells were encircled by a hydrophobic barrier. Rat1 fibroblasts were seeded at a density of $0.5x10^6$ onto 13mm inverted cover glasses (VWR) in 1ml D10 medium in a 24-well plate (Corning) and incubated overnight at 37^{o}C.

All sequential steps were carried out in a humidified chamber. Cells were washed once with 1ml PBS for 10 minutes and then permeabilised with 200µl of 0.1% Triton X-100 in 1x PBS (PBS-T) for 10 minutes at room temperature. Cells were fixed for 10 minutes in 200µl of 2% paraformaldehyde (PFA) in 1x PBS at room temperature. For samples that were assessed for DNA methylation an additional sequence of steps as detailed below was performed. Cells were washed once with 200µl PBS-T for 10 minutes prior to blocking with 200µl of blocking buffer (0.3% Triton X-100 / 5% normal goat serum (Cell Signalling Technology) / 1x PBS) for 1 hour. After blocking, cells were incubated with the appropriate primary antibody (*Table 2.4*) diluted in 200µl antibody dilution buffer (0.3% Triton X-100 / 1% BSA / 1x PBS) for 1 hour at room temperature. Cells were washed twice with 200µl PBS-T for 10 minutes prior to incubation with the appropriate secondary antibody (*Table 2.4*) diluted in 200µl antibody dilution buffer for 1 hour. Cells were washed twice with 200µl PBS-T for 10 minutes. Cells were mounted with Prolong Gold Anti-fade with DAPI (Cell Signalling Technology) and a cover glass. Slides were stored overnight at room temperature in the dark. Cells were stored at 4^{o}C until imaged. Images were acquired using a Retiga 6000 colour camera (Teledyne QImaging) at x100 magnification on a fluorescence microscope (Olympus BX51) powered by a U-RFL-T power supply (Olympus). The analysis of immunofluorescence experiments was performed largely by Dr Roberto Paredes. Reference Regions of interest (ROI) covering the entire positively stained area of the nuclei (DAPI stain) were used to analysed the signal level in the EVI1 and 5-mC stains (50+ cells per condition). The integrated density was determined by using the ImageJ software. To discard signal saturated ROIs, the images were analysed using HiLo intensity look up table (LUT). Dispersion plot (XY plot) were created in

GraphPad prism and Pearson coefficients were calculated to asses signal correlation (free open source Social Science Statistics).

For cells for which DNA methylation was assessed the following steps were performed: After fixation, cells were washed once with 200µl PBS-T for 10 minutes. Cells were denatured for 10 minutes with 200µl of 2N hydrochloric (HCl) acid in 1x PBS in a 37 °C incubator, then neutralised with 200µL of 0.1M Tris-HCl (pH 8.3) for 10 min at room temperature.

Table 2.4: Antibodies used for Immunofluorescence.

Antibody	**Host**	**Catalogue Number**	**Company**
DNMT3a (A-10)	Mouse	SC-373905	Santa Cruz Biotechnology
Anti 5-Methylcytidine	Mouse	MCA2201	Bio-Rad
EVI1 (C50E12)	Rabbit	2593S	Cell Signalling Technology
p-ATM (Ser1981)	Mouse	MA1-2020	Invitrogen
yH2AX	Rabbit	9718	Cell Signalling Technology
F(ab')2-Goat anti-Rabbit IgG (H+L) Cross-Adsorbed Secondary Antibody, Alexa Fluor 594	Goat	A11072	Invitrogen
Goat anti-Mouse IgG (H+L) Highly Cross-Adsorbed Secondary Antibody, Alexa Fluor 594	Goat	A11032	Invitrogen
Goat anti-Rabbit IgG (H+L) Highly Cross-Adsorbed Secondary Antibody, Alexa Fluor 488	Goat	A11034	Invitrogen

2.2 DNA

2.2.1 Generation of Plasmids

To study human EVI1 in overexpression experiments, the C-terminal FLAG-tagged vector under the control of a CMV promoter was used (*Table 2.5*). The plasmid pCMV-hEVI1-FLAG was previously generated by Dr Marion Schneider[131] (*Figure 2.5*). Here the pCMV-FLAG-5a (Sigma) (pCMV-FLAG) was used as a vector control (*Figure 2.5*). Site-directed mutagenesis of pCMV-hEVI1-FLAG to generate a non-phosphorylated and non-phosphorylatable hEVI1-S436A mutant is outlined in *Methods 2.2.12* (*Figure 2.5*).

For the study of EVI1 in a murine model, the lentiviral vector containing mEVI1co-IRES-eGFP was used (*Table 2.5*). The lentiviral pRRL.PPT.SF.mEVI1co.IRES.EGFP.pre plasmid (pLenti-mEVI1co-WT-GFP) (*Figure 2.6*) (gift from Professors Axel Schambach, Christoph Baum and Dr Olga Kustikova, Hanover[41,112]) contains a codon optimised EVI1 construct. The vector control (pLenti-GFP) was generated by Dr Marion Schneider through excision of the mEVI1co insert using the BamHI restriction site (*Figure 2.6*). Dr Marion Schneider also generated the mEVI1co-AQA mutant by site-directed mutagenesis (*Figure 2.6*) (*See Chapter 3.1*). For methods of site-directed mutagenesis to create the plasmid encoding mEVI1co-S436A construct (*Figure 2.6*) see Methods *2.2.12* (*See Chapter 3.3*).

The third-generation viral packaging plasmids were a gift from Dr Henri van de Vrugt, Amsterdam (*Table 2.5*) (*Figure 2.7*).

Table 2.5: Plasmids used throughout this Thesis.

Plasmid	Encoding	Source
pCMV-FLAG	C-FLAG	Sigma
pCMV-hEVI1-FLAG	C-FLAG Human EVI1	Generated by Dr Marion Schneider[131]
pCMV-hEVI1-AQA-FLAG	C-FLAG Human EVI1-AQA	Generated by Dr Marion Schneider[131]
pCMV-hEVI1-S436A-FLAG	C-FLAG Human EVI1-S436A	Generated by Dr Roberto Paredes[131]
pCMV-hDNMT3a-HA	N-HA Human DNMT3a	Generated by Dr Roberto Paredes
pRRL.PPT.SF.mEVI1co.IRES.EGFP.pre	Mouse codon optimised EVI1 -IRES-GFP	Gift from Kustikova[41,112]
pRRL.PPT.SF.IRES.EGFP.pre	IRES-GFP	Generated by Dr Marion Schneider[131]
pRRL.PPT.SF.mEVI1-AQAco.IRES.EGFP.pre	Mouse codon optimised EVI1-AQA-IRES-GFP	Generated by Dr Marion Schneider[131]
pRRL.PPT.SF.mEVI1-S436Aco.IRES.EGFP.pre	Mouse codon optimised EVI1-S436A-IRES-GFP	Thesis
pMD2.VSVg	VSVg envelope protein	Gift from Dr Henri van de Vrugt
pRSV-REV	REV protein	Gift from Dr Henri van de Vrugt
pMDLgpRRE	Viral polymerase Pol	Gift from Dr Henri van de Vrugt
pPLZF-luc	PLZF-firefly	Gift from Takashi[192]
pRenilla-luc	Renilla	Gift from Takashi[192]

2.2.1.1 Plasmid Maps

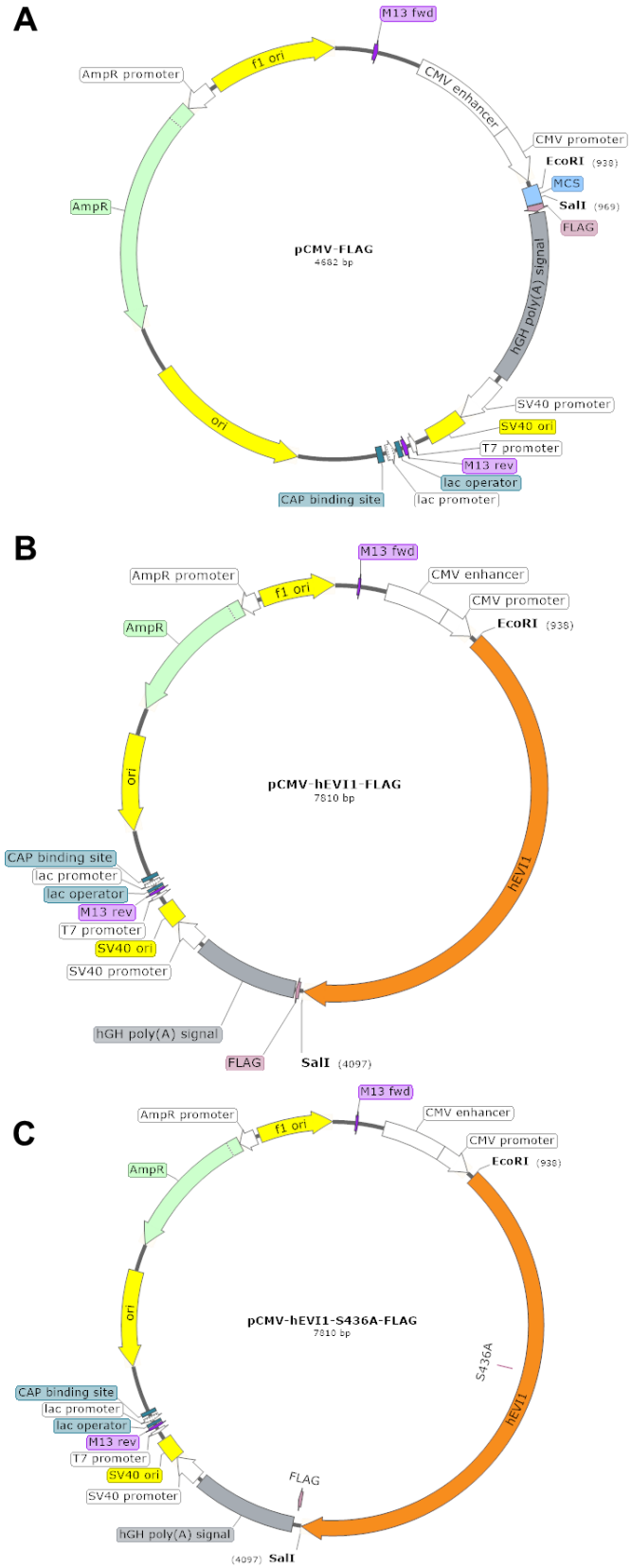

Figure 2.5: Plasmid Maps of the FLAG expression vectors. ***(A)*** *pCMV-FLAG was used as the backbone vector for EVI1-FLAG and used a vector control.* ***(B)*** *pCMV-hEVI1-FLAG plasmid*

encoding a C-terminal FLAG-tagged human EVI1 construct. The restriction sites EcoRI and SalI were used for cloning. This plasmid was generated by Dr Marion Schneider. ***(C)*** *pCMV-hEVI1-S436A-FLAG plasmid encoding the non-phosphorylated and non-phosphorylatable C-terminal FLAG-tagged human EVI1-S436A mutant construct. This plasmid was generated by site directed mutagenesis of pCMV-hEVI1-FLAG at 436aa (serine).*

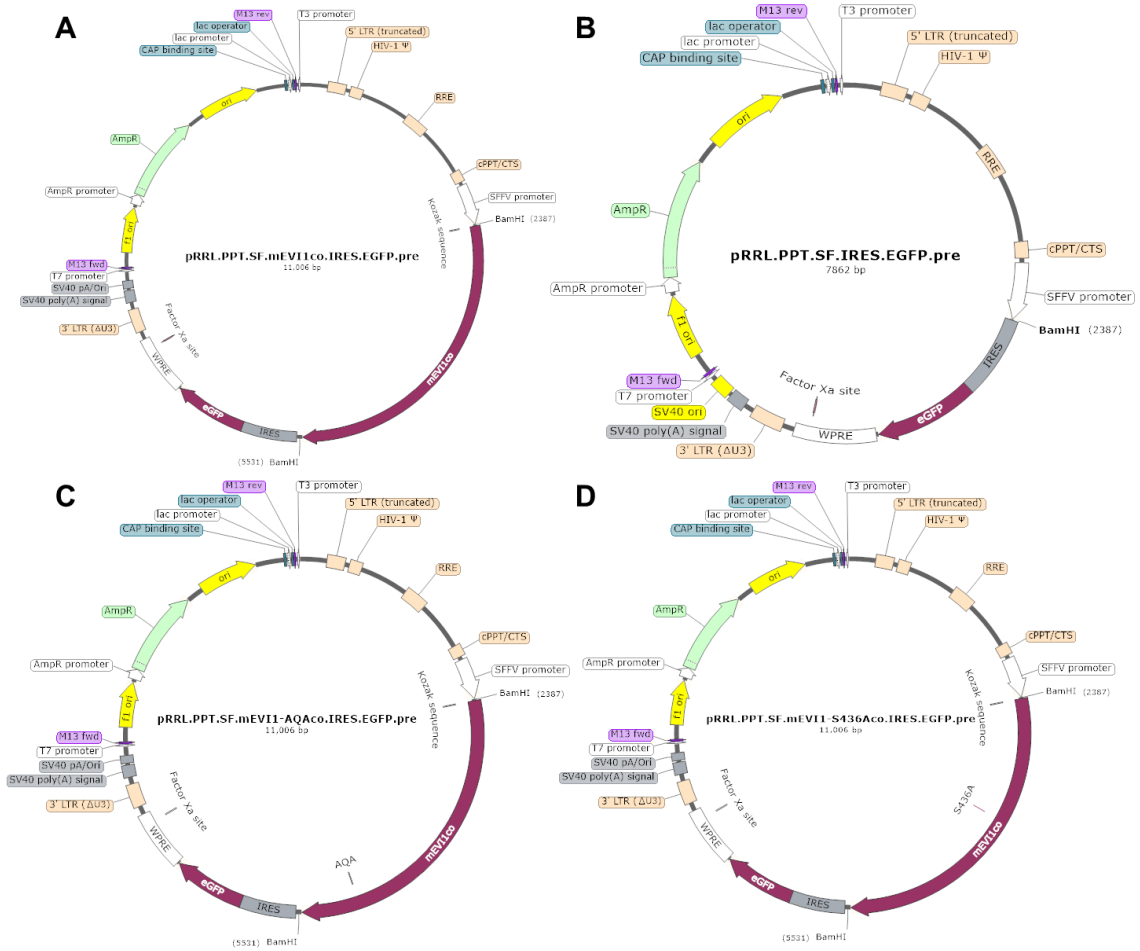

Figure 2.6: Plasmid Maps of the third generation lentiviral IRES-GFP expression vectors. ***(A)*** *pRRL.PPT.SF.mEVI1co.IRES.EGFP.pre plasmid encoding the codon optimised mouse EVI1 transcript with an IRES-GFP sequence.* ***(B)*** *pRRL.PPT.SF.IRES.EGFP.pre plasmid encoding the IRES-GFP sequence. This plasmid was used a vector control. The restriction site BamHI was used to excise the mEVI1co construct during cloning to generate the vector control.* ***(C)*** *pRRL.PPT.SF.mEVI1-AQAco.IRES.EGFP.pre plasmid encoding the non-phosphorylated and non-phosphorylatable EVI1-AQA mutant. This plasmid was generated by site directed mutagenesis of the 858/860aa SQS site. These plasmids were generated by Dr Marion Schneider.* ***(D)*** *pRRL.PPT.SF.mEVI1-S436Aco.IRES.EGFP.pre plasmid encoding the non-phosphorylated and non-phosphorylatable EVI1-S436A mutant. This plasmid was generated by site directed mutagenesis of pRRL.PPT.SF.mEVI1co.IRES.EGFP.pre at 436aa (serine).*

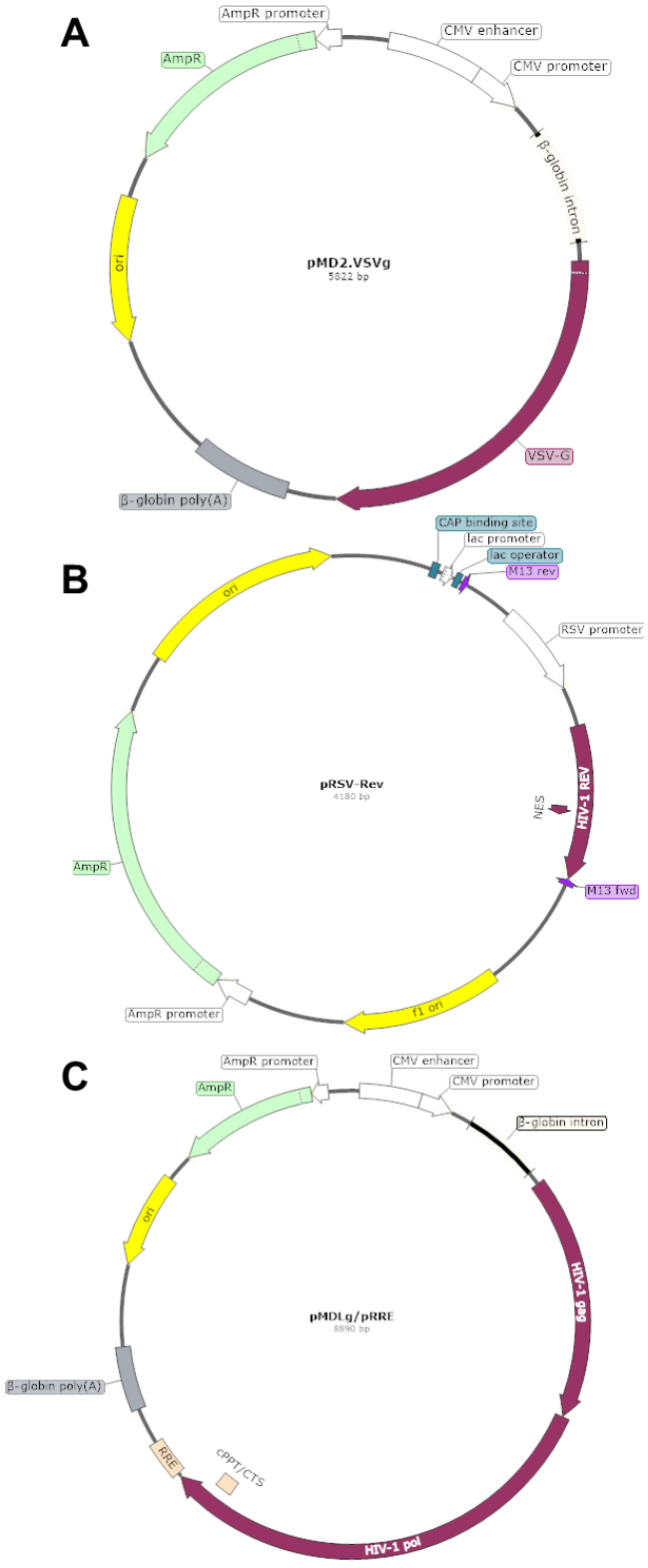

Figure 2.7: Plasmid Maps of the lentiviral packaging plasmids. (A) *pMD2.VSVg plasmid encoding for VSVg envelope protein under a CMV promoter.* ***(B)*** *pRSV-REV plasmid encoding REV protein under a RCV promoter.* ***(C)*** *pMDLgpRRE plasmid encoding Gag structural protein and the viral polymerase Pol under a CMV promoter. All plasmids carry an ampicillin resistance gene.*

2.2.2 Transformation of Bacteria

NEB (New England BioLabs) Stable High Efficiency E.coli was used for all bacterial transformations and thawed for 10 minutes on ice prior to use. A total of 50ng of plasmid was added to 50µl bacteria and incubated on ice for 30 minutes. Bacteria were then heat shocked at 42ºC for 30 seconds in a water bath (Grant) and placed on ice for 5 minutes. 950µl SOC medium (New England BioLabs) was added and cells were shaken horizontally at 30ºC for 1 hour. Cells were then spread at a 10:90 ratio onto LB ampicillin Agar plates (pre-warmed at 30ºC for 1 hour) and incubated at 30ºC overnight.

2.2.3 Plasmid Isolation from Transformed Bacteria

To isolate the desired plasmid a colony from the respective plate was added to 5ml LB broth supplemented with 100µg/ml ampicillin (Sigma) and incubated at 37ºC 250rpm overnight. The culture was then transferred to 250ml LB broth with 100µg/ml ampicillin in a 1L Erlenmeyer flask and incubated at 37ºC 250rpm overnight. Bacterial cultures were centrifuged at 5000rpm at 4ºC for 30 minutes and plasmid extracted by column purification using the EndoFree Plasmid Maxi Kit (Qiagen).

2.2.4 DNA Quantification

DNA quantification was performed using the Nanodrop200c Spectrophotometer (Thermo Scientific) measuring content in 1µl solution. The 260/280nm and 260/230nm ratios were monitored to ensure purity.

2.2.5 Sanger Sequencing

Sanger sequencing was carried out by CRUK Manchester centre core facility staff using an ABI 3130XL Capillary Sequencer (Applied Biosystems). Primers used for sequencing are outlined in the table below (*Table 2.6*). 300ng DNA or plasmid DNA was added with 15pmol of single primer to a final volume of 20µl ddH_2O. Sequence results were analysed using Sequence Scanner 2 (Applied Biosystems) software and BLAST (Basic Local Alignment Search Tool, National Library of Medicine).

Table 2.6: Sequencing Primers.

Target Sequence (bp)	Transcript	Primer (Pair)
1134 - 1559	mEVI1co	5'-CACTGGAGAAGATCAGCGAC-3' 5'-GTGGCTCCATCTTCAGTGGC-3'
2387 - 2703	mEVI1co	5'-GAAGAAGCACGAGAACGGCA-3' 5'-TCTGGGATCTCCTCGTCCAG-3'
- 149	mEVI1co	5'- GCTCTCGCTCTCCAGGTTC-3'
294 -	mEVI1co	5'- CTGCACCGGAAGAGCAAGAG-3'
1 - 500	hEVI1	5'- GCGAAGACTATCCCCATGAAAC-3' 5'-TGGATCGTGTGTATCTCTTGGA-3'
2479 - 3155	hEVI1	5' ACGGCTGCTTAAGTTCCTCT-3' 5'-GCACTTCACAGATAGCCTCA-3'

2.2.6 Polymerase Chain Reaction (PCR)

For cloning with incompatible restriction sites between vectors, PCR was required. Primers were designed to amplify the insert (*Table 2.7*). Additionally, these primers encoded restriction sites that were compatible with the recipient plasmid. For cloning involving a mismatch of restriction sites in the insert-plasmid and the recipient- plasmid, PCR of the insert with primers containing compatible restriction sites was required.

PCR was performed using Q5 High Fidelity DNA polymerase (New England Biolabs). The volumes and concentrations of the reagents used, along with cycle information, in a typical experiment listed in tables below (*Table 2.8 and 2.9*). PCR reactions were run in a PCR thermocycler (MJ Mini, Bio-Rad). PCR reactions were column purified using the Qiaquick PCR Purification Kit (Qiagen).

Table 2.7: PCR reaction mix.

Reagent	**Volume (µl)**	**Concentration**
5x Q5 Reaction Buffer	5	1x
10mM dNTPs	0.5	200µM
Forward Primer (10µM)	1.25	0.5µM
Reverse Primer (10µM)	1.25	0.5µM
Template DNA	variable	<1000ng
Q5 High Fidelity DNA polymerase	0.25	0.02U/µl
5x Q5 High GC enhancer	5	1x
Nuclease-free water	to 25	

Table 2.8: PCR cycle program.

Steps	**Initial Denaturation**	**Denaturation**	**Anneal**	**Elongation**	**Final Elongation**
		x30-35			
Temperature (^{o}C)	98	98	50-72	72	72
Time (s)	30	5-10	10-30	20-30/kb	120

Table 2.9: PCR Primers.

Insert Amplified	Insert Plasmid	Restriction Sites	Recipient Plasmid	Primer Pair (5'-3')
Human EVI1-WT	pCMV-EVI1-FLAG	AscI PacI	pCMV-3xHA	TAATGGGCGCGCCATATGAAGAGCGA AGACTATCCC GGCCGCTTAATTAAGGTCATACGTGG CTTATGGACTG
Human EVI1-WT	pCMV-EVI1-FLAG	AscI PacI	pCMV-3xFLAG	TAATGGGCGCGCCATATGAAGAGCGA AGACTATCCC GGCCGCTTAATTAAGGTCATACGTGG CTTATGGACTG
Human ΔEVI1	pCMV-ΔEVI1-FLAG	AscI PacI	pCMV-3xHA	TAATGGGCGCGCCATATGAAGAGCGA AGACTATCCC GGCCGCTTAATTAAGGTCATACGTGG CTTATGGACTG
Human ΔEVI1	pCMV-ΔEVI1-FLAG	AscI PacI	pCMV-3xFLAG	TAATGGGCGCGCCATATGAAGAGCGA AGACTATCCC GGCCGCTTAATTAAGGTCATACGTGG CTTATGGACTG
Human ΔEVI1	p50MΔ324-neo	EcoRI SalI	pCMV-FLAG	ATCGTGTCGACTACGTGGCTTATGGA CTGGAT ATGCTGAATTCATGAAGAGCGAAGACT ATCCC

2.2.7 Restriction Digests

Restriction digests were performed when the plasmid containing the desired insert and the recipient plasmid both had compatible restriction sites. Digests were performed using the appropriate New England Biolabs enzyme with a typical reaction outlined in the table below (*Table 2.10 and 2.11*). All incubations were carried out at 37^{o}C.

Table 2.10: Restriction digest reaction mix.

Reagent	Volume
Restriction Enzyme	1 µl
DNA	1 µg
10x NEBuffer	5 µl
Total Reaction Volume	50 µl

Table 2.11: Restriction enzymes used.

Enzyme (s)	Heat Inactivation (°C)	Insert Plasmid(s)	Insert(s) Excised	Recipient Plasmid	Resulting Plasmid
SacII	65°C	pCMV-3xHA-Reptin	Reptin	X	pCMV-3xHA
AscI PacI	80°C	pCMV-3xFLAG-Pontin	Pontin	X	pCMV-3xFLAG
AscI PacI	80°C	pCMV-hEVI1-FLAG (PCR)	hEVI1	pCMV-3xHA-Reptin	pCMV-3xHA-hEVI1
AscI PacI	80°C	pCMV-hEVI1-FLAG (PCR)	hEVI1	pCMV-3xFLAG-Pontin	pCMV-3xFLAG-hEVI1
AscI PacI	80°C	pCMV-hΔEVI1-FLAG (PCR)	hΔEVI1	pCMV-3xHA-Reptin	pCMV-3xHA-hΔEVI1
AscI PacI	80°C	pCMV-hΔEVI1-FLAG (PCR)	hΔEVI1	pCMV-3xFLAG-Pontin	pCMV-3xFLAG-hΔEVI1
EcoRI SalI	65°C	p50MΔ324-neo	hΔEVI1	pCMV-FLAG	pCMV-ΔEVI1-FLAG

2.2.8 Agarose Gel Electrophoresis

To analyse restriction digests and PCR reactions, DNA fragments were separated by electrophoresis using agarose gels (mobility determined by size, charge and conformation). Gels were made to concentrations of 0.8-2% (w/V) using agarose (Sigma) in 1x TAE buffer (40mM Tris, 20mM acetic acid and 1mM EDTA (Sigma)). This mixture was then heated in a microwave until the agarose had completely dissolved. GelRed Nucleic Acid Stain (Biotium) was

then added to visualise the DNA once the gel had cooled sufficiently. The mixture was then poured into a gel tank (Scotlab) with the appropriate comb and allowed to set. Once the gel had set, TAE buffer was added to the tank. Samples and DNA Molecular Wight Marker XIV, 100 base pair ladder (Roche) were loaded into their respective wells. Electrophoresis was then performed for 120 minutes at 80V. Once complete, gels were analysed using the ChemiDoc XRS Bioanalyzer (Bio-Rad) with UV light.

2.2.9 Gel Extraction from Agarose Gel

The band of interest was visualised using UV light on ChemiDoc XRS Bioanalyzer (Bio-Rad) and cut from the gel using a scalpel (Swann-Morton). DNA was then isolated from the gel by column purification using the Qiaquick Gel Extraction Kit (Qiagen).

2.2.10 Blunting

For cloning that requires blunting for incompatible restriction sites, the Quick Blunting Kit (New England BioLabs) was used. The purified DNA was incubated at room temperature for 30 minutes with the reaction mix outlined below (*Table 2.12*). Immediately after incubation the reaction mix was heated at 70^{o}C for 10 minutes to inactivate the blunting enzyme. Following blunting, inserts and backbone vectors underwent ligation.

Table 2.12: Quick Blunting reaction mix.

Reagent	**Volume (µl)**
10x Blunting Buffer	2.5
1mM dNTP Mix	2.5
Blunt Enzyme Mix	1
Purified DNA (up to 5µg)	to 25
Sterile dH_20	to 25

2.2.11 Ligation

Ligation of the insert into the respective vector backbone was performed using T4 DNA Ligase (New England BioLabs). Typical reaction is outlined in the table below (*Table 2.13*). Reactions were incubated overnight at 16ºC in a PCR thermocycler (MJ Mini, Bio-Rad). Following incubation, reactions were heat-inactivated at 65ºC for 10 minutes and sequentially transformed into competent bacteria as outlined above (*Methods 2.2.2*).

Table 2.13: Ligation reaction mix.

Reagent	Volume	Concentration
T4 DNA Ligase Buffer (10x)	2 µl	1x
Vector DNA (4kb)	50 ng	0.020pmol
Insert DNA (1kb)	37.5 ng	0.060pmol
T4 DNA Ligase	1 µl	-
Nuclease-free water	to 20 µl	

2.2.12 Site-Directed Mutagenesis

Site-directed mutagenesis was performed by amplification with mutagenesis primers and subsequent degradation of parent vector by methylation status using the QuikChange XL Site-Directed Mutagenesis Kit (Agilent) (*Table 2.14 and 2.15)*. Primers used to generate pCMV-hEVI1-S436A-FLAG and pLenti-EVI1-S436A-GFP are listed below (*Table 2.16*). Serine 436 in the human construct or serine 426 in the murine construct were substituted for alanine to mimic non-phosphorylatable and non-phosphorylated EVI1. Mutations were confirmed by Sanger sequencing (*Methods 2.2.5*) (*Figure 2.8*). Plasmids generated by site-directed mutagenesis were pCMV-hEVI1-S436A-FLAG and pLenti-mEVI1co-S436A-GFP.

Table 2.14: Mutagenesis reaction mix.

Reagent	Volume (µl)	Concentration
10× reaction buffer	5	1x
Template DNA	variable	10ng
Forward Primer	variable	125ng
Reverse Primer	variable	125ng
dNTP	1	-
QuikSolution	3	
PfuTurbo DNA polymerase	1	2.5U/µl
ddH_2O	to 50	

Table 2.15: Thermal cycler program.

Step	Cycles	Temperature (°C)	Time (s)
1	1	95	60
2	18	95	50
		60	50
		68	60/kb of plasmid length
3	1	68	420

Table 2.16: Mutagenesis primers.

Site (a.a)	Amino Acid Change	Transcript	Primer Pair (FW) (RV)
426	Serine to Alanine	mEVI1co	5'-CAGGTTCTGCAGGGGGGCGACTTTGTCCTTGAACA-3' 5'-TGTTCAAGGACAAAGTCGCCCCCCTGCAGAACCTG-3'
436	Serine to Alanine	hEVI1	5'-GGTAAAATGTTCAAAGACAAAGTAGCCCCTCTTCAGAATCTGGC-3' 5'-GCCAGATTCTGAAGAGGGGCTACTTTGTCTTTGAACATTTTACC-3'

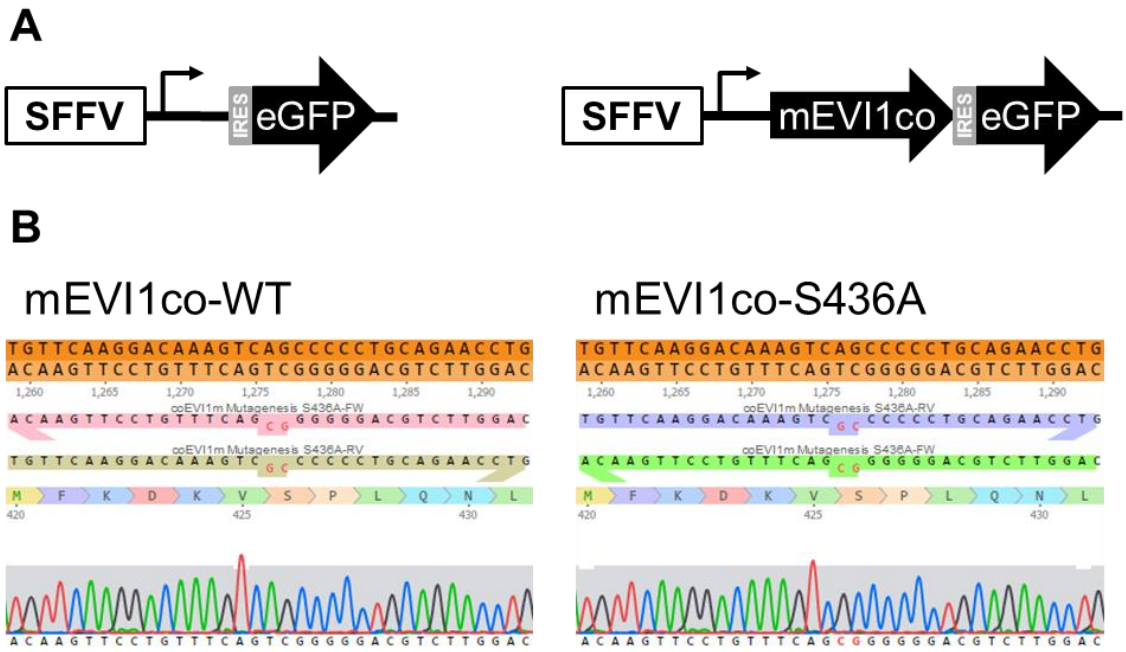

Figure 2.8: Confirmatory sequencing of site-directed mutagenesis for the S436A mutation. (A) *Schematic representation of the lentiviral IRES-eGFP vectors. The expression of the codon optimised murine EVI1 (mEVI1co) is under the control of the SFFV promoter. The plasmid contains an internal ribosomal entry site (IRES) that joins mEVI1co and eGFP to maintain equal expression. The plasmid containing no mEVI1co was used as a vector control.* ***(B)*** *Sanger sequencing results of mEVI1co-WT and mEVI1co-S436A confirming successful site-directed mutagenesis.*

2.3 RNA

2.3.1 qPCR

2.3.1.1 RNA isolation

Cells centrifuged at 400xg for 5minutes and washed with ice cold PBS. Cell pellets were either immediately stored at -80^{o}C or processed using the Qiagen RNeasy extraction kit (Qiagen). RNA was eluted in 30µl RNase free water.

2.3.1.2 RNA quantification

RNA quantification was performed using the Nanodrop200c Spectrophotometer (Thermo Scientific) measuring content in 1µl solution. The 260/280nm and 260/230nm ratios were monitored for purity.

2.3.1.3 cDNA Synthesis

For cDNA synthesis the amount of RNA used was dependent on the sample with the lowest RNA concentration in the experiment. The Transcriptor First Strand cDNA Synthesis Kit (Roche) was used for cDNA synthesis by reverse transcriptase. The reaction was performed in two steps. The reagents and PCR conditions and the setting for each step are outlined below (*Tables 2.17 and 2.18*). For consistency throughout the experiment, a master mix was made for all samples. A sample without reverse transcriptase was used as a control to monitor DNA contamination. cDNA was quantified used Qubit technology. cDNA was stored at -20^{o}C once synthesised.

Table 2.17: Reverse Transcription reaction mix.

Component	Volume (µl)	Concentration	Step
total RNA	variable	Up to 1µg	1
Anchored-oligo(dT) primer (50 pmol/µl)	1	2.5µM	
Random hexamer primer (600 pmol/µl)	2	60µM	
Water, PCR-grade	to 13		
5x Transcriptor Reverse Transcriptase Reaction Buffer	4	1x (8 mM MgCl2)	2
Protector RNase Inhibitor (40 U/µl)	0.5	20 U	
Deoxynucleotide Mix (10 mM)	2	1 mM	
Transcriptor Reverse Transcriptase (20 U/µl)	0.5	10 U	

Table 2.18: Reverse Transcription cycle program.

Step		Temperature (°C)	Duration (minutes)
1	Denaturation	65	10
2	Primer Extension	25	10
	cDNA synthesis	50	60
	Inactivation	85	5

2.3.1.4 Qubit Quantification of cDNA

cDNA was quantified using fluorescent dyes as part of the Qubit dsDNA HS Assay Kit (Invitrogen).

2.3.1.5 Quantitative Real-Time PCR (RT-qPCR)

All qPCR was performed in a MicroAmp Optical 384-well reaction plate (applied Biosystems) on a QuantStudio 5 Real-Time PCR System (Applied Biosystems). Plates were prepared in a UV PCR Workstation (UVP) using a Finnpipette (Thermo Scientific) in 3 technical replicates. TaqMan Fast Advanced Master Mix (Applied Biosystems) was used with reaction volumes, cycle details and primers as listed below (*Table 2.19, 2.20 and 2.21*). All primers were designed using the

Roche primer design online tool and validated by assessment of primer efficiency prior to use. Results were analysed using QuantStudio Design and Analysis (Thermo Fisher Scientific) software. To analyse the relative mRNA expression the ΔΔCt method was used[194] (*Equation 2.5*).

Equation 2.5: *Calculations for the ΔΔCt to analyse relative mRNA expression. Ct = threshold cycle.*

$$\Delta Ct = Ct(\text{target gene}) - Ct(\text{reference gene})$$
$$\Delta\Delta Ct = \Delta Ct(\text{sample}) - \Delta Ct(\text{control})$$
$$\text{Fold change} = 2^{-(\Delta\Delta Ct)}$$

Table 2.19: TaqMan qPCR reaction mix.

Components	**Volume (µl)**
TaqMan Fast Advanced Master Mix (Applied Biosystems)	5.5
Primer Pair Mix (2pmol per primer)	0.5
Roche Universal Probe (Roche) (1pmol)	0.25
cDNA (2ng/well)	to 4.75
Nuclease-free water	to 4.75

Table 2.20: TaqMan qPCR cycle program.

Step	**Hold Stage**		**PCR Stage**	
			40 cycles	
Temperature (°C)	50	95	95	60
Time (s)	120	120	1	20

Table 2.21: Primers for Taqman RT-qPCR.

Gene	Primer Pair (FW) 5'-3' (RV) 3'-5'	Roche Universal Probe
ALDOC	GGATCAGAACCCGAGCTGT TACGAGTGAGGCATGGTGAC	5
ABCD2	TGTCCATCTCTATCACATAGTTCAAA ACAGGACATCTTTCCAGTCCA	8
ADRGB2	AGCCACTGGAACCCCATC TTTTTCAGCAGCAAAATCCAC	23
HYDIN	TGGCGCTCTTAATTACAGCAA GCCCAAAGTCCACCTCTGTA	39
MOV10	ACCTGGGACCCTGTGGAC CGGCTCTCAGTCACTCCAG	64
SETX	TTTTTCCCTTTGATGGTATTGAA CTATTTGGAGAGTTGAGCCATTC	59
TMEM222	CCTGCTCTACGGGAAGTACG TGATGCCCAGGAGAAGGAT	71
TOM1L1	CCAGAAGGAAGCCACCAATA TGGGACTTAGGTCGAGGAGA	29
βACTIN	CCAACCGCGAGAAGATGA CCAGAGGCGTACAGGGATAG	64
YWHAZ	GATCCCCAATGCTTCACAAG TGCTTGTTGTGACTGATCGAC	30
EVI1	AGTGCCCTGGAGATGAGTTG TTTGAGGCTATCTGTGAAGTGC	64

2.3.2 RNA Sequencing and Analysis

To assess the effects of EVI1 phosphorylation on transcriptional regulation, two separate RNA-sequencing (RNA*seq*) experiments were carried out. To investigate the effect of genotoxic stress on EVI1-mediated gene expression, Dr Roberto Paredes transfected HEK1239FT cells with either EVI1-WT, EVI1-AQA or the vector-only control (*See Chapter 3.1.3*). Genotoxic stress was induced by treatment with 150μM H_2O_2 for 8 hours with RNA isolated as described above (*Methods 2.3.1.1*).

RNA*seq* was carried out by CRUK Manchester centre core facility staff. Libraries were prepared with the Lexogen QuantSeq 3′ mRNA-Seq Library Prep Kit for Illumina (FWD) using an input of 200 ng and performing 14 cycles of amplification. Indexed libraries were then quantified using the Kapa Illumina Library quantification kit (Cat. 07960336001) and pooled. 1 × 75 bp sequence reads were generated by clustering 2.0 pM of the library pool on a NextSeq500 High throughput run. Ordered BAM files were generated against the human genome feature file Homo_sapiens.GRCh38.90.gtf downloaded from Ensembl (ftp://ftp.ensembl.org/pub/current_gtf)[195].

Data analysis of this experiment was performed by Dr Adam Stevens using Qlucore Omics Explorer 3.3 (Qlucore, Lund, Sweden) with a FPKM (Fragments Per Kilobase Million) cut-off of 10. To identify significant differentially regulated transcripts, RNA*seq* expression data analysis was carried out by applying a group ANOVA with $p < 0.01$ to the entire dataset. For illustration of the comparisons between the effect on transcription with EVI1-WT and EVI1-AQA in relation to untransfected cells and empty vector-transfected control cells with and without DNA damage, values were normalized to the mean of 0 and a variance of one. In addition, differences between expression levels at individual conditions were assessed by two group comparison (t-test).

To assess effects of EVI1 transduction on transcription in Kit+ cells (*Figure 2.9*) (*see Chapter 3.3.3*), Kit+ cells were isolated as described above (*Methods 2.1.10.1-2*). A total of $5x10^5$ Kit+ cells were seeded in a 24-well plate in 250µl XVIVO (Kit) with 4µg/ml protamine. Cells were transduced by spinoculation (1250xg for 60 minutes at 32^{o}C) with the first batch of collected lentivirus. Cells were then again immediately transduced by spinoculation with the second batch of lentivirus and incubated overnight at 37^{o}C. Viral supernatant was removed and cells were cultured for an additional 24 hours in X-VIVO (Kit) medium prior to FACS selection of GFP+ cells. Cells were then sorted as described above (*Methods 2.1.10.6*). Immediately after sorting, half the cells were cultured in 1ml XVIVO (Kit) medium. The other half was processed and RNA isolated using the RNA/DNA Purification Micro Kit (Norgen Biotek Corporation). RNA was isolated from the cultured cells 24 hours after sorting. All RNA was stored at -80^{o}C post-

isolation. A total of 2.5ng RNA from each sample was used for quality control in the Eukaryote Total RNA Pico Assay (Agilent).

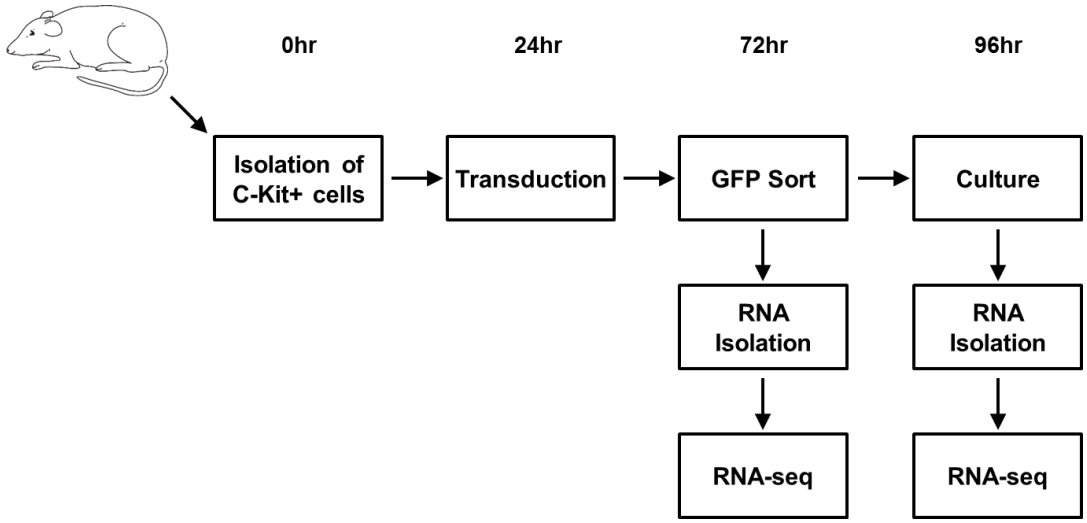

Figure 2.9: Schematic representation of the RNA-sequencing experiment. *Kit+ cells were transduced 24 hours post Kit+ isolation. GFP+ Kit+ cells were sorted and had RNA isolated 72 hours and 96 hours post Kit+ isolation.*

RNA*seq* was carried out by CRUK Manchester centre core facility staff. Libraries were prepared with the Lexogen QuantSeq 3' mRNA-Seq Library Prep Kit for Illumina (FWD) using an input of 200 ng and performing 14 cycles of amplification. Indexed libraries were then quantified using the Kapa Illumina Library quantification kit (Cat 07960336001) and pooled. 1 x 75bp sequence reads were generated by clustering 2.0pM of the library pool on a NextSeq500 High throughput run. Ordered BAM files were generated against the mouse genome feature file Mus_musculus_c57bl6nj.C57BL_6NJ_v1.96.gtf downloaded from Ensembl (ftp://ftp.ensembl.org/pub/current_gtf)[196].

Data analysis was performed by Dr Adam Stevens, Terence Garner and Dr Fabio MR Amaral using Qlucore Omics Explorer 3.3 (Qlucore, Lund, Sweden) with a FPKM (Fragments Per Kilobase Million) cut-off of 10. Deseq2 was used to convert read counts to a normalised value based using size factors to normalise for differences in the depth of sequence between samples (geometric size factor normalisation method) to calculate fold changes. To capture

similarities of changes mediated by EVI1-WT and EVI1-S436A transduction, data analysis was carried out by applying a false discovery rate (FDR)-modified ($p<0.05$) pair comparison of EVI1-WT vs vector control and EVI1-S436A vs vector control. A group ANOVA was applied for differences in median expression between EVI1-WT and EVI1S436A and vector only transduced cells with a p-value range of $2.3x10^{-8}$ to 0.01. In order to determine the connectivity of differentially regulated genes within the whole transcriptome of EVI1- WT and EVI1-S436A mutant cells, hypernetworks were used which allow compression of high dimensional relationships. Manhattan distance matrices were generated for EVI1-WT and EVI1-S436A transduced cells between all transcripts in each transcriptome. Manhattan distances were preferred over Euclidean distances as the former performs better in high dimensions[197]. Selecting only the genes identified as exclusively and significantly regulated in each group, a matrix, M, was generated which described the relationship between differentially expressed genes ($n^{WT}=78$, $n^{S436A}=106$) and all other genes ($n^{Total}=23766$). This matrix was binarised using a threshold of the 30th centile, so that only the closest relationships (smallest Manhattan distances) were retained. Multiplication of matrix M by the transpose of this matrix M^T results in a square hypernetwork matrix $M \times M^T$ whose values represent the number of binary relationships shared between a pair of genes. Connectivity was defined as the mean value for each hypernetwork. To assess organisation of the connections in these networks, entropy was calculated per gene in each hypernetwork. In order to test whether connectivity of each set of genes was greater than expected by random chance, a randomized iterative approach was used. Hypernetworks were generated 1000 times in each cell type, using a randomly selected set of genes ($n^{WT}=78$, $n^{S436A}=106$) each time, and connectivity and entropy were calculated.

2.4 Protein

2.4.1 Preparation of Protein Lysates

Protein was isolated from cells grown in a T75 to 90% confluency. Cells were centrifuged at 400xg for 5 minutes and pellets were washed twice with 5ml of ice cold PBS. Pellets were either stored at -80^{o}C or used immediately for protein isolation. Pellets were processed by addition of 3ml non-denaturing buffer (*Table 2.22*). Lysates were either stored at -80^{o}C or used immediately.

Table 2.22: Western Blot Whole Cell Lysis Buffer.

Component	**Stock Concentration**	**Final concentration**	**Volume for 1ml (µl)**
HEPES pH7.9	1M	20mM	20
$MgCl_2$	1M	2mM	2
NaCl	5M	250mM	50
Glycerol	100%	10%	100
NP-40	10%	1%	100
EDTA	0.5M	1mM	5
Protease inhibitor 1	100x	1x	10
Phosphatase inhibitor 1	100x	1x	10
Phosphatase inhibitor 2	100x	1x	10
Sodium Orthovanadate (Na_3VO_4)	100mM	1mM	10
Sodium Fluoride (NaF)	0.5M	10mM	20
Nuclease	250U/µl	0.5U/µl	2
H_2O	-	-	661

2.4.2 Immunoprecipitation

Cell pellets were re-suspended in an appropriate volume of immunoprecipitation buffer (IB) (*Table 2.23*) and placed on a rotor for 1 hour at 4^{o}C. Volume of buffer used was typically five-times the volume of the respective cell pellet. Lysed cell pellets were then centrifuged at 20,000g for 30 minutes at 4^{o}C. The supernatant was then split in a 1:10 ratio whereby 10% was used for the western blot input

and 90% was used for immunoprecipitation. The input was immediately processed by the addition of lithium dodecyl sulfate (LDS) buffer in a 1:1 ratio and stored at -80ºC. The remaining pellet was frozen as the insoluble fraction. For immunoprecipitation of Flag-tagged proteins, 50µl of Anti-FLAG M2 Magnetic Beads (Sigma) was added to the remaining supernatant and placed on a rotator for 2 hours at 4ºC. For immunoprecipitation of HA-tagged protein the Pierce Anti-HA Magnetic Beads (Thermo Scientific) were used. After incubation, tubes were placed on DynaMag Spin Magnet (Thermo Scientific) for 30 seconds prior to the removal of the supernatant. This supernatant was kept for the unbound fraction to test the efficiency of the bead-protein binding. After removal of the unbound fraction, beads were washed with 200µl of IB on the magnet and placed on the rotator for 5 minutes at 4ºC. This step was repeated twice. After the third wash, 65µl of LDS buffer was added to the bound beads to elute the bound protein and placed on a heat block for 10 minutes at 80ºC. The samples were then centrifuged at 15,000xg for 1 minute and supernatant was transferred to a fresh Eppendorf to remove any beads for the immunoprecipitation. Immunoprecipitated samples were stored at -80ºC until processing.

Table 2.23: Immunoprecipitation Buffer.

Component (Company)	**[Stock]**	**[Final]**	**Volume (1ml) (µl)**	**Function in Buffer**
N-(2-Hydroxyethyl)piperazine-N′-(2-ethanesulfonic acid) (HEPES pH7.9) (Sigma)	1M	20mM	20	Buffers pH between 7.2-8.2.
Magnesium Chloride ($MgCl_2$) (Sigma)	1M	2mM	2	Aids segregation of DNA.
Sodium Chloride (NaCl) (Sigma)	5M	250mM	50	Aid in protein solubilisation.
Glycerol (Sigma)	100%	10%	100	Aid protein solubility and in gel loading.
Nonidet P-40 Substitute (Roche)	10%	1%	100	Solubilising agent.
Ethylenediaminetetraacetic acid (EDTA) (Sigma)	0.5M	1mM	5	Acts as a chelating agent and dissociates proteins from RNA.
Tris(2-Carboxyethyl)Phosphine (TCEP) (Sigma)	0.5M	0.5mM	1	Break disulphide bonds within and between proteins (Reducing Agent).
Phenylmethylsulfonyl Fluoride (PMSF) (Sigma)	0.1M	0.1mM	1	Serine Protease Inhibitor (Minimal to none derivatisation of proteins).
Protease inhibitor 1 (Sigma)	100x	1x	10	Inhibits serine / cysteine / acid proteases and aminopeptidases.
Phosphatase inhibitor 2 (Sigma)	100x	1x	10	Inhibits L-isozymes of alkaline phosphatase and serine-threonine protein phosphatases.
Phosphatase inhibitor 3 (Sigma)	100x	1x	10	Inhibits a number of ATPases, protein tyrosine phosphatases, other phosphate-transferring enzymes and acid / alkaline / phosphoprotein phosphatases.

Sodium Orthovanadate (Na_3VO_4) (Sigma)	100mM	1mM	10	Inhibits protein tyrosine phosphatases, alkaline phosphatases and ATPases.
Sodium Fluoride (NaF) (Sigma)	0.5M	10mM	20	Inhibits protein phosphoseryl and phosphothreonyl phosphatases.
Pierce Universal Nuclease for Cell Lysis (Thermo Scientific)	250U/µl	0.5U/µl	2	Complete digestion of nucleic acids.
H_2O	-	-	659	

2.4.3 Western Blot

2.4.3.1 SDS page Gel Electrophoresis

Protein lysates were diluted in NuPAGE Sample Reducing Agent (Invitrogen) with NuPAGE LDS Sample Buffer (Invitrogen) prior and incubated at 90^{o}C for 10 minutes prior to loading on NuPAGE 4-12% Bis-Tris Gel (Life Technologies). A XCell Sure Lock tank (Invitrogen) were used along with NuPAGE MOPS SDS Running Buffer (Life Technologies) to run the samples. As size control, the Spectra Multicolour Broad Range Protein Ladder (Thermo Scientific) ladder was used. Samples were run at 150V for 90 minutes.

2.4.3.2 Transfer of Proteins to Membrane

After separation on the SDS page gel, proteins were transferred to a nitrocellulose blotting membrane (Amersham). The transfer procedure was run at 100V for 45 minutes in NuPAGE Transfer Buffer (Life Technologies) using an EPS2A200 (Hoefer) system with a tank and magnetic stirrer (Stuart). Once transfer was complete, the nitrocellulose membrane was incubated in Ponceau solution (Sigma) to confirm successful transfer. The membrane was then washed 3 times for 10 minutes in PBST (PBS+0.05% TWEEN-20).

2.4.3.3 Detection of Proteins

Prior to detection, to saturate non-specific binding, the membrane was blocked for 1 hour in PBST with 5% dried skimmed milk (Marvel). The membrane was again washed as described above (*Methods 2.4.3.2*). The primary antibody (*Table 2.24*) was then diluted in PBST with 5% milk and at a predetermined concentration dependent on the antibody and incubated overnight at room temperature. The membrane was then washed again. A secondary antibody (detailed below) was then added for 1 hour at room temperature. The secondary antibody was dependent on the primary antibody used. The membrane was then washed for a final time. Supersignal West Pico Chemiluminescent substrate (Thermo Scientific) was then used in conjunction with ChemiDoc XRS (Bio-Rad) machine to visualise the protein on the membrane. Image analysis was performed using ImageJ software. To visualise signals, images were processed in High-Low look up table. Quantification of specific protein bands was performed using the Analyse Tool of ImageJ. The integrated density of the band measured as a region of interest (ROI). For quantification of immunoprecipitation assays, the IP level of each condition was used to normalise co-immunoprecipitated proteins levels.

Table 2.24: Antibodies used for western blot analysis.

Antibody	Source	Catalogue No.
EVI1	Cell Signaling Technology	#2593
Phospho-EVI1 (Ser858/860)	Eurogentec	-
DNMT3a	Santa Cruz Biotechnology	#SC-373905
GAPDH	Ambion	#1303026
Phospho-ATM (Ser1981)	Invitrogen	#MA1-2020
ATM	Abcam	#ab78
Phospho-Histone H2A.X (Ser139)	Cell Signaling Technology	#9718
Histone H2AX	Cell Signaling Technology	#2595S
CtBP1	BD Biosciences	#612042
RUVBL2	NOVUS	#NBP1-40354
Phospho-p53 (Ser15)	Cell Signaling Technology	#9284
Histone H_3	Cell Signaling Technology	#9715
Anti-mouse IgG HRP Linked Whole Ab	Amersham	#NA931V
Anti-rabbit IgG HRP Linked Whole Ab	Amersham	#NA9340V

2.4.4 Mass Spectrometry

2.4.4.1 Identification of EVI1 Phosphorylation Sites

Protein preparation for mass spectrometry analysis was performed by Dr Roberto Paredes. Mass spectrometry analysis performed by Dr Bethany Geary. Immunoprecipitated EVI1 from 6×10^8 SB1690CB AML cells was analysed using multiple reaction monitoring-initiated detection and sequencing (MIDAS)[198]. Following SDS-PAGE gel electrophoresis, the EVI1 containing band was excised and digested with trypsin. Peptides were separated by liquid chromatography prior to MIDAS using electrospray mass spectrometry on a 4000 Q-TRAP mass spectrometer (AB Sciex). MRM transitions were designed to detect 7–24 amino acid EVI1 peptides with serine, threonine or tyrosine phosphorylation within a Q1 m/z range from 400 to 1300 and in both a double and triple charge state. A Q3 mass of either 216.0 Da or Q1 minus 98 Da was used to identify tyrosine or serine/threonine phosphorylation, respectively. MS/MS data were interrogated using MASCOT database software (MatrixScience) and confirmed by manual inspection of spectra.

2.4.4.2 Interactome Analysis of EVI1

Protein preparation for mass spectrometry analysis was performed by Dr Roberto Paredes. Mass spectrometry analysis was performed by Dr Bethany Geary. Interactome analysis was carried out on in-gel digested samples of EVI1-immunoprecipitate Flag-IP of Flag-tagged EVI1-WT or EVI1-S436A transfected HEK293 cells (*Methods 2.5.2*). IP products were separated by SDS-PAGE gel electrophoresis with each lane separated into fractions. The gel was then subject to alkylation and reduction. Gel pieces were then digested using trypsin overnight, and analysed with an Ultimate 3000 HPLC (Dionex, Sunnyvale, CA) in-line with a TripleTOF 6600 mass spectrometer (Sciex, Warrington, UK). The trapping column was an Acclaim PepMap 100 C18 cartridge (Thermo, Loughborough, UK) and the analytical column was an Acclaim PepMap 100 C18 NV column (Thermo). Buffer A comprised of 98% water, 2% acetonitrile and 0.1% formic acid, buffer B comprised of 80% acetonitrile, 20% water, 0.1% formic acid. Peptides were eluted over a gradient from 0 to 40% buffer B. Peptides were fragmented in a data-dependent manner. Spectral data was searched using MASCOT (version 2.5.1) against the Uniprot human database (downloaded on: 20/06/2018). Downstream analysis and data processing was performed using R (version 3.4.1).

2.4.5 Protein Sequence Alignment

Alignment of EVI1 protein sequences from NCBI database was performed using ClustalW2 or Clustal Omega programs[199]. These protein sequences were analysed and illustrated using the Uniprot knowledgebase[200] and the Jalview software[201].

2.4.6 *In silico* analysis of kinase prediction and protein modelling

In silico kinase prediction for EVI1 S436 phosphorylation was carried out using the PHOSHONET platform[202]. Protein modelling was carried out by Dr Batool Almarzouq, Liverpool: To model the structure of the 426-598aa region of EVI1 the Iterative Threading ASSEmbly Refinement (ITASSER) was used (https://zhanglab.ccmb.med.umich.edu/I-TASSER/)[203]. Five structures were predicted for EVI1 and assessed by C- and TM-score (confidence scores for estimating the quality of predicted models by I-TASSER). The model prediction with maximum C-score (-0.94) and TM-scores (0.60±0.14) was selected, quantifying the accuracy of the model built. The EVI1-CtBP1 interaction was simulated through modelling of protein-protein docking using ClusProserver applying the initial coordinates of the structure of CtBP1, (28-378), which has largely been resolved (PDB:6CDR)[204,205]. Proteins were *in silico* positioned in a cubic periodic box with each side at least 1nm away from the protein. The complexes were parameterized using GROMOS 54A7 force field in a cubic box solvated with SPC water model[206,207]. Both CtBP-binding motifs were used when setting attraction in the docking parameters in ClusPro. In order to examine the phosphorylation at S436 of EVI1, the ViennaPTM tool was used to modify EVI1-CtBP1 PDB file and obtain force-field parameters for phosphorylated EVI1-CtBP1[208]. A neutral charge was introduced at 150mM NaCl. Long-range interactions were defined using the particle mesh Ewald (PME) algorithm[209]. Energy minimization was carried out using steepest descent after applying position restraints to heavy atoms. This was followed by a 100ps NVT ensemble at 300K, and a100ps NPT ensemble at 300K and 1bar[210,211]. Production MD was performed at 300K and 1 bar for 400ns with frames written every 2 pico seconds. GROMACS modules such as gmx *rms*, gmx *rmsf*, and gmx *energy* were used to analyse the stability and behaviour of each system[212–214]. Root Mean Square Fluctuation (RMSF) was calculated for of Cα atoms coordinates of EVI1 in the EVI1-CtBP1 complex, and the p(S436) EVI1-CtBP1 complex in the last 350ns to ensure the complex reached equilibrium. The g_mmpbsa tool was used to calculate the binding free energy of EVI1-CtBP1 complex and the contribution of S436 to the binding energy by

means of energy decomposition[213]. All molecular dynamics (MD) work was generated through High Performance Computing facility (Barklacluster, University of Liverpool) using Gromacsv.5.1.4[210,212].

Chapter 3 Results

Some of the results presented in this thesis have been carried out as part of a broader effort to understand EVI1 by the group. For completeness, collaborative work which has mainly been generated by other people is included and clearly marked with my own contributions accurately indicated.

3.1 Carboxy-Terminal Phosphorylation of EVI1

Previous work performed by our group had identified a phosphorylation of EVI1 at serine 860 (S860) in the EVI1-overexpressing SB1690CB AML cells[131], confirming the previous reports of EVI1 phosphorylation at this site[95,125,132,135,136,215]. Further analysis of immunoprecipitated EVI1 by mass spectrometry from SB1690CB AML cells treated with irradiation revealed also a doubly phosphorylated EVI1-peptide at residues S858 and S860 (*Appendix Figure 7.1)*. This double phosphorylation of EVI1 at S858/860 after genotoxic stress was confirmed by western blot analysis with a specific antibody (*Appendix Figure 7.1)*.

3.1.1 EVI1 S858/860 Phosphorylation is Mediated by ATM

The SQS motif has been identified as an ATM (ataxia telangiectasia mutant)-kinase specific motif[215]. ATM is a protein kinase with an essential role in cell cycle progression and the DNA damage response[216]. Sequence alignment analysis of the amino acid sequences harbouring this phosphorylation site reveals a high degree of conservation of the motif across species, suggesting that the SQS motif is relevant to EVI1 function (*Figure 3.1 A*). Experimental work previously performed by Dr Daniel White in the group using an antibody specifically raised against an EVI1 peptide phosphorylated both at S858 and S860 confirmed the rapid induction of doubly phosphorylated EVI1 both at S858 and S860 together after irradiation treatment (*Figure 3.1 B*). The double phosphorylation was detected at minimal levels in non-

stressed cells. Cells pre-treated with the ATM inhibitor KU55933 showed decreased serine 858/860 phosphorylation after irradiation treatment (*Figure 3.1 B*).

The activation of ATM in response to hydrogen peroxide (H_2O_2) treatment was assessed in Rat1 fibroblasts by immunofluorescence. H2AX phosphorylation and ATM serine 1981 phosphorylation was used as control for induction of genotoxic stress and ATM activity. In both vector-only and EVI-WT transduced Rat1 fibroblasts treated with H_2O_2, there was a sharp induction in the phosphorylation of both H2AX and ATM when compared to the untreated cells (*Figure 3.1 C*). These results confirm that hydrogen peroxide induces the activation of ATM in Rat1 fibroblasts and that ATM is mediating the double phosphorylation of EVI1 at S858/860 after genotoxic stress. It should be noted that H_2O_2 treatment is likely inducing differential genotoxic stress responses in the different models used within this thesis, particularly primary cell populations. However, at the concentrations tested, H_2O_2 is sufficient to result in ATM activation and phosphorylation of EVI1.

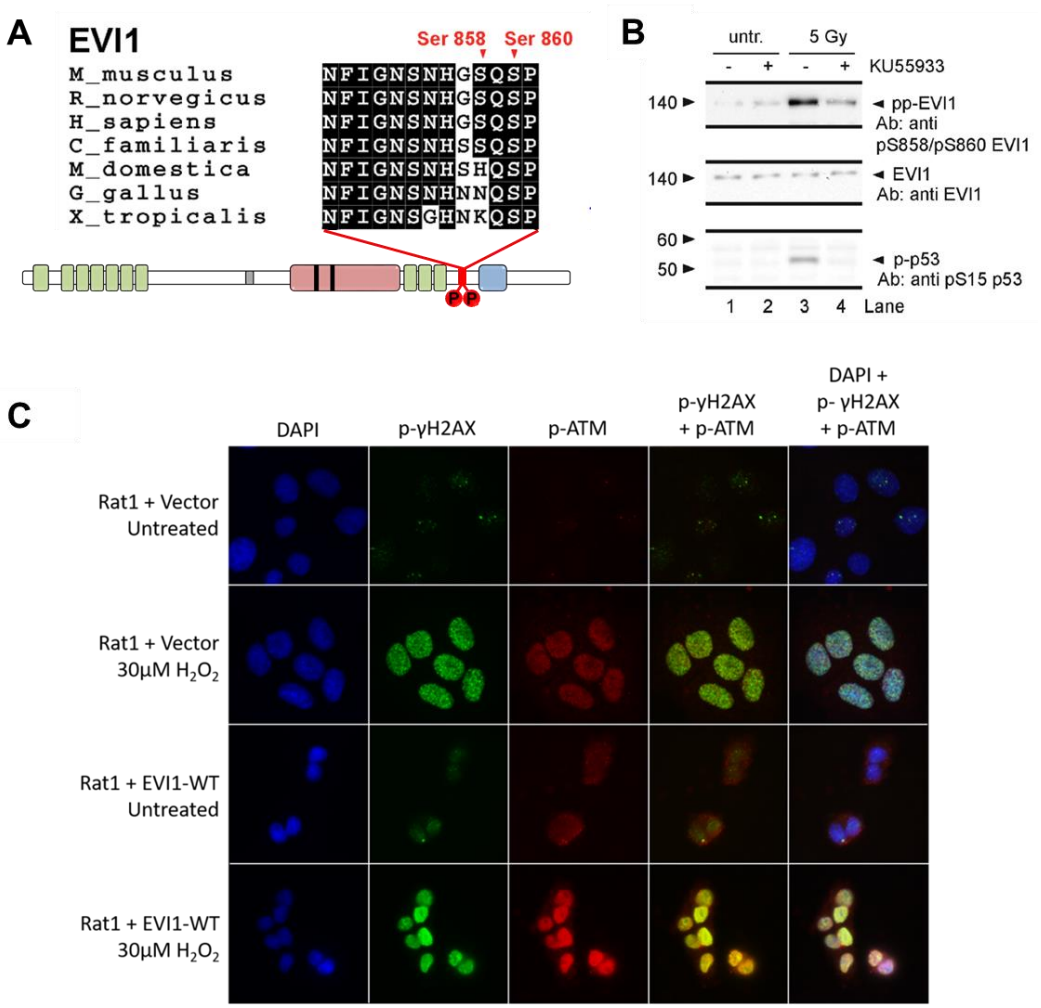

Figure 3.1: ATM phosphorylates the EVI1 carboxy-terminal SQS motif. (A) *Schematic representation of the EVI1 protein with sequence alignment from other species for the peptide sequence surrounding the carboxy-terminal SQS motif. Red circles = Carboxy-terminal SQS motif. Image adapted from Paredes et al.*[131] ***(B)*** *Western blot (WB) of EVI1-immunoprecipitates from untreated (lanes 1 and 2) and irradiated (lanes 3 and 4) SB1690CB cells pre-treated (1 h) with 10μM ATM-kinase inhibitor KU55933 (lanes 2 and 4), and not pre-treated (lanes 1 and 3).Membranes were probed for doubly phosphorylated EVI1 with anti-pS858/pS860-EVI1 antibody. Middle panel: membrane as upper panel re-probed with pan-EVI1 antibody. Lower panel: WB of p-p53 (Ser15) carried out on input samples as positive control for ATM-activity and ATM-inhibition. Western blot analysis performed by Dr Daniel White.* ***(C)*** *Immunofluorescence of Rat1 fibroblast stable transduced with either vector-only control or EVI1-WT encoding lentiviral plasmids. Cells either left untreated or treated with 30μM H_2O_2 for 2 hours and then probed for p-H2AX to monitor a genotoxic stress response, p-ATM for activation of ATM and DAPI as a nuclear stain.*

3.1.2 Functional Analysis of the Carboxy-Terminal EVI1 Phosphorylation

The effect of carboxy-terminal phosphorylation was studied using a non-phosphorylated and non-phosphorylatable construct of EVI1. The EVI1-WT S858/860 amino acid sequence SQS was mutated to EVI1-AQA to generate a non-phosphorylated, non-phosphorylatable EVI1. (*Methods 2.2.12*). Here the functional aspects of EVI1 that are altered by phosphorylation of the SQS motif are investigated.

3.1.2.1 EVI1 Carboxy-Terminal Phosphorylation Sustains EVI1 Transforming Ability in the DNA Damage Response

To investigate the effect of the carboxy-terminal SQS phosphorylation of EVI1 on Rat1 fibroblast transformation, the EVI1-AQA and EVI1-WT constructs were compared with respect to their ability to transform Rat1 fibroblasts in the absence and presence of genotoxic stress. Stable transduced Rat1 fibroblast expressing EVI1-WT, EVI1-AQA or vector-only control constructs were established as described above (*Methods 2.1.5*). Equal expression of EVI1 protein in EVI1-WT and EVI1-AQA transduced cells was confirmed by western blot analysis (*Figure 3.2 A*). A dose

response curve was generated for Rat1 fibroblasts to determine the optimal concentration for H_2O_2 treatment. A concentration of 30μM was chosen for subsequent treatment to avoid excessive cell death or apoptosis (*Figure 3.2 B*). Treatment with H_2O_2 did not result in a change in EVI1 expression levels (*Figure 3.2 A*).

Rat1 fibroblasts transduced with EVI1-WT formed significantly more colonies after 14 days compared with vector-only transduced cells. Under standard conditions colony numbers were not significantly different from Rat1 fibroblasts transduced with the EVI1-AQA mutant (*Figure 3.2 C*). However, when genotoxic stress was induced by treatment with H_2O_2, EVI1-WT conferred a significant increase in colony numbers compared to both vector-only and EVI1-AQA (*Figure 3.2 D*). These results show that in the absence of genotoxic stress EVI1-WT and EVI1-AQA have equal ability to transform Rat1 fibroblasts. In the presence of genotoxic stress, however, mutation of the SQS motif completely abrogates transforming ability, suggesting that the transformation of Rat1 fibroblasts was dependent on the phosphorylation of the SQS motif.

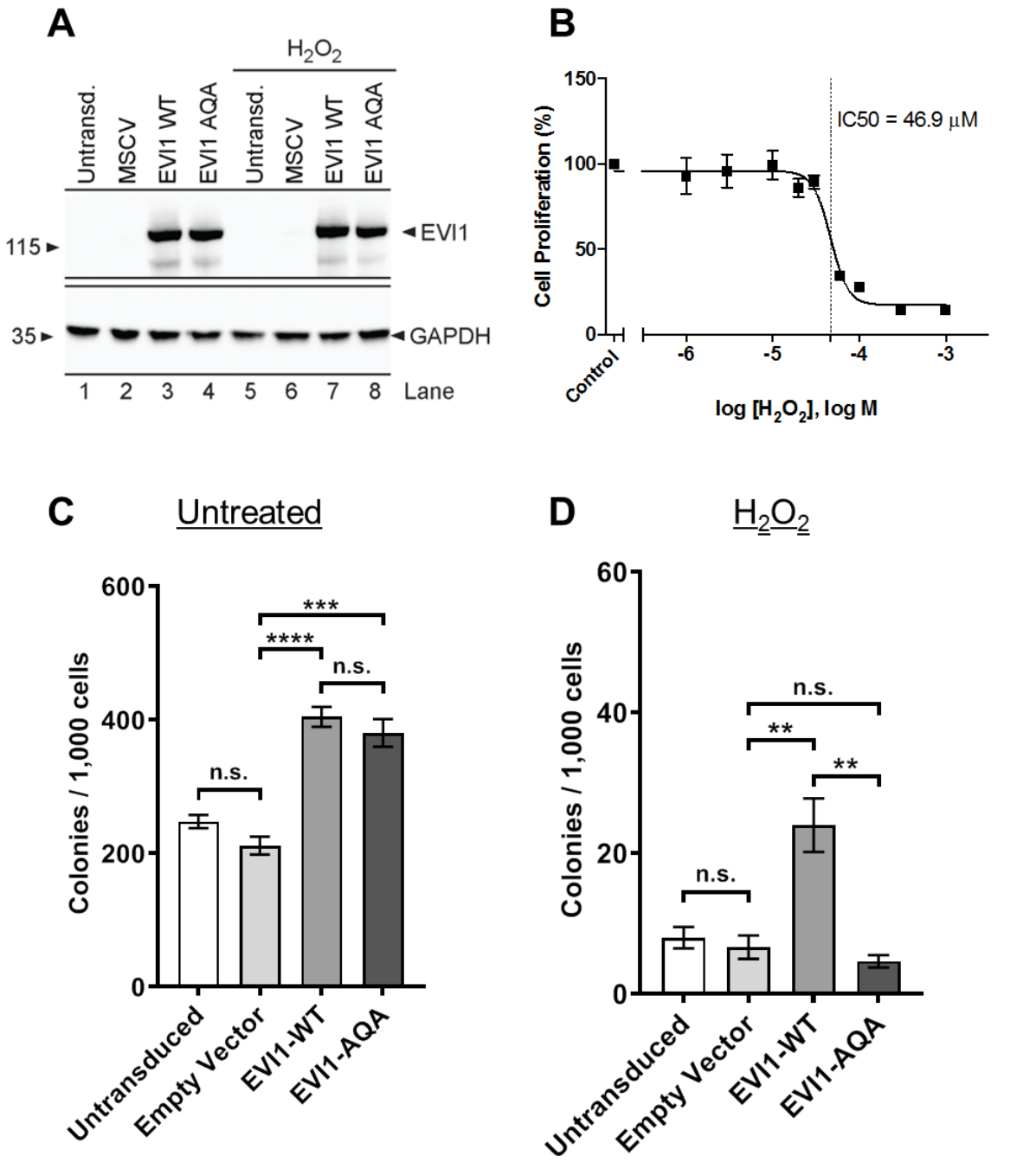

Figure 3.2: EVI1-mediated transformation of Rat1 fibroblasts. (A) *Western blot demonstrating comparable expression of EVI1 in the stably transduced Rat1 fibroblasts.* ***(B)*** *The tolerance of Rat1 fibroblasts to hydrogen peroxide treatment at a 1000/well cell density (n=3) (IC50=46.9µM).* ***(C)*** *Rat1 fibroblast stable transduced with either vector-only control, EVI1-WTor EVI1-AQA-IRES-GFP lentiviral plasmids untreated* ***(D)*** *or treated with H_2O_2 and plated in Methocult. Untransduced Rat-1 fibroblasts were used as controls. Statistical analysis: one-way ANOVA, Tukey posttest (n=3) (** p<0.01, *** p<0.001, **** p<0.0001, ns=not significant).*

3.1.2.2 The EVI1 Carboxy-Terminal SQS Motif Sustains Haematopoietic Self-Renewal

The transduction of murine haematopoietic Kit+ stem and progenitor cells (Kit+ HSPCs) with EVI1 has previously been shown to increase re-plating capacity[112,217]. To investigate the role of the carboxy-terminal phosphorylation of EVI1 in haematopoiesis in response to genotoxic stress, Kit+ HSPCs were transduced with EVI1-WT, the EVI1-AQA mutant or vector-only control (*Methods 2.1.10*). When transduced with either EVI1-WT or EVI1-AQA, equal levels of GFP positive cells and median fluorescence intensity of GFP signal were measured (*Figure 3.3 A & B*). It should be noted that transduction with the vector-only control produced significantly more GFP positive cells; this could be due to the smaller construct size[218]. Additionally, cells transduced with either EVI1-WT or EVI1-AQA had equal levels of *EVI1* transcript (*Figure 3.3 C*). Taken together these results indicate equal expression of EVI1 after transduction.

To induce a genotoxic stress response in Kit+ HSPCs, a concentration of 30μM H_2O_2 was chosen (*Figure 3.3 D*). The re-plating capacity of Kit+ HSPCs transduced with EVI1-WT or EVI1-AQA was investigated in three rounds of re-plating in the presence or absence of genotoxic stress (H_2O_2). It was confirmed that EVI1-WT confers re-plating capability of Kit+ HSPCs for three rounds of re-plating untreated and in the presence of genotoxic stress[112,125] (*Figure 3.3 E, F & G*). In the first round of plating, transduction with EVI1-AQA did not affect re-plating efficiency compared to EVI1-WT (*Figure 3.3 E*). However, when re-plated in the second and third round, transduction with EVI1-AQA had significantly reduced re-plating capability compared to EVI1-WT, corresponding to fewer colonies formed (*Figure 3.3 F & G*). In the presence of genotoxic stress the significant reduction in re-plating ability of EVI1-AQA transduction compared to EVI1-WT was even more profound (*Figure 3.3 F & G*). The non-phosphorylatable mutated EVI1-AQA was unable to significantly sustain re-plating of Kit+ HSPCs in the presence of genotoxic stress

Phenotypic assessment of the colonies formed revealed both macrophage (CFU-M) and granulocyte-macrophage (CFU-GM) colonies, which was expected due to the cytokines used (*Figure 3.4 A*). In line with the increased re-plating observed, morphological assessment of the colonies revealed myoblast-derived lineage cells in addition to mitotic cells, indicating a proportion of progenitor cells within the colony

that are sustaining colony formation (*Figure 3.4 B*). Morphological analysis of EVI1-WT transduced colonies revealed a significant proportion of cells with a blast-like morphology (*Figure 3.4 C*). When compared to EVI1-WT, EVI1-AQA colonies had significantly fewer blast-like cells in particular in the presence of genotoxic stress (*Figure 3.4 D*). These results indicate that the EVI1-mediated maintenance and self-renewal of haematopoietic stem cells is partially dependent on the phosphorylatable carboxy-terminal SQS motif.

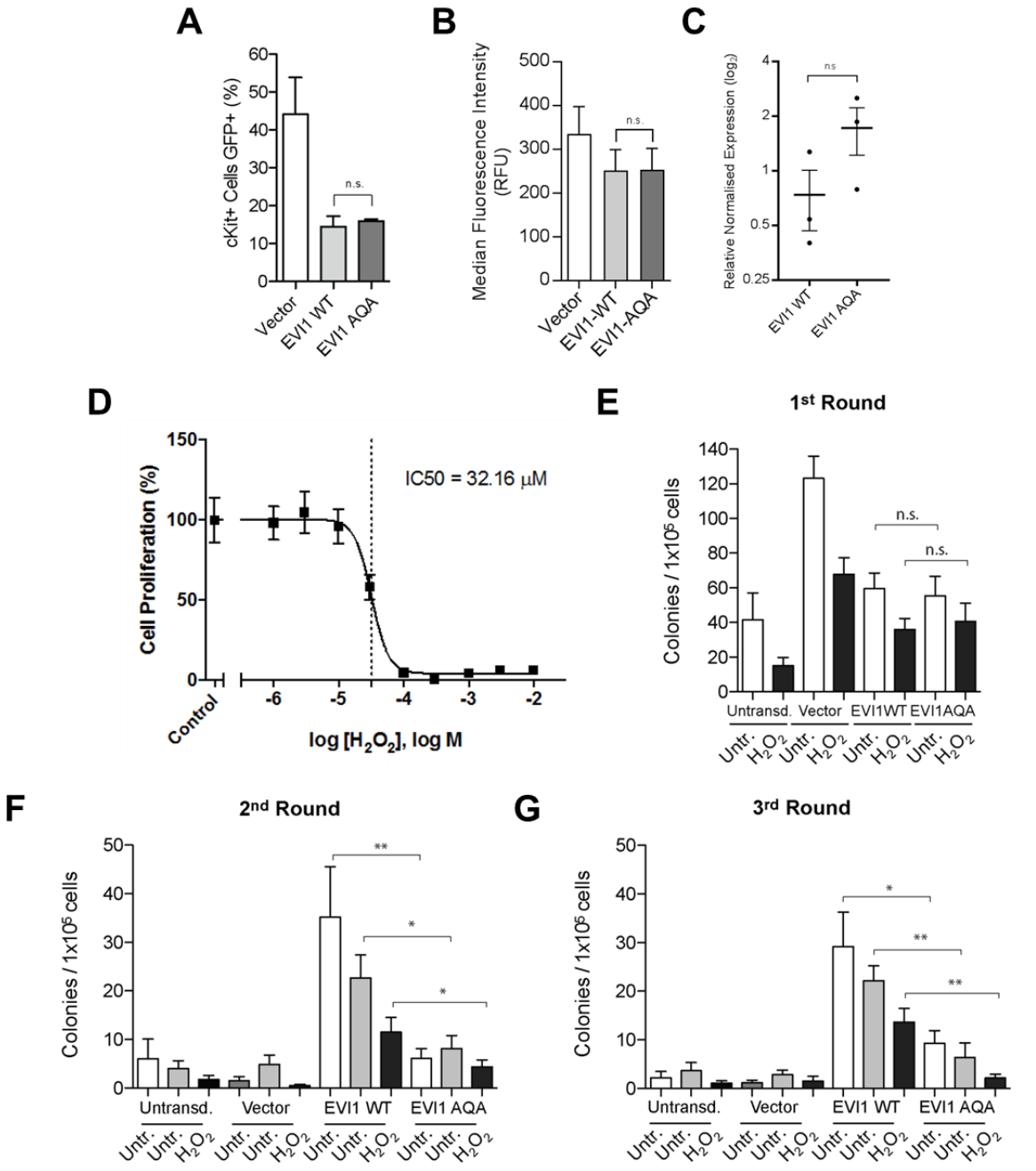

Figure 3.3: EVI1-mediated serial re-plating of Kit+ HSPCs. (A) *Percentage of transduction of Kit+ HSPCs calculated by the GFP expression using flow cytometry.* ***(B)*** *Median Fluorescent Intensity of cells transduced with lentiviral plasmids.* ***(C)*** *mRNA expression of the EVI1 encoding constructs in transduced primary murine bone marrow progenitors as determined by RT-qPCR.* ***(D)*** *Tolerance of Kit+ HSPCs to treatment with H_2O_2 (IC50=32.16µM).* ***(E)*** *Colony counts after first round of plating Kit+ HSPCs transduced with EVI1-WT / -AQA and vector-only control encoding lentiviral plasmids in Methocult. Untransduced cells were plated as a control.* ***(F/G)*** *Colonies counts after the second and third rounds of re-plating. (White: Untreated. Grey: Untreated cells re-plated from previously H_2O_2 treated colonies. Black: treated with H_2O_2.) Statistical analysis: paired t-test (n=8, eight different mice) (* p<0.05, **p<0.01, n.s. = not significant).*

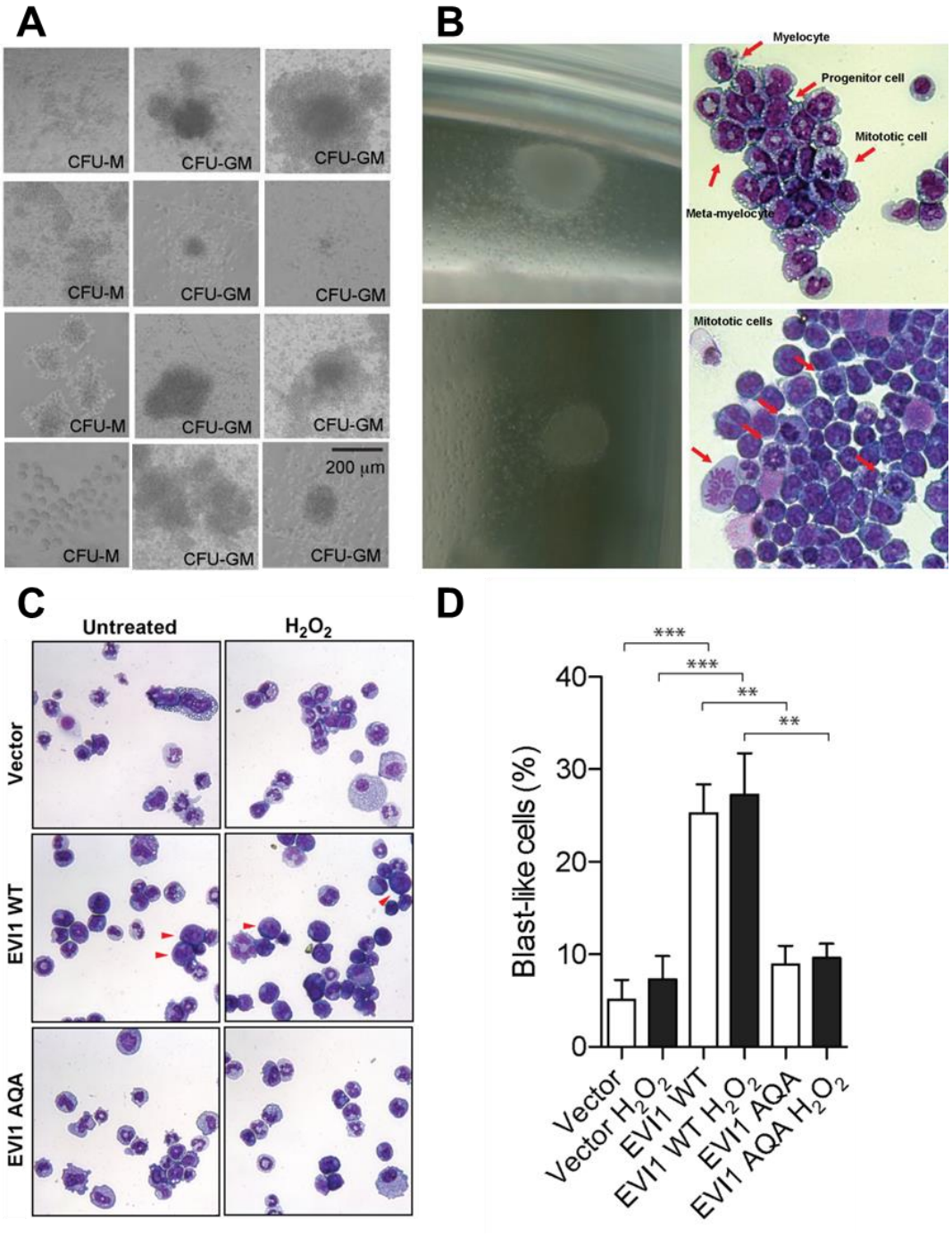

Figure 3.4: The morphology of Kit+ HSPCs in the serial re-plating assay. (A) *Typical Kit+ HSPCs colony morphology in methylcellulose-based medium after 7 days in culture.* ***(B)*** *Kit+ HSPCs single colony May-Grünwald Giemsa stain (right hand side panels) showing the presence of active cell division (mitotic cells, arrows) and differentiated cells (arrows) in the same colonies. Direct bright field microscopy (left hand side panels) was used to score colony morphology.* ***(C)*** *May-Grünwald Giemsa stain of cell collected from colonies (1st round) prior to be re-plated (2nd round). Red arrowheads point to typical blast-like cell morphology.* ***(D)*** *Blast-like cells quantitation from the 1st round of colony growth. Statistical analysis: one-way ANOVA (n=8) (** p<0.01, *** p<0.001).*

3.1.3 EVI1 transcriptional changes in the DNA damage response are sustained by carboxy-terminal SQS-phosphorylation

Complementary work performed by the group (Dr Roberto Parades) investigated the change in transcriptional patterns by EVI1 in response to genotoxic stress[131]. HEK293FT cells were transfected with the EVI1-WT and EVI1-AQA constructs along with the vector-only control. Genotoxic stress was induced by treatment with 150µM H_2O_2 for 8 hours. RNA*seq* analysis was performed by Dr Adam Stevens to determine to what extent the transcriptional changes in response to DNA damage are modulated by the phosphorylation of EVI1 at Ser858/860 (*Figure 3.5*). Applying a group ANOVA with a $p<0.01$ identified 1306 significantly differentially expressed transcripts when comparing transduction status and the presence or absence of genotoxic stress. (For full dataset please refer to the GEO site: https://www.ncbi.nlm.nih.gov/geo/query/acc.cgi?acc=GSE115643).

Analysis of untreated EVI1-WT and EVI-AQA compared to vector-only transfected cells by two-group ANOVA comparison revealed a strong overlap in gene expression patterns (*Figure 3.5*). EVI1-WT transfection resulted in 62 significantly up-regulated transcripts when compared to vector-only control. From the 62 up-regulated by EVI1-WT, 22 are also significantly up-regulated as a result of EVI1-AQA transfection. Of the 90 transcripts significantly repressed with EVI1-WT transfection, 30 are also significantly repressed with EVI1-AQA transfection. However, in the presence of genotoxic stress the effect on gene expression patterns was more diverse. Only 10 of 41 transcripts significantly up-regulated with EVI1-WT transfection overlapping with EVI1-AQA transfection. Of the significantly repressed transcripts only 7 of 47 were also repressed by EVI1-AQA.

Graphical representation of the 1306 differentially expressed transcripts identified by the group ANOVA as a heatmap illustration clearly divided the dataset into two halves by induction of genotoxic stress (*Figure 3.5*). The horizontal dendrogram delineation separated untreated EVI1-transfected cells, when compared to the controls, into two main clusters of EVI1-regulated transcripts (*Figure 3.5 – boxed*). Cluster 1 contains 139 transcripts that are downregulated by EVI1 transduction. Cluster 2 contains 328 transcripts that are upregulated with EVI1 expression. In untreated cells, patterns of differentially regulated transcripts (clusters 1A and 2A)

are strikingly similar with transduction of EVI1-WT and EVI1-AQA. However, when comparing expression patterns mediated by EVI1-WT with EVI1-AQA in the presence of genotoxic stress, gene expression patterns are more diverse.

In cluster 1B, there was a distinct sub-cluster of 14 transcripts that are repressed in untreated EVI1-WT and EVI1-AQA transfected cells, but in response to genotoxic stress are only repressed in EVI1-WT transfected cells (*Figure 3.5 – arrow*). In cluster 2B, a sub-cluster of 93 transcripts have a higher expression in untreated and damaged EVI1-WT transfected cells that was not maintained in response to genotoxic stress in EVI1-AQA transfected cells (*Figure 3.5 – dashed box*). For selected genes, the patterns seen in the RNAseq experiment were confirmed by RT-qPCR (*Figure 3.6*). The gene expression patterns modulated by EVI1-WT and EVI1-AQA are strikingly similar in untreated cells. In the presence of genotoxic stress there was divergent modulation, indicating that the SQS phosphorylation was important in sustaining EVI1 function in the presence of genotoxic stress.

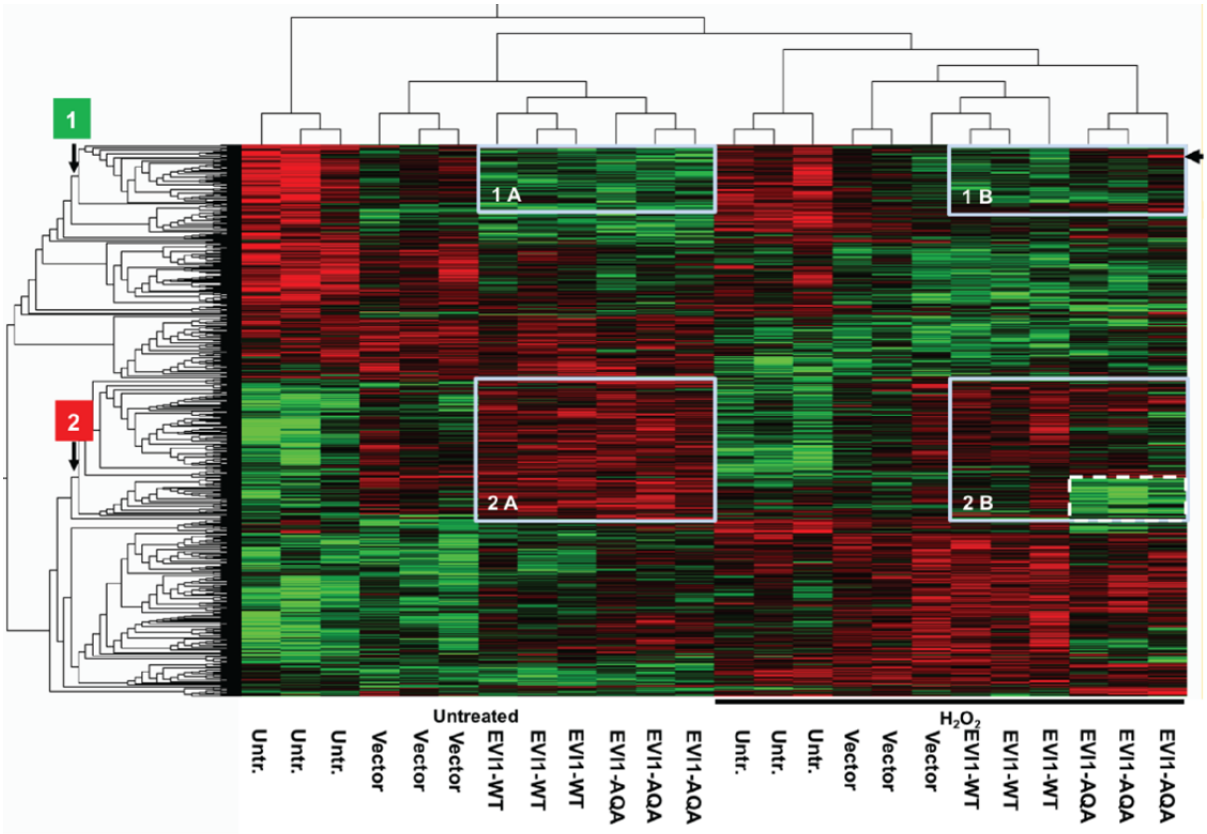

Figure 3.5: Effect of genotoxic stress on EVI1-mediated gene expression. *Heat-map illustration of differential expressed transcripts (n=1,306) (p<0.01, ANOVA) in untransfected, vector-only control, EVI1-WT and EVI1-AQA transfected cells left untreated, and treated with H_2O_2 (150μM), indicated by black line. Clusters of EVI1 regulated transcripts by dendrogram delineation, boxed for repressed (green), and upregulated transcripts (red). Patterns of sub-clusters in H_2O_2 treated cells with different changes comparing EVI-WT with EVI1-AQA indicated by arrow in 1B and dashed box in 2B. (Data generated by Dr Roberto Parades with data analysis performed by Dr Adam Stevens).*

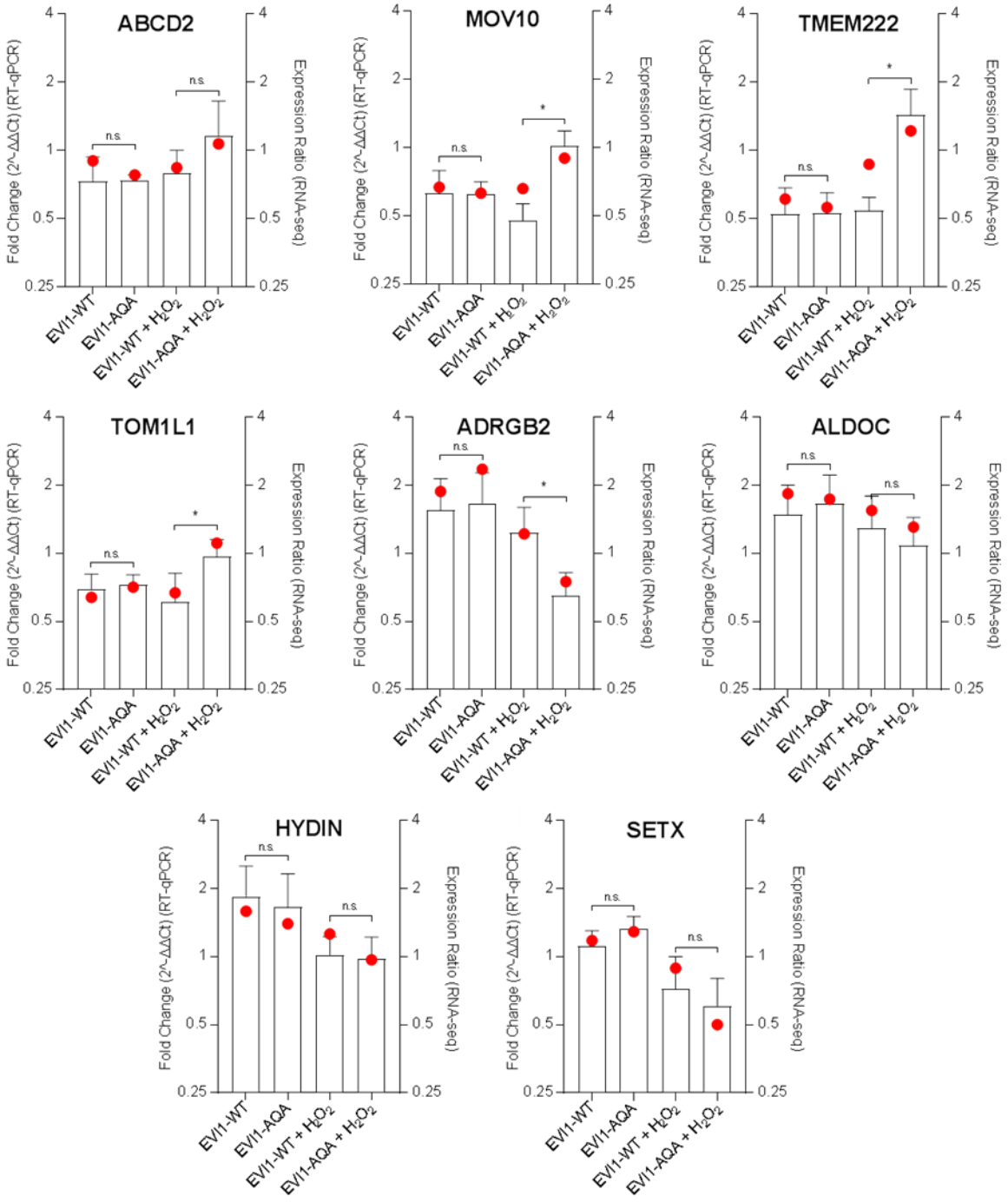

Figure 3.6: Confirmation of the effect of genotoxic stress on EVI1-mediated gene expression. ***(A-H)*** *Modulation of EVI1 regulated gene expression in HEK293FT cells transfected with either EVI1-WT or EVI1-AQA in the presence or absence of hydrogen peroxide by RT-qPCR (n=3) (plotted on left y-axis as bars). RNAseq expression ratios are plotted on the right y-axis as red dots. Values are normalised to the respective untransduced cells for both the RNAseq and RT-qPCR data. The reference genes βACTIN and YWHAZ are also used for the normalisation of the RT-qPCR data. Statistical analysis of RT-qPCR data: T-test (* p<0.05, ns=not significant).*

3.2 ATM Inhibition Affects EVI1 function

ATM has been identified as a potential therapeutic target in cancer treatment for its essential role in the DNA damage response[219]. Inhibition of ATM might enhance the therapeutic window for radiation and DNA-damaging chemotherapy[186]. Several ATM inhibitors have been developed as a potential therapeutic and are currently in clinical evaluation[188]. The identification of a functionally important ATM phosphorylation site on the EVI1 protein suggests that ATM inhibition might have an unexpected effect by targeting also EVI1 oncogenic function. To further investigate ATM-inhibition as a potential therapeutic strategy for EVI1-overexpressing leukaemia or solid tumours, the effect of ATM inhibitors on EVI1 function was investigated.

3.2.1 ATM Inhibition has Minimal Effect of EVI1-Mediated Transformation of Rat1 Fibroblasts

For the inhibition of ATM, two compounds currently undergoing clinical evaluation (AZD0156 and AZD1390) were used (Provided in collaboration with AstraZeneca)[187,188]. Both AZD0156 and AZD1390 are potent inhibitors of ATM with reported cellular IC50's of 0.58nM and 0.78nM respectively[188]. AZD1390 was developed with superior selectivity, solubility and blood-brain-barrier penetration over AZD0156, and has shown efficacy in combination with irradiation in patient-derived xenograft (PDX) models of glioblastoma multiforme (GBM)[188].

First, the effect of AZD0156 and AZD1390 on Rat1 fibroblast proliferation was investigated. When comparing the IC50 of AZD0156, AZD0156 treatment was equally potent in all cell lines (*Figure 3.7 A & B*). However, EVI1-WT transduced cells showed some sensitivity to AZD0156 treatment in the dose response curve when compared to vector-only and EVI1-AQA transduced cells (*Figure 3.7 A & B*). In contrast, when comparing the IC50 of AZ1390, ATM inhibition has a significant but small effect on proliferation only on phosphorylatable EVI1-WT (*Figure 3.7 C & D*).

To investigate the effect of ATM inhibition on EVI1 function with respect to transformation, AZD0156 and AZD1390 were tested in the Rat1 fibroblast colony

forming assay. The concentrations of AZD0156 and AZD1390 in this assay were chosen to normalise the effect seen in the Wst-1 proliferation assay and to ensure ATM inhibition with respect to the reported cellular IC50[188]. Consistent with the data above, transduction with EVIT-WT or EVI1-AQA resulted in significantly more colonies than the vector-only control cells (*Figures 3.7 E & F*). There was a general trend that treatment with either AZD0156 or AZD1390 reduces colony formation across all cell lines, but this was insignificant when compared to the untreated cells (*Figures 3.7 E & F*). Although treatment with AZD0156 and AZD1390 resulted in a reduction in the proliferation of EVI1-WT transduced Rat1 fibroblasts, inhibition of ATM had minimal to no effect on EVI1-mediated transformation of Rat1 fibroblasts in the absence of genotoxic stress.

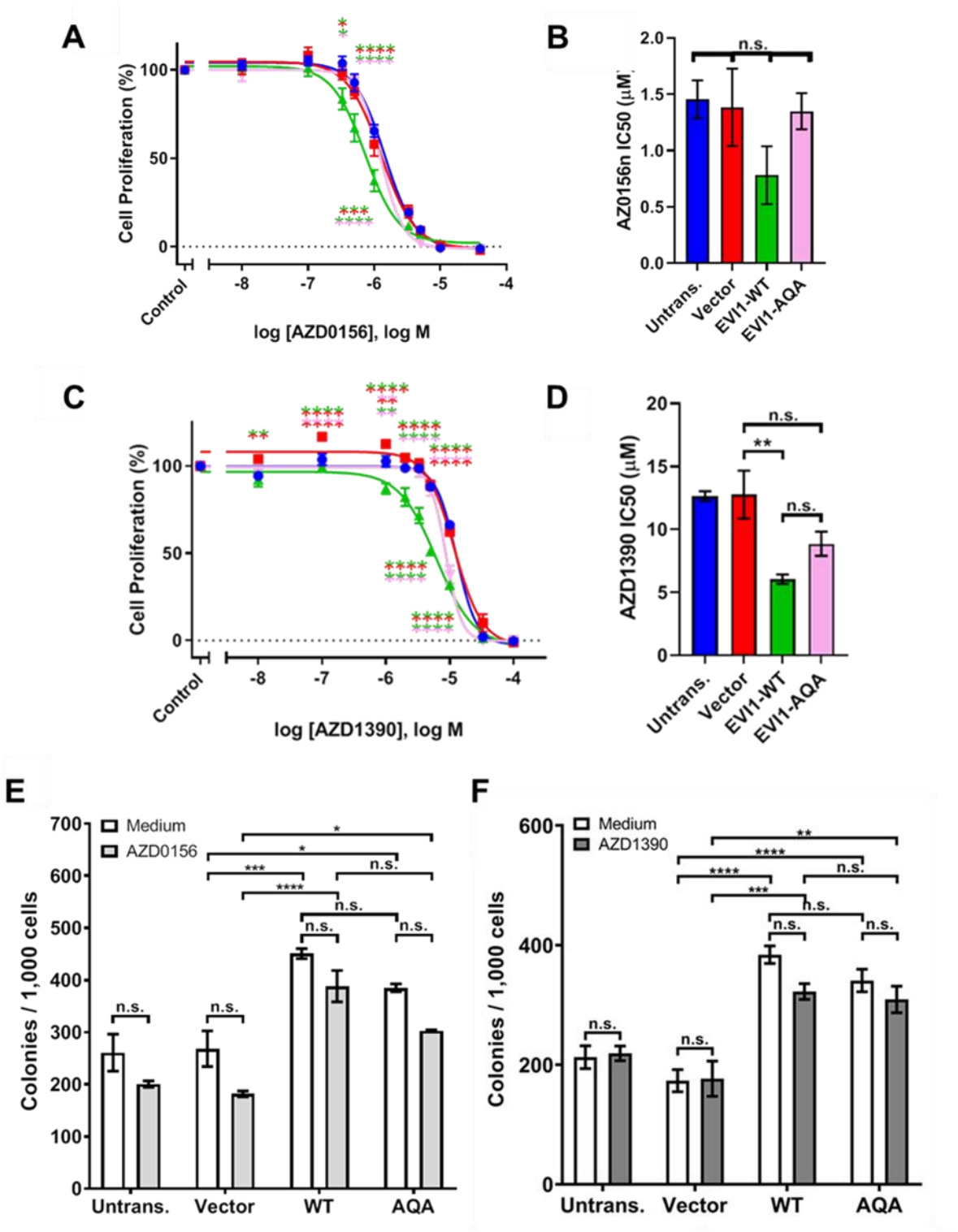

Figure 3.7: The effect of ATM inhibition of Rat1 fibroblast proliferation and colony formation. ***(A)*** *The proliferation of stable transduced Rat1 fibroblast to AZD0156* ***(C)*** *or AZD1390 by WST-1 measurement 72 hours post treatment. Cells plated at 1000/well density. Green and red * indicate significance when comparing EVI1-WT transduced cells to the vector-only control Statistical analysis: Two-way ANOVA (n=4) (* p<0.05, *** p<0.001, ****p<0.0001).* ***(B)*** *The IC50 of AZD0156* ***(D)*** *or AZD1390 in the Rat1 fibroblast lines as determined by non-linear regression of the drug titration curve.* ***(F)*** *Rat1 fibroblast stable transduced lines untreated or treated with 58nM AZD0156* ***(E)*** *or*

*78nM AZD1390, and plated in Methocult. Untransduced Rat-1 fibroblasts were used as controls. Statistical analysis: one-way ANOVA, Tukey posttest (n=5) (*p<0.05, ** p<0.01, *** p<0.001, **** p<0.0001, ns=not significant).*

3.2.2 Synergistic Effect of ATM Inhibition with Genotoxic Stress

Given that ATM mediated SQS phosphorylation sustains EVI1 function in the presence of genotoxic stress mediated by H_2O_2, potential additive or synergistic effects of ATM inhibition with genotoxic stress were investigated. Activation of ATM and its inhibition was controlled by H2AX phosphorylation and auto phosphorylation of pS1981 of ATM.

In the Rat1 fibroblast model, pre-treatment with 580nM AZD0156 eliminated H_2O_2 induced activation of ATM (*Figure 3.8 A*). As previously demonstrated (*Figure 3.8 D*), Rat1 fibroblast transduced with EVI1-WT form significantly more colonies than vector-only or EVI1-AQA transduced cells in the presence of genotoxic stress (*Figure 3.8 B & C*). Strikingly, combination treatment with AZD0156 significantly reduces EVI1-WT-mediated colony formation in the presence of genotoxic stress (*Figure 3.8 B*). Similarly, combination of AZD1390 with H_2O_2 significantly reduces EVI1-WT-mediated transformation of Rat1 fibroblasts when compared to H_2O_2 treatment alone (*Figure 3.8 C*).

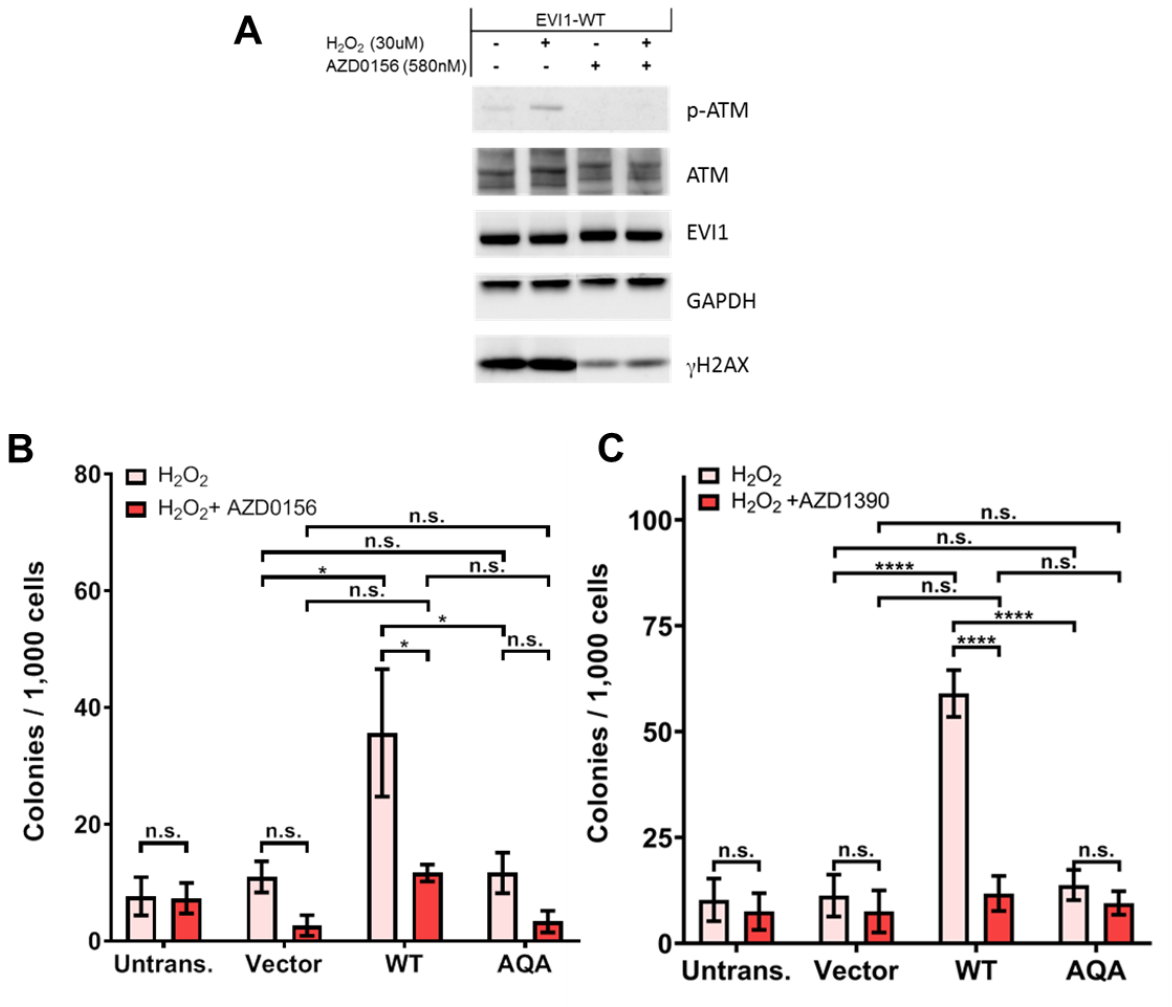

Figure 3.8: Synergistic effect of ATM inhibition with genotoxic stress by H_2O_2. (A) *Western blot of whole cell lysates from Rat1 fibroblast stable transduced with EVI1-WT encoding lentiviral plasmid. Cells were either un-treated (lanes 1 and 2) or pre-treated with the ATM inhibitor AZD0156 (580nM) for 1 hour (lanes 3 and 4) then either left untreated (lanes 1 and 3) or treated with 30uM hydrogen peroxide for 2 hours (lanes 2 and 4). Cells were probed for activation of ATM by p-ATM, p-H2AX for a genotoxic stress response, GAPDH for loading control, EVI1 to confirm transduction status and ATM for a control to p-ATM. Rat1 fibroblast stable transduced lines treated with 30μM H_2O_2 or treated with 30μM H_2O_2 and 58nM AZD0156* ***(B)*** *or 78nM AZD1390* ***(C)****, and plated in Methocult. Untransduced Rat1 fibroblasts were used as controls. Statistical analysis: one-way ANOVA, Tukey posttest (n=5) (*p<0.05, **** p<0.0001, ns=not significant).*

3.2.3 Synergistic Effect of ATM inhibition with Chemotherapy on EVI1-mediated Transformation

To investigate if ATM inhibition on EVI1 might have also synergistic effects with chemotherapeutic compounds used clinically for the treatment of AML, ATM inhibition was next investigated in combination with Etoposide, Daunorubicin and Cytarabine.

Pre-treatment with AZD1390 eliminates chemotherapy induced activation of ATM in Rat1 fibroblasts (*Figure 3.9*). Compared to untreated cells (*Figure 3.7 F*), treatment with chemotherapy results in a marked decrease in the anchorage independent growth of transduced Rat1 fibroblasts (*Figure 3.10 A, B & C*). However, when treated with chemotherapy, EVI1-WT and EVI1-AQA confer a significant increase in colony numbers compared to vector-only (*Figure 3.10 A, B & C*).

Upon Etoposide treatment, Rat1 fibroblasts transduced with EVI1-WT form significantly more colonies compared to the vector-only control (*Figure 3.10 A*). However, EVI1-AQA transduced cells form significantly more colonies compared to EVI1-WT transduction in response to Etoposide treatment (*Figure 3.10 A*). Combination treatment of Etoposide with AZD1390 results in complete elimination of colony formation in both EVI1-WT and EVI1-AQA transduced cells (*Figure 3.10 A*). In the same trend, EVI1-WT and EVI1-AQA maintain colony formation in response to Daunorubicin treatment, but it is the EVI1-AQA mutant that confers greater colony forming potential (*Figure 3.10 B*). Upon combination treatment with AZD1390 and Daunorubicin, EVI1-WT and EVI1-AQA are unable to maintain colony formation with the number of colonies completely abrogated compared to Daunorubicin treatment alone (*Figure 3.10 B*). In contrast to the effect of Etoposide and Daunorubicin treatment, both EVI1-WT and EVI1-AQA transduction resulted in similar levels of colony formation that are significantly higher compared to the vector-only control (*Figure 3.10 C*). Combination treatment of AZD1390 with Cytarabine results in a significant decrease in the number of colonies formed in both EVI1-WT and EVI1-AQA transduced cells when compared to Cytarabine treatment alone (*Figure 3.10 C*). Conversely to both Etoposide and Daunorubicin combination treatment with AZD1390, treatment with AZD1390 and Cytarabine does not completely abolish

colony formation. The enhanced protective effect of the EVI1-AQA mutant in response to Etoposide and Daunorubicin treatment contrasts the protective effect of EVI1-WT in response to H_2O_2 induced genotoxic stress described above (*Figure 3.8 C*).

The increased sensitivity of EVI1-WT transduced cells to chemotherapy treatment was also seen in dose-response experiments (*Figure 3.11*). In the dose-response curve, EVI1-AQA transduced cells had an increased resistance to Etoposide when compared to EVI1-WT transduced cells that was not reflected in the comparison of the IC50 (*Figure 3.11 A & B*). In both the dose-response curves and in comparison of IC50's, EVI1-AQA transduced cells are significantly more resistant to Daunorubicin and Cytarabine treatment when compared to EVI1-WT transduced cells (*Figure 3.11 C, D, E & F*).

In summary, there was a strongly synergistic effect of ATM inhibition with chemotherapy treatment on EVI1-mediated transformation of Rat1 fibroblasts. However, EVI1-AQA mutation had diverse effects in response to H_2O_2 compared with chemotherapy, implying that the SQS phosphorylation is in particular relevant for the response to oxidative stress.

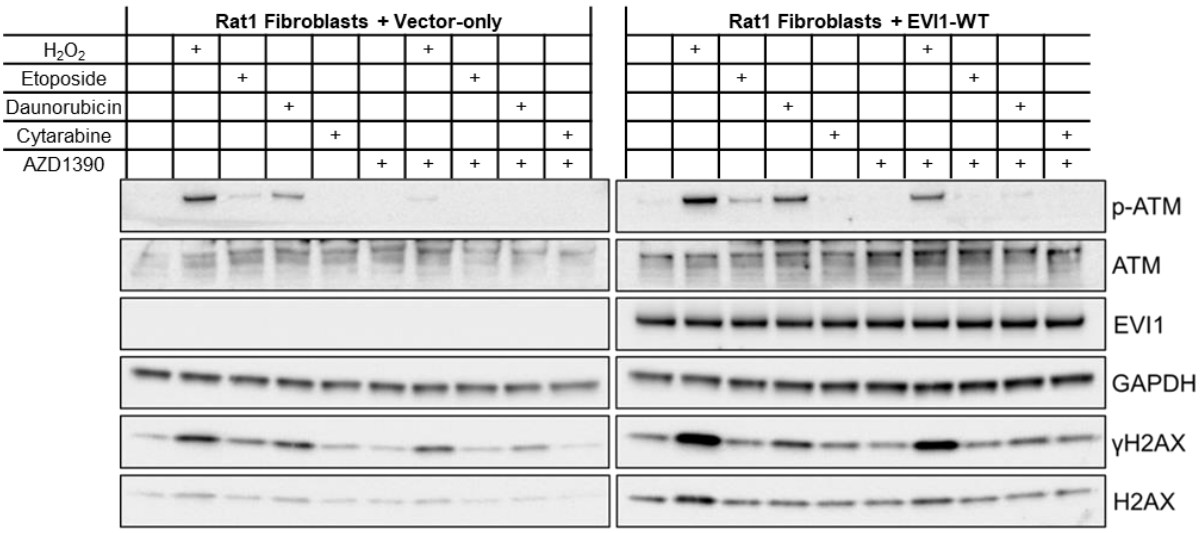

Figure 3.9: ATM inhibition and Etoposide, Daunorubicin and Cytarabine treatment. *Western blot analysis of whole cell lysates from Rat1 fibroblast stably transduced with vector-only control or EVI1-WT encoding lentiviral plasmid. Cells were either un-treated (lanes 1) or pre-treated with the ATM inhibitor AZD1390 (78nM) for 1 hour (lanes 5) then either left untreated (lanes 1 and 5) or treated with 30uM hydrogen peroxide (lanes 2 and 7)/1uM Etoposide (lanes 3 and 8)/100nM Daunorubicin (lanes 4 and 9)/100nM Cytarabine (lanes 5 and 10) for X hours. Cells were probed for activation of ATM by p-ATM, p-H2AX for a genotoxic stress response, GAPDH for loading control, EVI1 to confirm transduction status, ATM for a control to p-ATM and H2AX for a control to p-H2AX.*

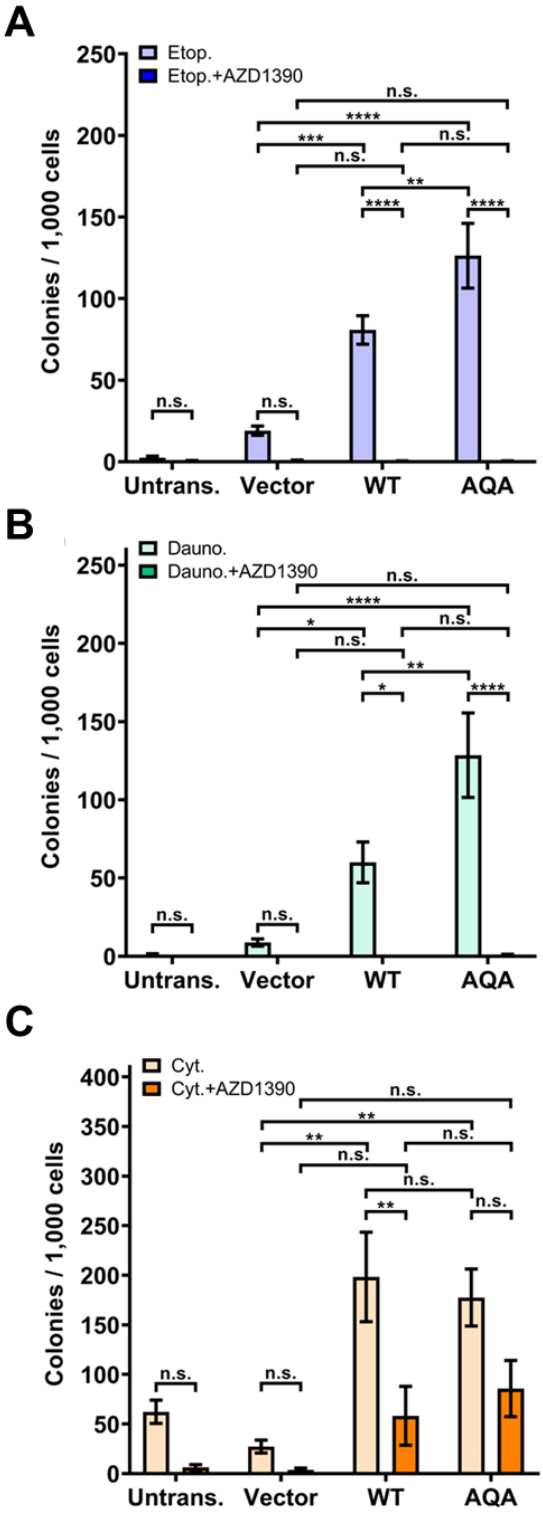

Figure 3.10: Synergistic effect of ATM inhibition with Etoposide, Daunorubicin and Cytarabine in Rat1 fibroblast transformation. (A) *Rat1 fibroblast stable transduced lines treated with 1uM Etoposide or 1uM Etoposide and 78nM AZD1390* ***(B)*** *treated with 100nM Daunorubicin or 100nM Daunorubicin and 78nM AZD1390* ***(C)*** *treated with 100nM Cytarabine or 100nM Cytarabine and 78nM AZD1390 and plated in Methocult. Untransduced Rat1 fibroblasts were used as controls. Statistical analysis: one-way ANOVA, Tukey posttest (n=5) (*p<0.05, ** p<0.01, **** p<0.0001, ns=not significant).*

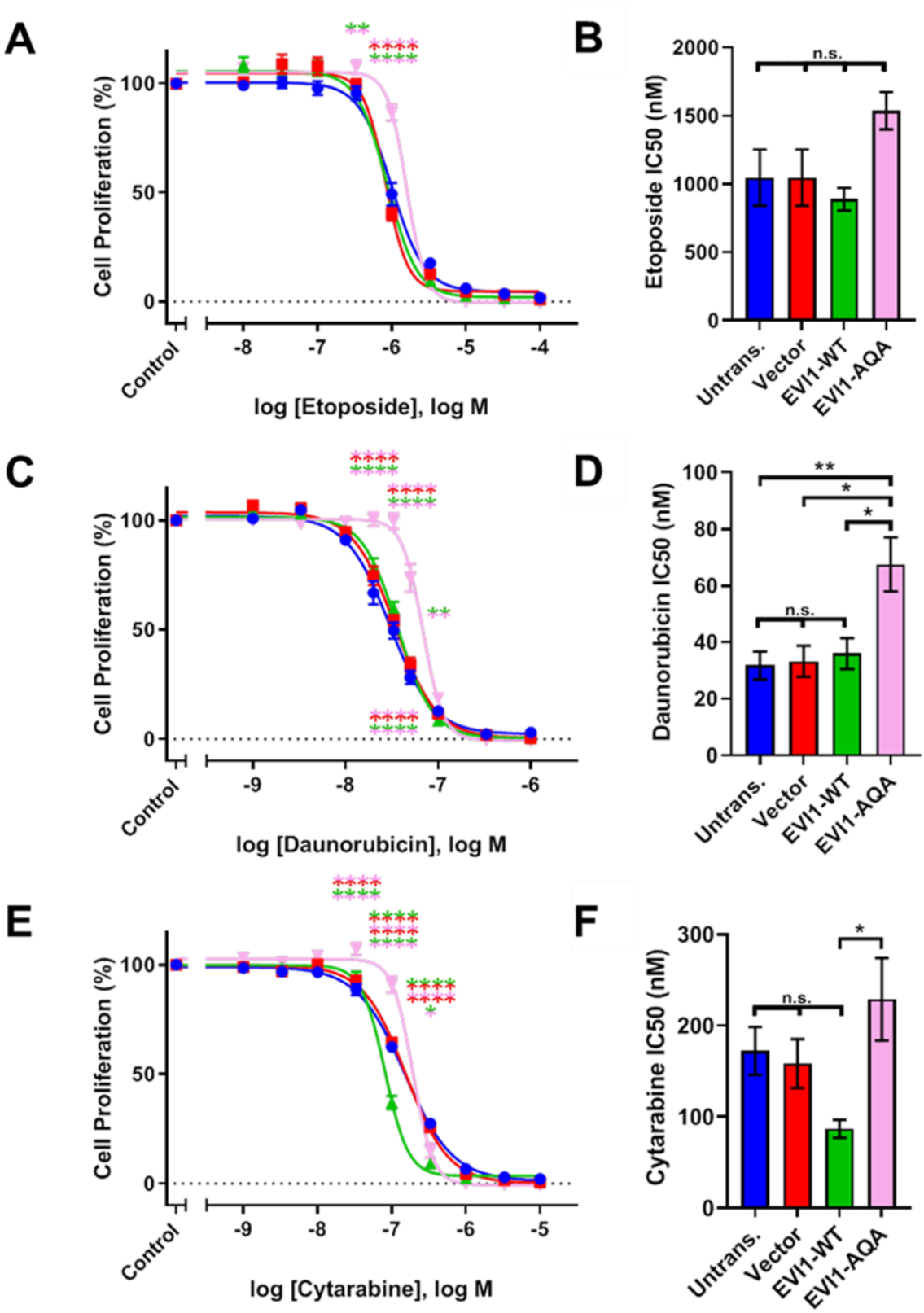

Figure 3.11: Rat1 fibroblast sensitivity to Etoposide, Daunorubicin and Cytarabine. (A) *The tolerance of stable transduced Rat1 fibroblast to Etoposide* ***(C)*** *or Daunorubicin* ***(E)*** *or Cytarabine treatment by WST-1 measurement 72 hours post treatment. Cells plated at 1000/well density. Green and red asterix indicate significance when comparing EVI1-WT transduced cells to the vector-only*

control. Green and pink asterix indicate significance when comparing EVI1-WT to EVI1-AQA transduced cells. Pink and red asterix indicate significance when comparing EVI1-AQA transduced cells to the vector-only control. ***(B)*** *The IC50 of Etoposide in corresponding stable transduced Rat1 fibroblast. (Untransduced: 1047.13nM. Vector: 1047.1nM. EVI1-WT: 888.7nM. EVI1-AQA: 1536.33nM.)* ***(D)*** *The IC50 of Daunorubicin corresponding stable transduced Rat1 fibroblast. (Untransduced: 31.814nM. Vector: 33.283nM. EVI1-WT: 36.013nM. EVI1-AQA: 67.4733nM.)* ***(F)*** *The IC50 of Cytarabine in corresponding stable transduced Rat1 fibroblast. (Untransduced: 172.2nM. Vector: 158.4nM. EVI1-WT: 86.956nM. EVI1-AQA: 228.9nM.). Statistical analysis: Two-way ANOVA (n=4) (* p<0.05, ** p<0.01, ****p<0.0001, ns=not significant).*

Summary of EVI1 Carboxy-Terminal Phosphorylation Results

This study has demonstrated that the EVI1 carboxy-terminal S858/860 phosphorylation is mediated by ATM and is essential to EVI-mediated haematopoietic self-renewal. As the phosphorylation event was discovered in response to genotoxic stress, this study demonstrates the effect on gene expression patterns in response to genotoxic stress that are modulated by the carboxy-terminal phosphorylation. It was shown that the EVI1-mediated transformation of Rat1 fibroblasts in the presence of genotoxic stress was mediated by the carboxy-terminal phosphorylation and that ATM inhibition abrogates this. EVI1 transduction conferred transformation of Rat1 fibroblast in response to treatment with Etoposide, Daunorubicin and Cytarabine. In contrast to hydrogen peroxide induced genotoxic stress, it is the non-phosphorylatable EVI1-AQA mutant that confers greater transforming capability in response to chemotherapy treatment. Combination treatment of the chemotherapy compounds with ATM inhibition was exhibiting a synergistic effect: While ATM inhibition in the doses tested had no effect of colony forming and Rat1 transformation, there was a significant increase of the cytotoxic effect of Daunorubicin, Etoposide and Cytarabine.

3.3 Functional analysis of EVI1 S436A phosphorylation

EVI1 is phosphorylated at multiple sites[95]. Of particular interest is the S436 phosphorylation site, as it is not present in the ΔEVI1 isoform. Previous mass spectrometry conducted by colleagues in the group identified the EVI1 peptide DKVSPLQNLASINNK (aa 433 to 447) unmodified and phosphorylated at S436 in SB1690CB AML cells, which overexpress both EVI1 and ΔEVI1 (*Appendix Figure 7.2*)[131]. This phosphorylation event has been listed in a number of global proteomic studies[130,132,134–139]. A non-phosphorylated and non-phosphorylatable EVI1 mutant (EVI1-S436A) was generated by site-directed mutagenesis (*Methods 2.2.12*). Here I investigated the function of the S346 phosphorylation by comparing the EVI1-WT with S436 available for phosphorylation with a mutant EVI1 S436A, where the 436 site cannot be phosphorylated.

3.3.1 S436A mutation does not affect EVI1 Nuclear Localisation, DNA Binding or Rat1 Fibroblast transformation

The S436 phosphorylation site is located near a putative NLS site (*Figure 1.2*). To test the hypothesis, that the S436 phosphorylation might direct localisation of the EVI1 protein, the effect of S436 availability for phosphorylation on EVI1 nuclear localisation was investigated. Both the EVI1-WT and EVI1-S436A transduced Rat1 fibroblasts had a positive stain for EVI1 compared to the vector-only negative control, confirming stable transduction (*Figure 3.12 A*). Consistent with previously published data[96,144,220], the staining of EVI1 in the EVI1-WT transduced Rat1 fibroblasts was speckled and contained within the nucleus, sparring the nucleolus (*Figure 3.12 A*). When compared to EVI1-WT transduced cells, EVI1-S436A mutant showed identical nuclear staining patterns (*Figure 3.12 A*). In murine Kit+ HSPCs transduced with EVI1-WT or EVI1-S436A, the EVI1 stain was also speckled and contained within the nucleus, sparring the nucleolus (*Figure 3.12 B*). Both in stable transduced cell lines and transduced primary cells, the S436A mutation did not alter EVI1 nuclear localisation.

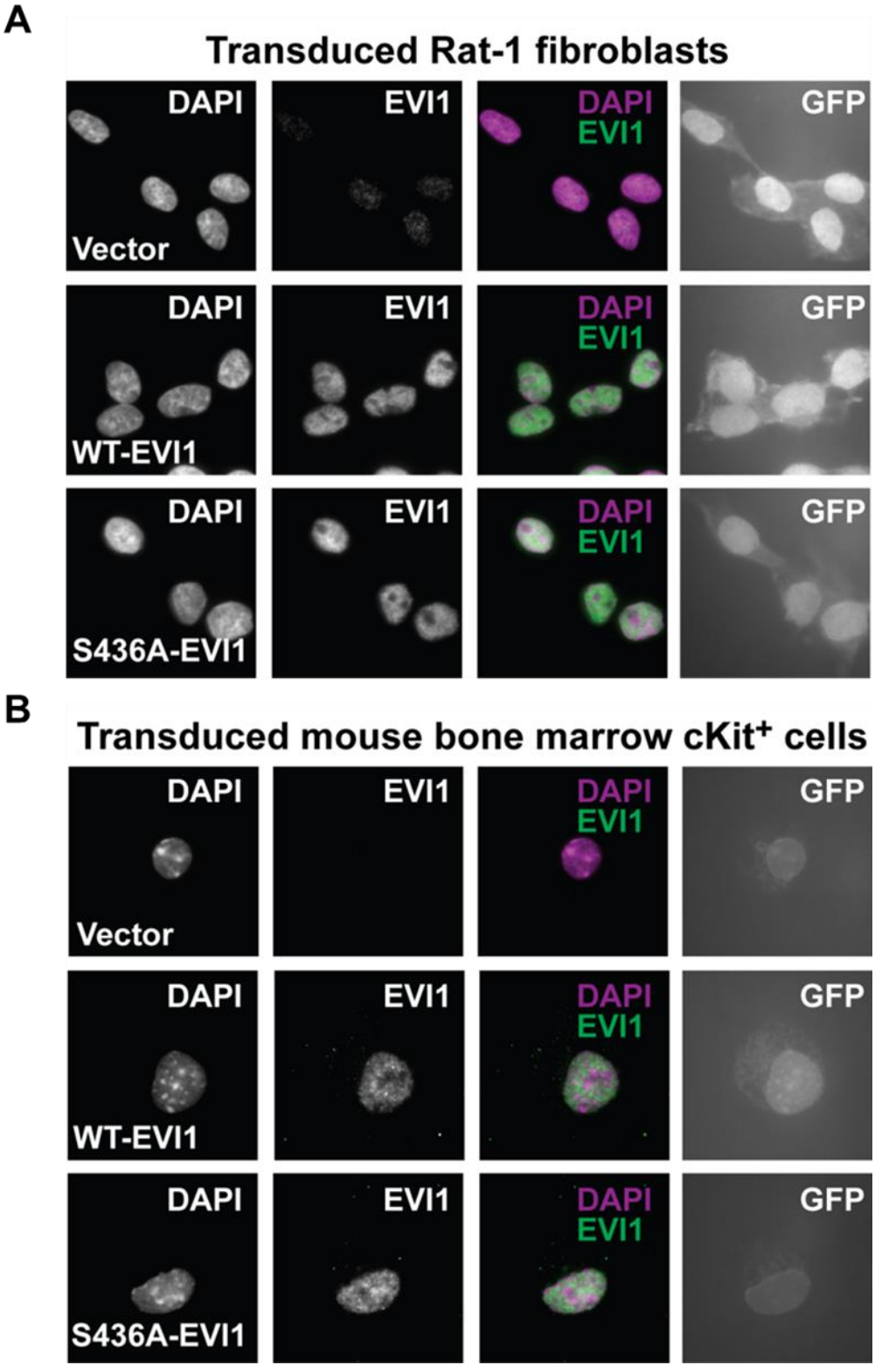

Figure 3.12: The nuclear localisation of EVI1-WT and EVI1–S436A in transduced Rat1 fibroblast and Kit+ HSPCs. (A) *Rat1 fibroblasts transduced with either vector-only control or EVI1-WT or EVI1-S436A containing lentiviral plasmids.* ***(B)*** *Kit+ HSPCs transduced with either vector-only control or EVI1-WT or EVI1-S436A containing lentiviral plasmids. Samples were stained with EVI1 C50 antibody. DAPI was used as a nuclear co-stain. Imagine acquisition was controlled for exposure.*

It was next assessed whether S436A mutation affects EVI1 target-gene repression. EVI1 mediates the repression of the *PLZF* promoter via the n-terminal zinc-finger motif of EVI1 and the *FOS* promoter via the C-terminal zinc-finger motif[192,193] (*Figure 3.13 A*). In Rat1 fibroblasts, transfection with EVI1-WT results in significant repression of both *FOS* and *PLZF* promoters when compared transfection with vector-only (*Figure 3.13 B*). Transfection with the EVI1-S436A mutant also resulted in significant repression of both *FOS* and *PLZF* promoters compared to vector-only control (*Figure 3.13 B*). No effect of S436A mutation on N-terminal or C-terminal zinger finger mediated transcriptional repression mediated by EVI1 could be demonstrated.

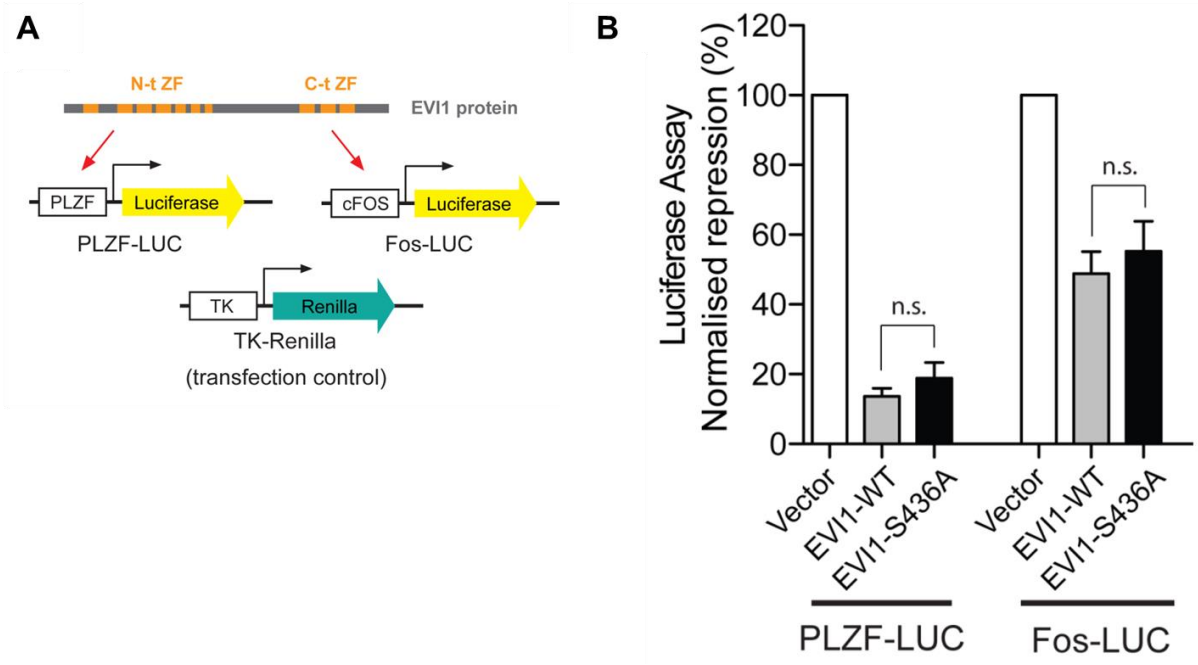

Figure 3.13: EVI1-mediated minimal promoter repression. (A) *Schematic representation of the vectors used in the dual-luciferase assay along with the zinc-finger domains known to mediate the promoters within the vectors.* ***(B)*** *The repression of both the PLZF-luc (left panel) and Fos-LUC (right panel) minimal promoters in Rat1 fibroblast transfected with either vector-only control, EVI1-WT or EVI1-S436A encoding plasmids. Vector-only control was used to normalise repression. (T-test, ns=not significant) (n=3).*

I next investigated EVI1-WT with S436 available for phosphorylation compared with EVI1-S436A in the Rat1 fibroblast model. Initially the effect of S436A mutation on proliferation was investigated in Rat1 fibroblasts. Cellular proliferation over 72 hours

was not altered by transduction with EVI1-WT or EVI1-S436A compared to vector-only control (*Figure 3.14 A*). At both 96 and 120 hours the EVI1-WT and EVI1-S436A transduced cells had proliferated significantly more than the vector-only control transduced cells. There was no significant difference between EVI1-WT and EVI1-S436A. As previously demonstrated (*Figure 3.2*), transduction with EVI1-WT resulted in significantly more colonies than the vector-only control (*Figure 3.14 B*). Transduction with EVI1-S436A also resulted in a significant increase in colony formation compared to the vector-only control, but there was no difference when compared to EVI1-WT transduction (*Figure 3.14 B*). To control for the effect of site-directed mutagenesis on the transformation of Rat1 fibroblasts, cells were also treated with H_2O_2. Mutation of the S436 site had no effect on colony forming ability in the presence of genotoxic stress (*Figure 3.14 B*).

EVI1-WT with S436 available for phosphorylation was also investigated in mouse embryonic fibroblasts (MEFs). Historically MEFs have been used as feeder cells for the culture of mouse embryonic stem cells[221]. However, more recently the transformation of these cells have been used to study oncogenes[222]. Transduction with either EVI1-WT or EVI1-S436A produced significantly more colonies than the vector-only control in the presence or absence of genotoxic stress (*Figure 3.14 C*). Again, there was no difference when comparing EVI1-WT to EVI1-S436A transduction. These results confirm that mutation of the EVI1 S436 phosphorylation site did not alter the colony forming ability in Rat1 fibroblasts and MEFs.

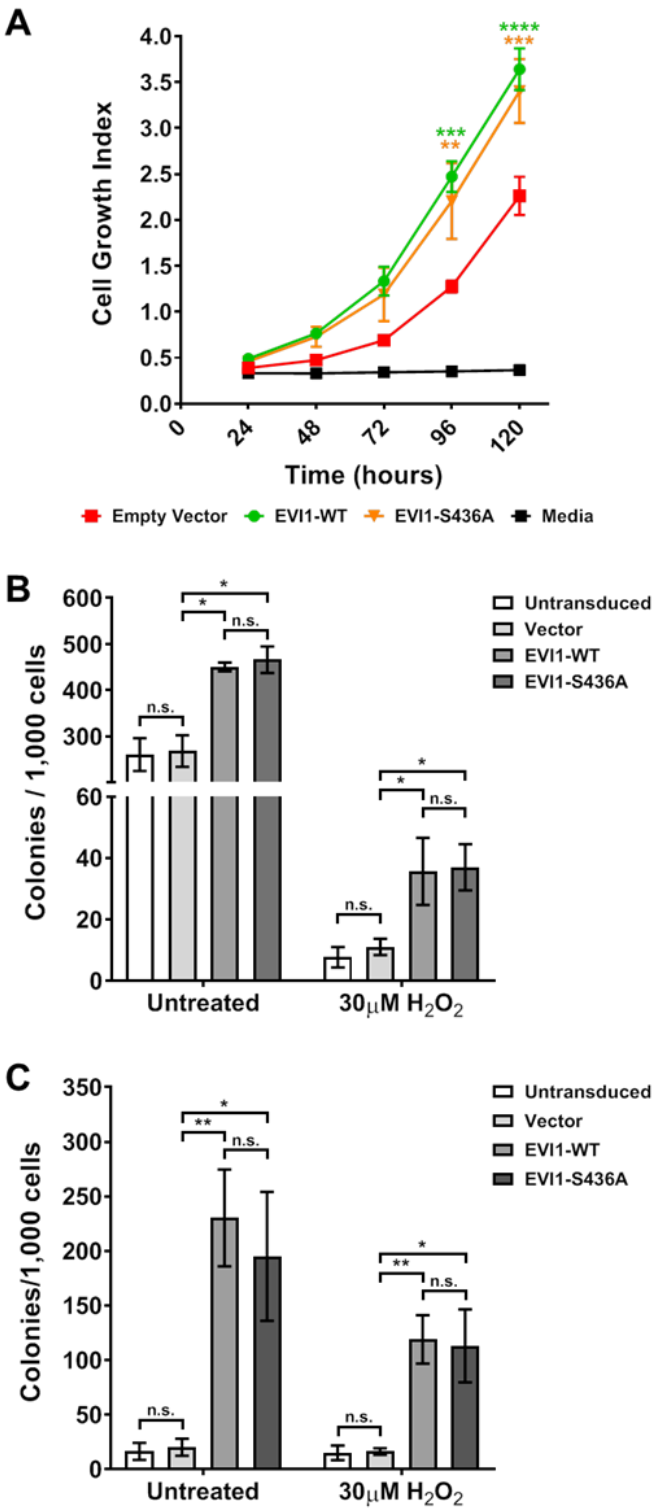

Figure 3.14: EVI1-mediated transformation of Rat1 Fibroblast and Mouse Embryonic Fibroblasts. (A) *The proliferation of stable transduced Rat1 fibroblast with vector-only control, EVI1-WT or EVI1-S436A encoding lentiviral plasmids over a 120 hour period. WST-1 used as a marker for proliferation. Statistical analysis: two-way ANOVA, Tukey posttest (n=3) (** p<0.01, *** p<0.001, **** p<0.0001).* ***(B)*** *The colony formation of stable transduced Rat1 fibroblast with either vector-only*

control, EVI1-WT or EVI1-S436A. Additional control included non-transduced Rat1 fibroblast. Statistical analysis: one-way ANOVA, Tukey posttest (n=4) (p<0.05, ** p<0.01, *** p<0.001, **** p<0.0001, ns=not significant).* ***(C)*** *The colony formation of stable transduced mouse embryonic fibroblasts with either vector-only control, EVI1-WT or EVI1-S436A. Additional control included non-transduced mouse embryonic fibroblast. Statistical analysis: one-way ANOVA, Tukey posttest (n=3) (* p<0.05, ** p<0.01, ns=not significant)*

3.3.2 S436 Availability for Phosphorylation is Required for EVI1-Mediated Haematopoietic Self-Renewal

The function of or effect of the availability of S436 for phosphorylation was investigated in murine haematopoietic Kit+ stem and progenitor cells (Kit+ HSPCs). Transduction of Kit+ HSPCs with either EVI1-WT or EVI1-S436A resulted in equal levels of GFP positive cells and median fluorescence intensity of GFP signal by FACS sorting (*Figures 3.15 A & B*). Transduction resulted in equal levels of expression of either *EVI1-WT* or *EVI1-S436A* mRNA, suggesting equal expression of EVI1 after transduction (*Figures 3.15 C*).

Consistent with previously published data[112,125,131], and results above with respect to the workup of the SQS motif (*Figure 3.3*), transduction of murine Kit+ HSPCs with EVI1-WT confers re-plating potential over three rounds of plating when compared to vector-only transduced cells (*Figures 3.15 D*). In comparison to EVI1-WT, transduction with EVI1-S436A resulted in significantly fewer colonies beyond round two of re-plating (*Figures 3.15 D*). The levels of colony numbers with EVI1-S436 were similar to vector-only in rounds two and three. This was in contrast to the transformation of Rat1 fibroblasts and MEFs, in which proliferation and colony forming ability was not affected by the S436A mutation, emphasizing the higher sensitivity of Kit+ re-plating assay (*Figure 3.14*).

Upon morphological assessment, transduction with EVI1-WT sustained significantly more blast-like cells compared to vector-only transduction over all three rounds of re-plating (*Figures 3.15 E & F*). In agreement with the decreased re-plating observed, transduction with the EVI1-S436A mutant was unable to sustain an elevated level of blast-like cells compared to vector-only transduction beyond the first round of re-plating (*Figures 3.15 E & F*). Only transduction with EVI1-WT sustains clonogenic

activity of Kit+ HSPCs in comparison with vector-only control cells over three rounds, not the EVI1-S436A mutant. The S436A mutation abrogates EVI1-mediated colony forming potential, suggesting an essential function for EVI1-S436 site available for phosphorylation in sustaining EVI1-mediated self-renewal of murine Kit+ HSPCs.

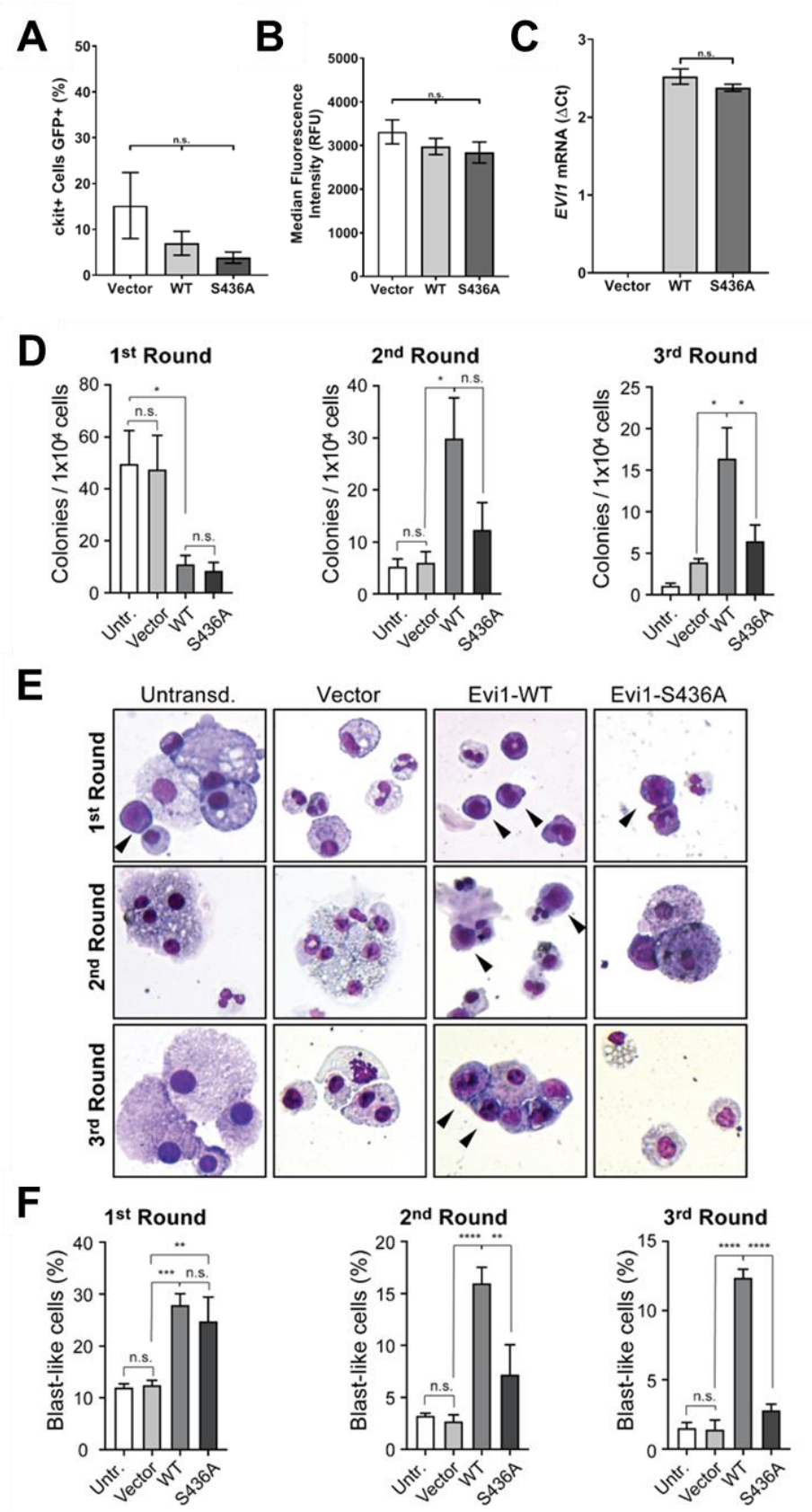

Figure 3.15: The EVI1-mediated self-renewal in Kit+ HSPCs. (A) *Percentage of GFP positive cells during FACS sorting of Kit+ HSPCs transduced with either EVI1-WT, EVI1-AQA or vector-only control*

lentiviral plasmids. ***(B)*** *Median Fluorescence Intensity (MFI) of vector-only, EVI1- WT and EVI1-S436A sorted Kit+ HSPCs.* ***(C)*** *Quantitative RT-PCR EVI1-WT and EVI1-S436A mRNA expression in sorted Kit+ HSPCs from A.* ***(D)*** *Colony counts (n= 6, 6 different mice) of transduced Kit+ HSPCs after 1st round (left), 2nd round (middle) and 3rd round (right) of re-plating.* ***(E)*** *Representative panels of the May- Grünwald stain of cells collected and cytospan from the colonies produced after the first, second and third rounds of re-plating from D. Black arrowheads indicate a typical blast-like cell morphology.* ***(F)*** *Quantitation of the blast-like cells from 1st round (left), 2nd round (middle) and 3rd round (right) of re-plating as a percentage of total cells counted. Statistical analysis for A/B/D/F: one-way ANOVA, Tukey posttest (n=6) (* p<0.05, ** p<0.01, *** p<0.001, n.s.= not significant). Statistical analysis for C: two-tailed t-test (n=3) (n.s.=not significant)*

3.3.3 Phosphorylatable S436 EVI1 Directs transcriptional Changes Associated with Self-Renewal

To investigate the effect of phosphorylatable S436 on the transcriptome, EVI1-WT and EVI-S436A were expressed in murine Kit+ HSPCs for 48 hours, and the effects on EVI1-mediated transcriptional patterns were compared by RNA sequencing (RNAseq) (*Methods 2.3.2*). Vector-only transduced and untransduced controls were also analysed in biological triplicates. The analysis was carried out by Dr Adam Stevens and Dr Fabio Amaral. Unsupervised principal component analysis of gene expression patterns showed tight clustering of replicates for EVI1-S436A transduced samples, while in concordance with availability of S436 for phosphorylation EVI1-WT-transduced replicates clustered with a wider distribution and partial overlap with EVI1-S436A (*Figure 3.16 A*). A group comparison between EVI1-WT and vector-only transduced cells revealed a total of 653 genes significantly changed, 497 upregulated and 156 downregulated by applying a cut off log-fold change (FC) of >0.6 and a false discovery rate (FDR)-adjusted p-value of <0.05 (*Figure 3.16 B*). Amongst these were known EVI1-regulated genes such as the stem cell marker *Aldha1a*, and more than half of the top 40 upregulated genes identified in a previous study investigating the effect on EVI1-transduction on murine haematopoietic precursors[112]. In this group was also downregulated *Cepba*, previously shown to be repressed by EVI1-mediated interference in myeloid maturation[223] (*Figure 3.16 C*). Comparing EVI1-S436A with vector-only controls, expression of 816 genes changed significantly (567 upregulated, 249 downregulated) (*Figure 3.16 B*). Strikingly, 444 of

these genes changed concordantly with EVI1-WT, including *Aldh1a1* (*Figure 3.16 B, C & D*). Amongst 372 genes changing significantly exclusively with EVI1-S436A the upregulation of *Spi1* was identified, which is involved with EVI1-driven myeloid haematopoietic skewing[224], and downregulation of *Ms4a3*, of which repression has previously been implicated in EVI1-mediated malignant progression[225]. Also *Gbp6*, *Nqo1* and *Cdh17*, which were previously shown to be regulated by EVI1 in murine progenitor cells[112], were significantly changed exclusively via the non-phosphorylatable EVI1-S436A. Many genes, including *Spi1* and *Ms4a3* showed concordant changes both with EVI1-WT and EVI1-S436A, albeit not reaching significance in one or the other group (*Figure 3.16 C*), further illustrating a broad overlap of EVI1-WT and EVI1-S436A mediated gene expression patterns after 48hrs.

In order to delineate expression patterns that significantly discriminate EVI1-WT from EVI1-S436A transduced cells, a group ANOVA test was applied to the dataset: 620 genes discriminated EVI1-WT, EVI1-S436A and vector-only transduced cells with a p-value range of 2.3x10-8 to <0.01 (*Figure 3.17 A*). Significantly and exclusively modulated by EVI1-WT, were 78 genes. Of these, 64 genes were upregulated (*Figure 3.17 A - green cluster*), and 14 downregulated (*Figure 3.17 A - orange cluster*). Significantly and exclusively upregulated by EVI1-S436A were 19 genes (*Figure 3.17 A - yellow cluster*) and repressed exclusively by EVI1-S436A were 87 genes (*Figure 3.17 A - brown clusters*). Comparing EVI1-WT (with EVI1-S436 available for phosphorylation) with EVI1-S436A transduction, it was demonstrated that genes exclusively and significantly regulated by EVI1-WT displayed a significantly narrower diversity of connections than EVI1-S436A ($p < 2.2x10-16$) (*Figure 3.17 B & C*). Moreover, a hypernetwork generated with the EVI1-S346A mutant regulated patterns had significantly higher entropy than EVI1-WT regulated ($p < 2.2x10-16$), demonstrating that coordination of the higher connectivity between the genes in S436A regulated patterns was low (*Figure 3.17 D*). It follows that the effect on the entire transcriptome conferred by EVI1-WT transduction, correlating with self-renewal, had a significantly more coordinated and focussed effect than that of non-phosphorylatable EVI1-S436. Hypernetwork connectivity and entropy were greater with EVI1-S436A transduction than in hypernetworks of the same size

generated from randomly selected genes iterated 1000 times (p<2.2x10-16) (*Figure 3.17 E & F*).

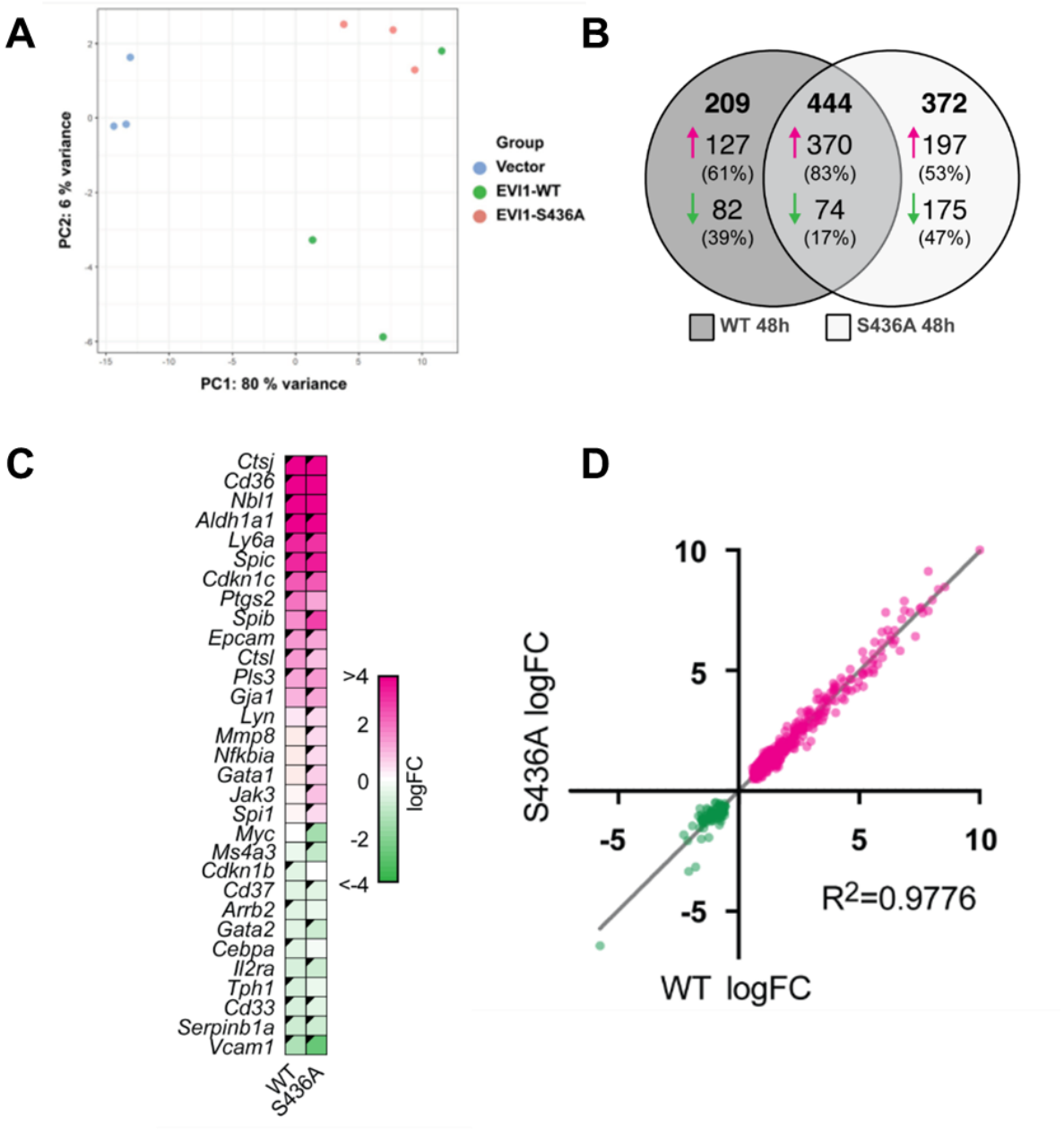

Figure 3.16: Gene expression of EVI1 in Kit+ HSPCs by RNAseq analysis. (A) *Unsupervised principal component analysis of transcriptomic data. Data was processed and regularised log transformed in DEseq2. The top 500 gene based on variance were used to generate the figure.* ***(B)*** *Two way comparison of RNAseq data. EVI1-WT vs vector-only and EVI1-S436A vs vector-only transduced Kit+ HSPCs. Venn diagram of transcripts significantly changed by EVI1-WT or EVI1-S436A (adj. p>0.05, FC>0.6).* ***(C)*** *Heatmap illustration of selected differentially expressed genes in the two way comparison (black triangle: adj.p<0.05).* ***(D)*** *Regression analysis comparing fold-change of significantly (p<0.05) changing transcripts in EVI1-WT and EVIi1-S436A transduced cells.*

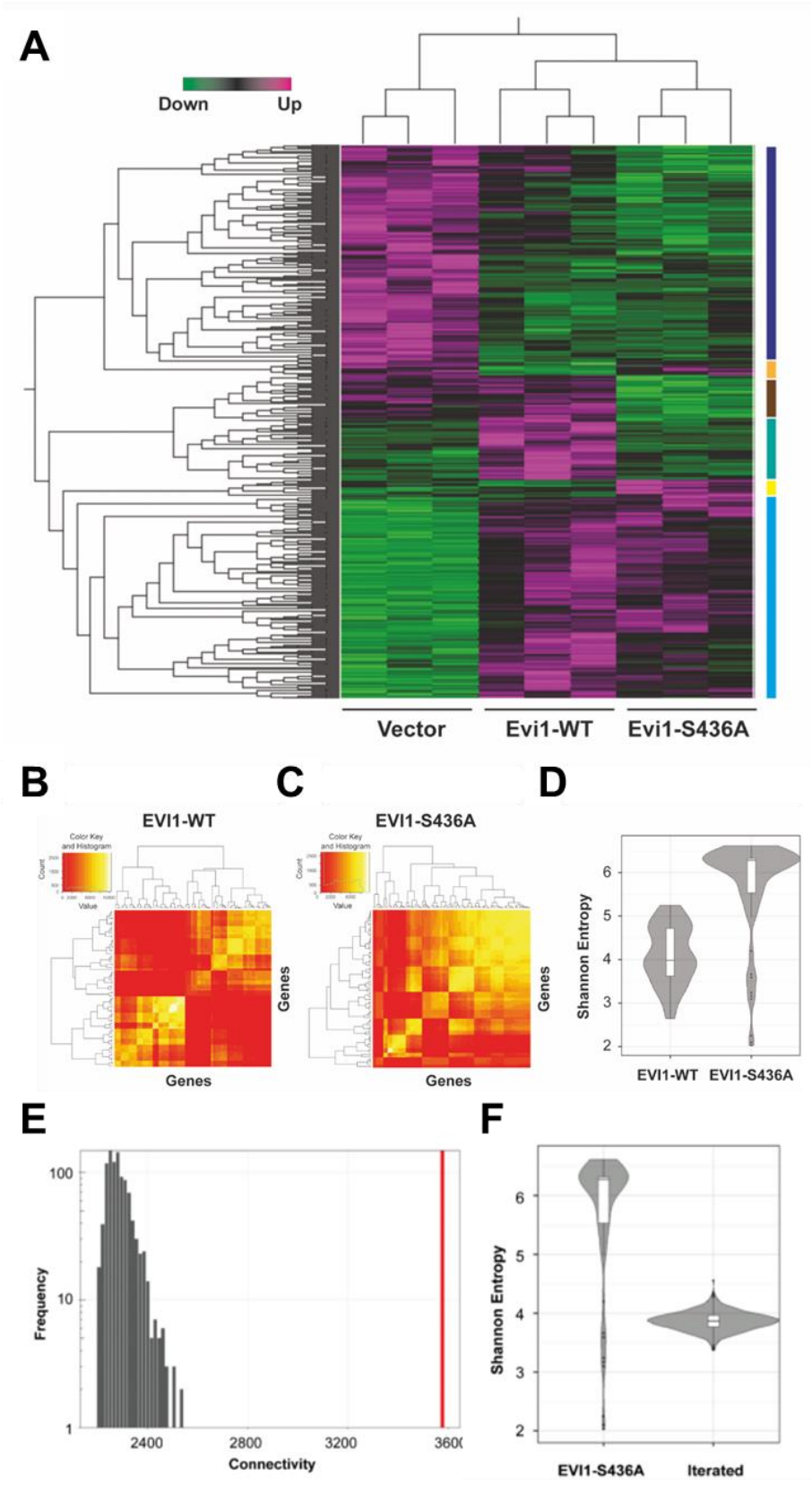

Figure 3.17: Gene expression of EVI1 in Kit+ HSPCs by RNAseq analysis. (A) *Heat map illustration of group-ANOVA analysis of vector-only, EVI1-WT and EVI1-S436 transduced Kit+ HSPCs, adj. p -value range of 2.3e-8 to <0.01.* ***(B & C)*** *Hypernetwork heatmap for EVI1-WT (n=78*

transcripts, mean connectivity = 2376) and EVI1-S436A (n=106 transcripts, mean connectivity = 3561) respectively. Colour intensity represents number of binary relationships shared between a pair of transcripts with the rest of the transcriptome (n=23766 total transcripts). ***(D)*** *Shannon entropy in EVI1-WT (n=78) and EVI1-S436A (n=106) induced hypernetworks (p<2.2e-16).* ***(E)*** *Iterated connectivity and Hypernetwork connectivity (number of binary relationships shared between a pair of transcripts with the rest of the transcriptome (n=23766)) of a random set of 106 genes iterated 1000 times. Red line indicates the comparison of mean connectivity of the EVI1-S436A hypernetwork (p<2.2e-16).* ***(F)*** *Entropy analyses Shannon entropy calculated from EVI1-S436A hypernetwork compared with hypernetworks generated from 106 randomly selected genes iterated 1000 times (p<2.2e-16).*

3.3.4 EVI1-S436 phosphorylation negatively affects interaction with CtBP1

Given the location of S436 between the EVI1 zinc finger motifs (*Figure 1.2*), and as mutation of the site did not affect promoter affinity with respect to repression of *PLZF* and *FOS* (*Figure 3.13*), the gene expression patterns directed by phosphorylation of S436 are unlikely to be a result of differential DNA binding. Therefore it was investigated whether mutation of S436 alters the EVI1-protein interaction with the transcriptional regulator CtBP1, as the S436 site is located in close proximity to the CtBP binding motifs (*Figure 1.2*), and interaction with CtBP1 has been shown to be essential for EVI1-mediated haematopoietic self-renewal[93,94,118]. The subsequent *in silico* analysis was performed by Dr Batool Almarzouq with the *in vitro* confirmation of the analysis and co-IP with RUVBL carried out by me.

Cross species sequence alignment of the region of EVI1 (426-598aa) revealed conservation of the serine 436 and both CtBP binding motifs suggesting the region was important for structure and function of the EVI1 protein (*Figure 3.18 A*). As the tertiary structure of EVI1 is not fully resolved, the structure of the region was modelled using Iterative-Threading Assembly Refinement (I-TASSER)[203]. This analysis predicted several α-helix formations involving S436 and both CtBP binding sites (*Figure 3.18 A & B*). Given that the crystal structure of CtBP1 is largely resolved[204,226,227], the docking of the predicated 426-598aa region of EVI1 with CtBP1 was modelled using ClusPro[205] (*Figure 3.18 C*). Using *Gromacs* with 400ns molecular dynamics (MD)[209,213,214], the effect of S436 phosphorylation on EVI1-

CtBP1 interaction was also simulated. This analysis predicted a stable α-helix configuration within the 553-557 CtBP binding site (*Figure 3.18 A*) for modelled docking with CtBP1 residues 28-378 (*Figure 3.18 B & C*). However, phosphorylation of S436 was predicted to destabilise the α-helix formation, which would potentially disrupt the EVI1-CtBP1 interaction (*Figure 3.18 D*). Using Molecular Mechanics-Poisson Bolzmann Surface Area (MM-PBSA)[213], the binding affinity of the 426-589 region of EVI1 to CtBP1 was calculated. Estimation of the binding energy for the EVI1-CtBP1 interaction predicts that S436 phosphorylation unfavourably shifts the binding energy by approximately 100 kJ/mol ($\Delta G_{binding} > 0$) as a result of the phosphate group altering electrostatic energy (*Figure 3.18 E*). EVI1 non-phosphorylated at S436 had favourable ($\Delta G_{binding} < 0$) binding energy in the EVI1-CtBP1 complex (*Figure 3.18 F*), where phosphorylation at S436 shifts the mean contribution unfavourably from -2.9 KJ/mol to 19.47 KJ/mol. Here the modelling predicts that S436 phosphorylation negatively impacts the affinity of EVI1 for CtBP1.

To verify these predictions experimentally, co-immunoprecipitation of CtBP1 with FLAG-tagged EVI1-WT and EVI1-S436A in HEK293FT cells was quantified. In agreement with the *in silico* prediction, there was a significant increase in the association of non-phosphorylatable EVI1-S436A with CTBP1 compared to EVI1-WT (*Figure 3.19 A & B*). As a control to exclude any non-specificity in the higher CtBP1 affinity of EVI1-S436A, the co-immunoprecipitation of the AAA-ATPase RUVBL2 was also quantified. RUVBL2 has previously been shown to interact with EVI1[95] and is functionally relevant for other leukaemogenic transcription factors[140,228]. In contrast to CtBP1 affinity, phosphorylatable EVI-WT showed significantly higher affinity to RUVBL2 compared to the non-phosphorylatable EVI1-S436A (*Figure 3.19 A & B*).

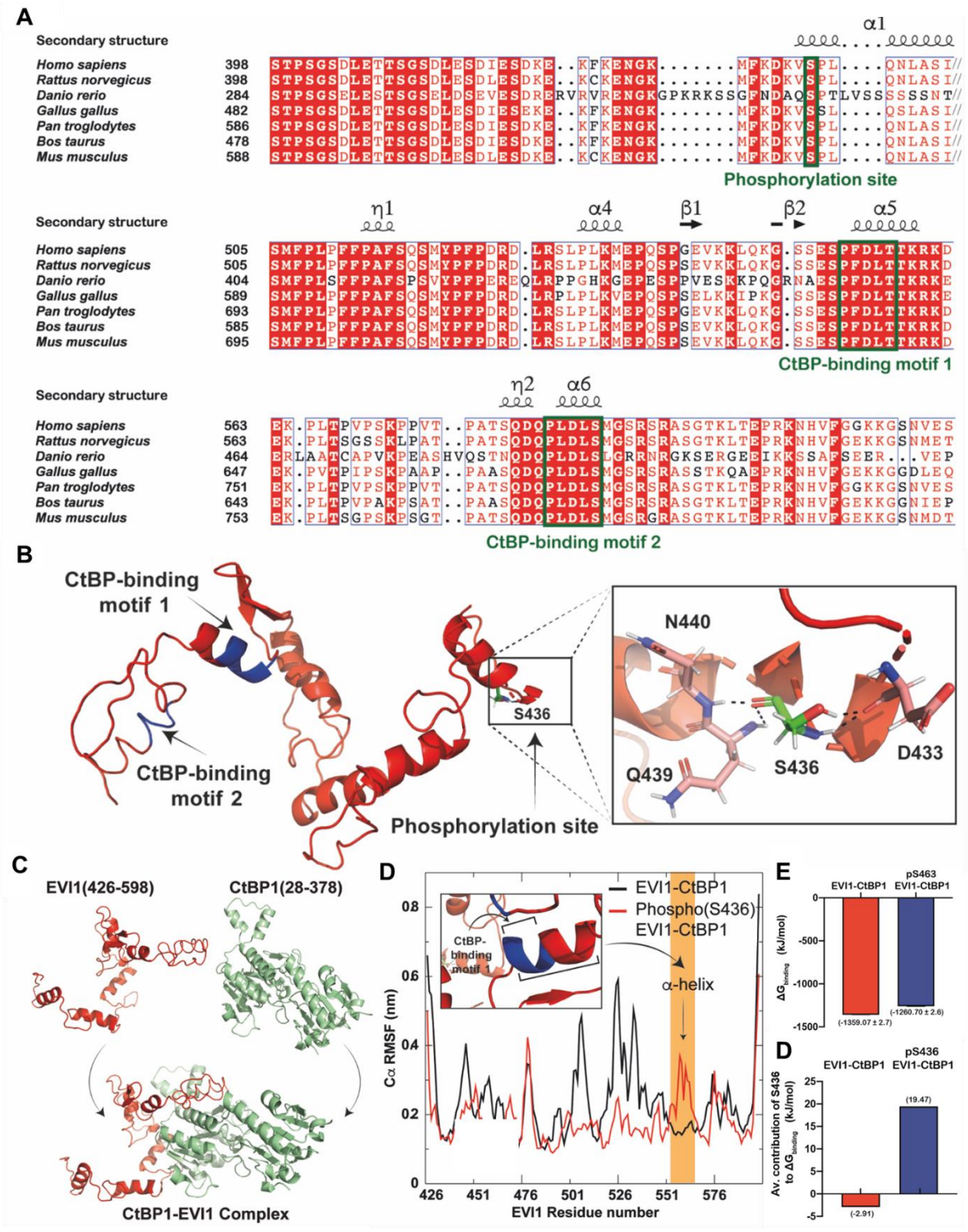

Figure 3.18: Modelling of EVI1-S436 phosphorylation on CtBP1 affinity ***(A)*** *Alignment for the full-length amino acid sequences of EVI1 in Homo sapiens (Uniprot Q03112), Mus musculus (Uniprot P14404), Rattus norvegicus (Uniprot D3ZM26), Danio rerio (Uniprot F1Q834), Gallus gallus (Uniprot A0A3Q2U4Z4), Pan troglodytes (Uniprot A0A2I3RS65) and Bos taurus (Uniprot A0A3Q1LI16) were aligned using MUSCLE and visualized by ESPript and aligned.* ***(B)*** *Three dimensional prediction of*

the I-TASSER generated structure of the EVI1 region as in A. Both CtBP-binding motifs (blue) and the S436 site are part of predicted α-helix structures. Hydrogen bonds formed by Ser436 with Gln440, Gln439 and Asp433 residues (dashed lines). ***(C)*** *I-TASSER-generated model of EVI1(aa426-598) for modelling the interaction between EVI1 and CtBP1 using ClusPro server. Both CtBP-binding motifs were used when setting attraction in the docking parameters in ClusPro.* ***(D)*** *Modification of the complex according to the force field parameters of GROMOS 54A7 for effect of EVI1-S436 phosphorylation. Molecular dynamics simulations (400ns) for modelling EVI1 complexation with CtBP1. Root mean square fluctuation (RMSF) plot of Cα atoms of EVI1 in EVI1-CtBP1 complex and phospho(S436) EVI1-CtBP1 complex. Yellow: region of EVI1 structure (553-566) affecting the α-helix stability containing the CtBP1-binding motif 1 (553-557).* ***(E)*** *Comparative estimation of binding energy in EVI1-CtBP1 complex with and without EVI1-S436 phosphorylation, calculated using the Molecular Mechanics-Poisson Bolzmann Surface Area (MM-PBSA). Phosphorylation at S436 in EVI1-CtBP1 complex changes the binding energy by 100 kJ/mol.* ***(F)*** *Contribution of S436 to the binding free energy was calculated by means of energy decomposition which shows that the average contribution of S436 to the binding energy in EVI1-CtBP1 complex had shifted unfavourably from -2.9 KJ/mol to 19.47 KJ/mol after phosphorylation.*

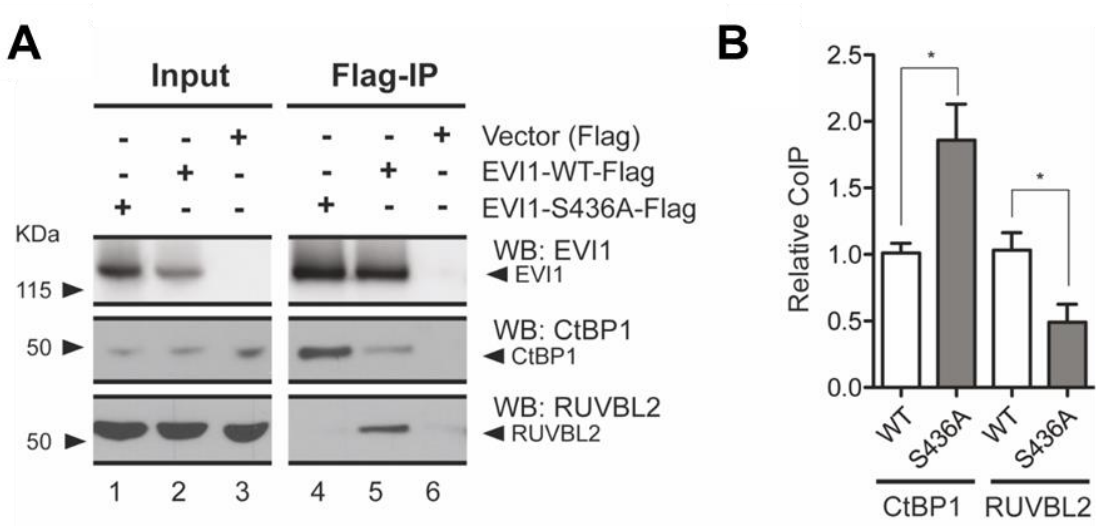

Figure 3.19: Experimental confirmation of EVI1-S436 phosphorylation on CtBP1 affinity. (A) *HEK293 cells transfected with flag-tagged EVI1-WT or EVI1-S436A; protein extracts were subjected to Flag-magnetic beads immunoprecipitation to quantify EVI1-CtBP1 co-Immunoprecipitation. Quantitation of immunoprecipitated RUVBL2 used as a control.* ***(B)*** *Quantitation of independent Co-IP assays (n=3, unpaired, two-tailed Student's t-test * p<0.05) as shown in E.*

3.3.5 Preferential Association of EVI1-WT with Target-Specific Kinases and DNMT3a

To investigate the effect of phosphorylatable S436 on EVI1-protein affinity and to determine possible kinases involved, a colleague in the group (Dr Roberto Paredes) expressed FLAG-tagged EVI1-WT and EVI1-S436A in HEK293 cells and carried out affinity purification by FLAG-IP. Mass spectrometry analysis versus vector-only control was performed by Dr Bethany Geary. Data analysis considered another MS study of MECOM encoded proteins and previously described protein interactions[95,146] (*Appendix Table 7.2*). In addition, further analysis was performed using the "CRAPome" platform to consider non-specific interactions[229]. With EVI1-WT and EVI1-S436A 926 and 702 proteins were co-immunoprecipitated respectively. Of these, 263 proteins co-immunoprecipitated with both EVI1-WT and EVI1-S436A (*Figure 3.20 A*). The number of detected proteins was similar to that in the interactome study concerning MECOM encoded proteins in T47D breast cancer cells[146]; with which there was a considerable overlap: 209 proteins in the dataset (22%) were also found in the Ivanochko study (*Appendix Table 7.2*). Of these 209 proteins, 89 were detected exclusively in the EVI1-WT interactome, 65 in both IPs, and 55 exclusively in the EVI1-S436A interactome. Of the previously described 102 proteins that interact with EVI1[95] (*Appendix Table 7.2*), 21 were identified in the dataset, of which 17 were detected exclusively in the EVI-WT IP, and three in both. Only one previously described EVI1-interacting protein (PRDX1) was detected exclusively with EVI1-S436A[95]. Here it was demonstrated that phosphorylatable EVI1-WT interacts with more proteins and co-immunoprecipitates with more known EVI1-interactors than EVI1-S436A.

Several kinases were identified in the EVI1-WT interactome. An *in silico* analysis of the DKVSPLQNLASINNK sequence of EVI1, using *PhosphoNet*[202]*,* showed that EVI1-S436 is located in a protein sequence that is a putative target of multiple kinases (*Figure 3.20 B*), including CDK2 and CDK3. Both CDK2 and CDK3 were detected in the EVI1-WT interactome. The casein kinase CSNK2A1 was also detected, which has previously been implicated in EVI1 phosphorylation[95]. Only a few of the proteins that co-immunoprecipitated with EVI1 have been investigated functionally for potential biological relevance, and for most, a role in haematopoietic self-renewal is elusive. However, in the EVI1-WT, but not in the EVI1-S436A

interactome the DNA methyltransferase DNMT3A was detected. DNMT3A has an essential role in haematopoiesis, interacts with EVI1[168,175], and has been suggested to mediate EVI1-directed methylation patterns in AML[165]. To confirm this MS finding, HEK293 cells were transfected with HA-tagged DNMT3A, and with EVI1-WT and EVI1-S436A. Quantitative co-immunoprecipitation of EVI1 and DNMT3A demonstrated a higher affinity of EVI1-WT with DNMT3A compared with EVI1-S436A (*Figure 3.20 C & D*), corroborating the MS findings.

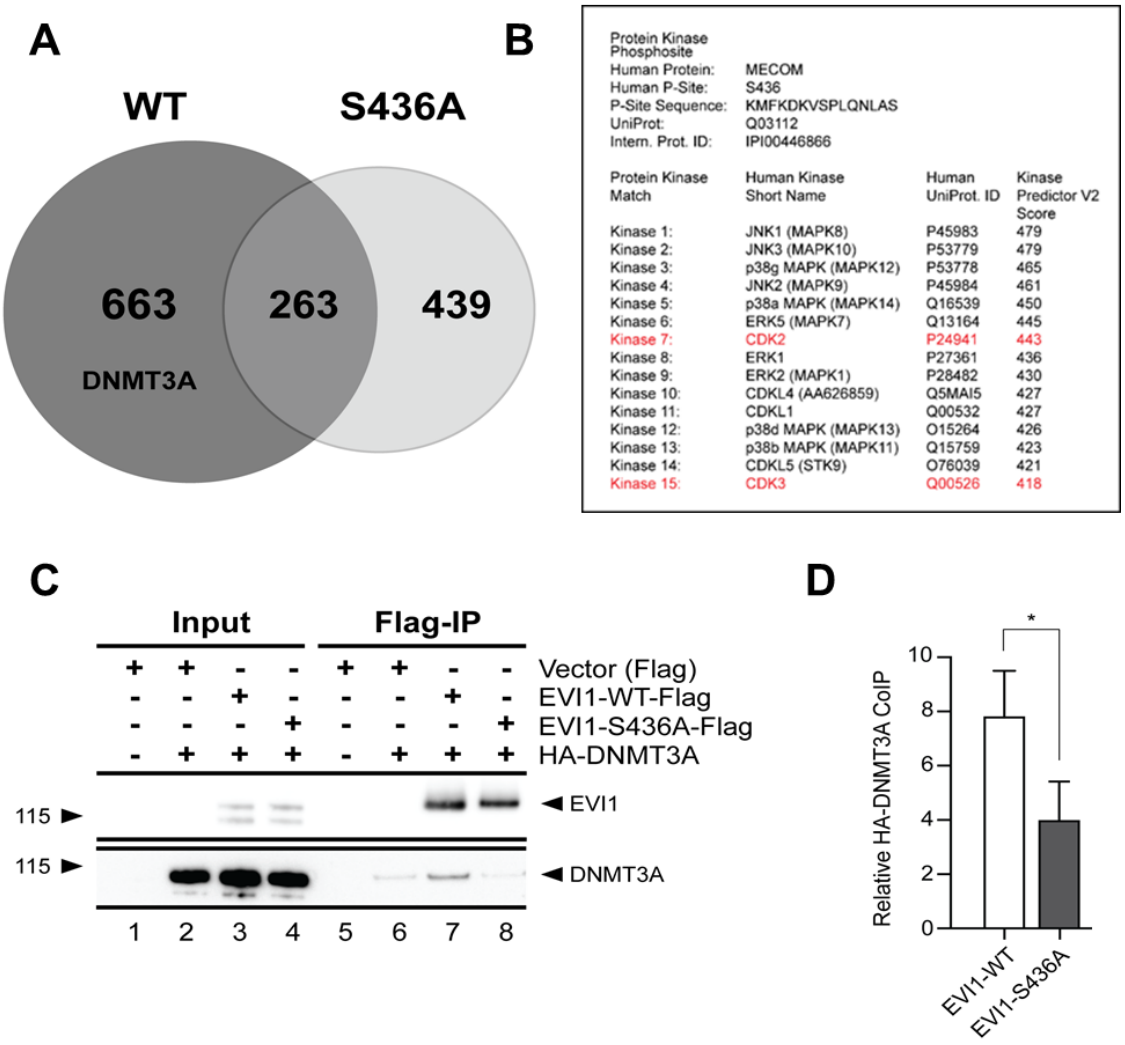

Figure 3.20: Protein association of EVI1-WT and EVI1-S436A. (A) *Venn diagram showing the number of proteins associated with EVI1- WT (dark grey) or EVI1-S436A analysed by affinity purification and mass spectrometry of co-immunoprecipitated proteins.* ***(B)*** *In silico analysis of the EVI1 protein sequence, using PhophoNet (Kinexus) (http://www.phosphonet.ca/). Listed are the top 15 candidate kinases that phosphorylate the DKVSPLQNLASINNK sequence of EVI1.* ***(C)*** *Co-immunoprecipitation of Flag-tagged EVI1-WT and EVI1-S436A, and HA-tagged DNMT3A in HEK293*

cells and western blotting. ***(D)*** *Signal quantitation of co-immunoprecipitated DNMT3A (n=3. unpaired, two-tailed Student's t-test; * p<0.05).*

3.3.6 S436 Available for Phosphorylation is Required for EVI1-Mediated DNA-Methylation Patterns

As previously outlined (*Introduction 1.4.6.2*), DNMT3a is an essential mediator of *de novo* cytosine DNA methylation in haematopoietic self-renewal[168]. One of the biologically probably highly relevant findings was the preferential interaction of DNMT3a with phosphorylatable EVI1-WT. This was first further investigated in the Rat1 fibroblast model, where I assessed methylation by 5-methylcytosine (5mC) staining. Transduction with EVI1-WT resulted in a significant increase in DNMT3a staining compared to vector-only transduction (*Figure 3.21 A & B*). There was some degree of co-localisation between the EVI1 and DNMT3a stains. The EVI1-S436A mutant also conferred an increased in DNMT3a staining compared to the vector only control, but there was no significant change in staining compared to EVI1-WT (*Figure 3.21 A & B*). The indication of increased co-localisation of DNMT3a staining and EVI1 staining in EVI1-WT transduced cells was in agreement with the preferential interaction of EVI1-WT with DNMT3a. The majority of cells transduced with EVI1-WT have little to no staining for 5mC (*Figure 3.21 C*). Quantification of the 5mC staining reveals significantly less staining in cells transduced with EVI1-WT compared to the vector-only control (*Figure 3.21 C & D*). Transduction with EVI1-S436A also resulted in significantly less 5mC staining compared to the vector control (*Figure 3.21 C & D*). However, the EVI1-S436A mutant was not associated with a reduction of 5mC staining to the same extent as EVI1-WT: the majority of cells still had some degree of 5mC staining (*Figure 3.21 C & D*). The lower levels of 5mC staining with phosphorylatable EVI1-WT could be causatively linked to the preferential protein interaction with DNMT3A.

The 5mC staining patterns were next investigated in the transduced Kit+ HSPCs model. First it was confirmed that untransduced Kit+ HSPCs had the distinct speckled 5mC staining as previously described[230] (*Figure 3.22*). In cells transduced with EVI1-WT, but not with EVI1-S436A, there was a distinct population of 5mC negative cells (*Figure 3.23 A, E & F*). This observation was quantified by correlating

the signal distribution of 5mC with the EVI1 signal in Kit+ HSPCs transduced with EVI1-WT and EVI1-S436A. With EVI1-WT transduction there was no correlation between EVI1 and 5mC staining (r=0.0379, range -1 for total exclusion, 1 for total association)) (*Figure 3.23 B & E*) as a result of the distinct population with high EVI1 signal but low or absent 5mC staining (*Figure 3.23 C & D*). In contrast, the absence of a cell population with low or absent 5mC staining in EVI1-S436A transduced Kit+ HSPCs resulted in a significantly higher correlation of the 5mC with the EVI1 signal (*Figure 3.23 B & F*) (r=0.517). These results suggest that the EVI1-S436 available for phosphorylation was important to the methylation patterns in cells with overexpression of EVI1.

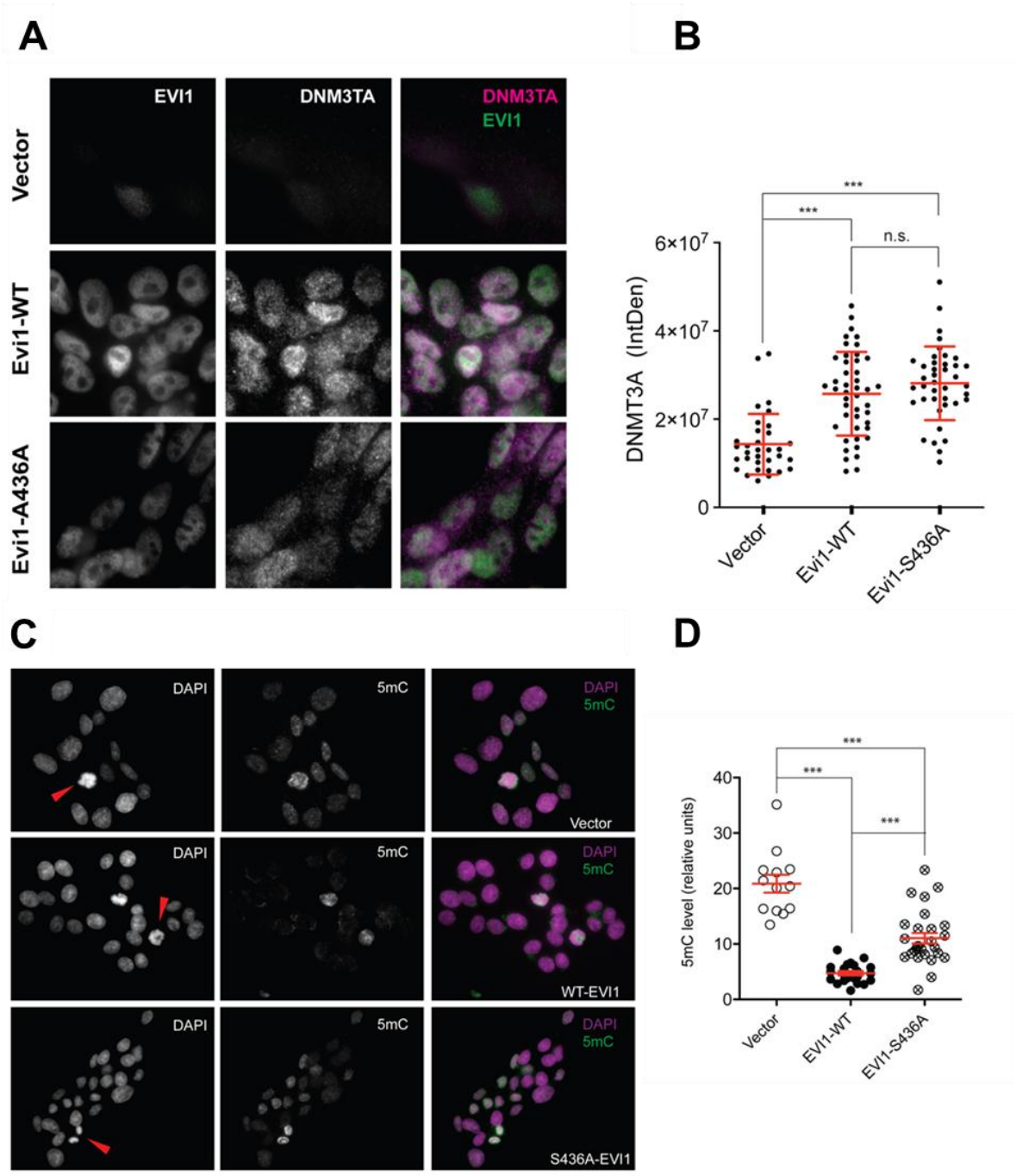

Figure 3.21: EVI1 association with 5mC methylation and co-localisation with DNMT3a in Rat1 fibroblasts. (A) *Immunofluorescence of EVI1 and DNMT3a in transduced Rat1 fibroblast cell lines. White staining in column three indicates co-localisation of the stain.* ***(B)*** *Quantification of the DNMT3a stain signal by integrated density. Statistical analysis: one-way ANOVA, Tukey posttest (n=3) (*** p<0.001, n.s.= not significant)* ***(C)*** *Immunofluorescence of DNA methylation by 5-methylctyosine (5mC) staining and nuclear staining with DAPI. Orange arrowheads indicate cells in mitosis.* ***(D)*** *Quantification of the 5mC stain signal by integrated density. Statistical analysis: one-way ANOVA, Tukey posttest (n=3) (*** p<0.001, n.s.= not significant)*

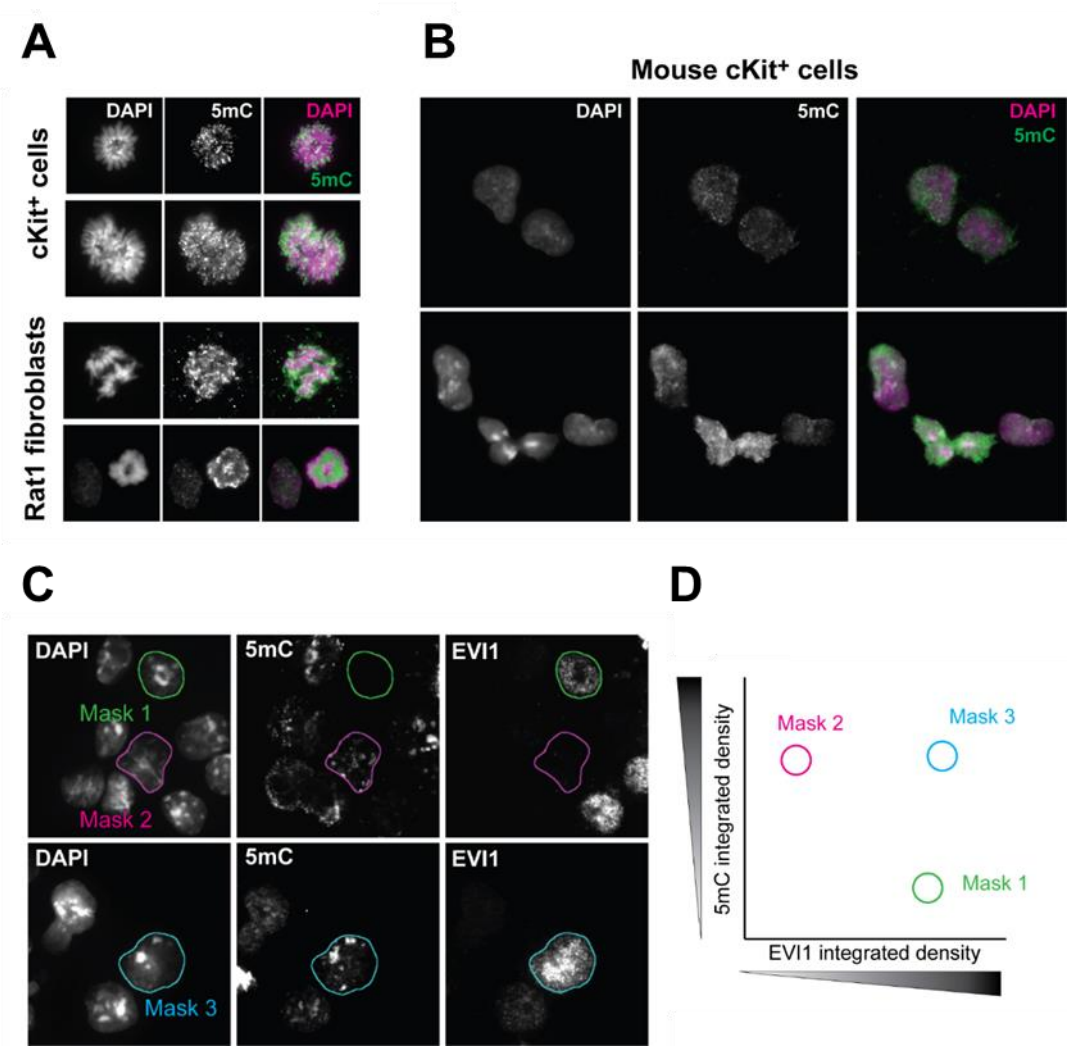

Figure 3.22: Validation of 5-mC immunofluorescence. *(**A)** Kit⁺ (upper panels) or Rat1 fibroblasts (bottom panels) mitotic cells were stained with the 5mC antibody. DAPI: chromatin **(B)** Kit+ HSPCs were stained with the 5-mC antibody. DAPI: chromatin **(C)** Quantitation of 5-mC and EVI1 signals. Reference Regions of interest (ROI) covering the entire positively stained area of the nuclei (DAPI stain), annotated as mask, and were used for analysis of signal level of EVI1 and 5-mC. The integrated density was calculated to generate a dispersion plot **(D)** Schematic representation. Cells with high EVI1 and 5-mC signals score a high Pearson's coefficient (Mask 3). Cells with high EVI1 signal and low 5-mC signal (Mask 1), score a low Pearson's coefficient.*

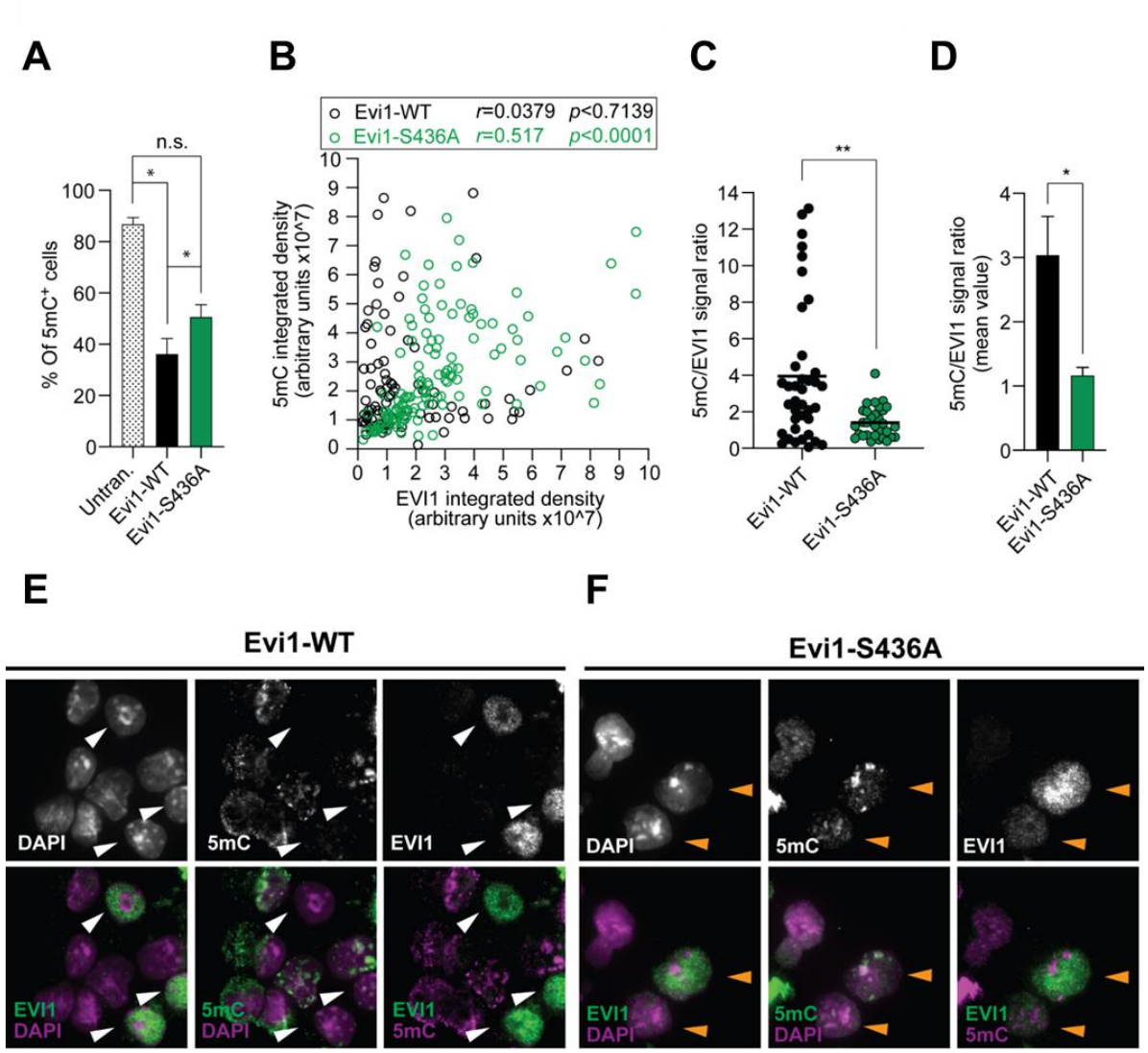

Figure 3.23: DNA methylation patterns in EVI1-transduced Kit+ HSPCs. . (A) *Quantitation of total 5-meC signal in Kit+ HSPCs after transduction with EVI1-WT or EVI1-S436A. Cells were scored by presence or absence of 5-meC IF stain (One-way ANOVA, Tukey posttest, * p<0.05).* ***(B)*** *Correlation of the EVI1 and 5-meC signals by Pearson's test (r range -1 for total exclusion, 1 for total association) for EVI1-WT (black circles) and EVI1-S436A (green circles).* ***(C)*** *Signal ratio of EVI1 and 5-meC (T-test; ** p<0.01).* ***(D)*** *Quantitation as in E of 3 independent experiments (* p<0.05).* ***(E and F)*** *Top panels illustrate individual stains (grayscale) of EVI1, DAPI and 5-meC, bottom panels merged. Arrows indicate cells in corresponding upper and lower panels with high EVI1-WT signal and absent 5mC signal (white), and cells with high EVI1-S436A signal cells with high EVI1 signal and high 5mC signal (orange).*

Summary of EVI1 S436 Phosphorylatability Results

This study has demonstrated the important role of serine 436 available for phosphorylation in EVI1-mediated haematopoietic self-renewal by directing transcriptional regulation. Complimentary modelling of the motif revealed the phosphorylation modulated protein interaction and co-immunoprecipitation results supported a dynamic CtBP1 interaction. Mass spectrometry also confirmed dynamic protein interactions mediated by the serine 436 motif available for phosphorylation. Of interest was the preferential interaction of EVI1-WT with DNTM3a, a DNA methyltransferase that is implicated in leukaemogenesis when perturbed. Analysis of methylation by 5mC staining suggested that the self-renewal mediated by EVI1-WT is associated with the maintenance of a cell population with low 5mC staining.

Chapter 4 Discussion

The transcriptional regulator EVI1 plays an increasingly recognised role in normal development in particular for normal haematopoiesis. However, aberrantly high EVI1 is one of the most oncogenic events in human leukaemia, and high *EVI1* expression is an also increasingly recognised oncogene in other malignancies. Investigations into the function of the EVI1 protein not only shed light on its function in normal development, but might also have therapeutic implications for leukaemia and other cancers that overexpress EVI1. The focus of this thesis is the functional investigation of EVI1 phosphorylation events.

There is increasing evidence that phosphorylation of oncoproteins are critical to their oncogenic function. The phosphorylation of MLL at serine 516 by ATR in response to genotoxic stress is required for progression through the cell cycle[231]. Phosphorylation of RUNX1 at serine 48, 303 and 424 by CDK stimulate proliferation of Lin- murine bone marrow progenitors[232]. Additionally, phosphorylation of GATA2 at serine 401 by AKT has been suggested to impair GATA2 DNA-binding activity[233]. Targeting of these phosphorylation sites as therapeutic strategies have not been fully explored. There have been suggestion of targeting the phosphorylation of RUNX1 in inv(16) leukaemia[234,235]. Furthermore there has been success using the ovarian cancer SKOV-3 cells, which overexpress the EVI1 isoforms, in targeting the phosphorylation of AKT[236]. Therefore study of the EVI1 phosphorylation might provide further insight into EVI1 role leukaemogenesis and present a therapeutic avenue in EVI1-overexpressing AML.

Mass spectrometry performed by the group prior to the start of this project discovered dynamic phosphorylation events of EVI1 at serine 858/860 and serine 436, in SB1690CB leukaemia cells, which had previously been listed in global proteomic and phosphoproteomic studies in other malignancies[95,135]. In order to investigate these phosphorylation sites, site-directed mutagenesis was used to generate non-phosphorylated and non-phosphorylatable EVI1 mutants at serine 436 and serine 858/860. There is argument made whether site-directed mutagenesis is suitable to study post-translational modifications due to amino acid substitution's potential effect on protein structure[237]. Therefore, EVI1 functionality was assessed

after site-direct mutagenesis by nuclear localisation, minimal promoter affinity and transformation of Rat1 fibroblasts that confirmed no functional impact as a result of the site directed mutagenesis. Some studies that have investigated phosphorylation events by site-directed mutagenesis have also generated phosphomimetic mutants in which phosphorylation of the motif is mimicked by mutation of the amino acid to aspartic acid, which to some extend resembles the charge associated with a phosphorylation[125]. However a phosphomimetic mutant was not generated within this study as this substitution can have drastic charge and structural changes that compromise protein functionality and does not mimic the special features of the phosphorylation[237].

The two main models chosen for the study of the EVI1 non-phosphorylatable mutants in this thesis were the Rat1 fibroblast and the Kit+ HSPCs. The Rat1 fibroblast model has historically proven successful in identifying the role of protein domains[94,97], and post-translational modifications[125,131] for EVI1 oncogenic potential. Within this thesis the Rat1 fibroblasts were successful in determining the role of the carboxy-terminal phosphorylation in response to hydrogen peroxide induced genotoxic stress. However, the model lacked the sensitivity needed to detect the importance of the S436 and S858/860 phosphorylatability in sustaining the re-plating of the Kit+ HSPCs. An alternative model, mouse embryonic fibroblasts (MEFs), that has recently been used to assess the oncogenic potential[222], was also employed. Although the MEFs were unable to fully replicate the results seen in the Kit+ HSPCs, they were more sensitive to the oncogenic effect of EVI1-mediated transformation as a result of low colony formation in control cells. The MEF cells would be preferable to Rat1 fibroblasts in future studies to assess more subtle changes in EVI1 function due to the sensitivity of the model. Furthermore, MEFs allow for increased flexibility and transition into *in vivo* models, in which CRISPR-Cas technology could be used to alter motifs subject to post-translational modification or to replicate the somatic mutation seen in patients with malignancies associated with germline MECOM mutations. However, the best model for the study of EVI1 in particular in a hematopoietic context remains the transduced Kit+ HSPCs which most closely replicates the biology of EVI1 driven leukaemogenesis. This model also offers the ability to transition into *in vivo* models, whereby reconstitution of the bone marrow of

irradiated mice with EVI1-transduced BM progenitors could provide an EVI1-induced murine AML model for study[238].

EVI1-mediated maintenance and self-renewal of haematopoietic stem cells is partially dependent on the phosphorylatable carboxy-terminal SQS motif. In an effort to further define the dynamic effect of carboxy-terminal phosphorylation, a previous member of the group (Dr Marion Schneider) investigated the effect of carboxy-terminal phosphorylation on EVI1-protein interactions[131]. The EVI1-CtBP1 is essential for EVI1-mediated self-renewal of murine haematopoietic progenitor cells[94,118]. Dr Paredes and Dr Schneider found that EVI1 interaction with CtBP1 is dynamically and finely modulated by the ATM-mediated EVI1-SQS phosphorylation and enhanced by genotoxic stress[131]. The loss of CtBP1 affinity to the EVI1-AQA mutant in the presence of genotoxic stress could explain the inability of the EVI1-AQA mutant to maintain EVI1-transcriptional patterns in response to genotoxic stress. Further, the dynamic interaction with CtBP1 that is mediated by carboxy-terminal phosphorylation might provide insight into the differential response to chemotherapy treatment seen between EVI1-WT and EVI1-AQA transduced or transfected cells. Here a study of the EVI1 interactome in SB1690CB cells, or clinical samples, in response to chemotherapy treatment and genotoxic stress induced by hydrogen peroxide would inform about the differential protein interactions mediated by the carboxy-terminal phosphorylation. Additionally, a MIDAS-MS experiment would be beneficial in determining whether the carboxy-terminal SQS motif is phosphorylated also in response to chemotherapy treatment

The data presented within this study support the concept that EVI1 carboxy-terminal phosphorylation links the DNA damage response and ATM to EVI1-mediated transformation, self-renewal and transcriptional regulation. These findings could be therapeutically relevant for EVI1-overexpressing malignancies as EVI1 might induce chemo-resistance via ATM-mediated carboxy-terminal phosphorylation. Small molecule inhibitors for ATM inhibition, AZD0156 and AZD1390, are currently in phase 1 clinical evaluation[187,188]. AZD0156 has shown efficacy in MLL-rearranged AML mouse models[239]. Although the study did not assess for *EVI1* expression, MLL-rearranged leukaemia typically results in aberrant *EVI1* expression[64], suggesting a potential link between EVI1 and the efficacy of ATM inhibition.

The poor response to chemotherapy seen in AML with high *EVI1* expression is well documented in patients, however this resistance has not been studied extensively *in vitro*. Within this study, there is contrasting data regarding the effect of EVI1 on the chemo-resistance of Rat1 fibroblasts. Within the drug titration assays it is not EVI1-WT that confers protection to Cytarabine treatment, rather the EVI1-AQA mutant. However within the colony forming assay, both EVI1-WT and EVI1-AQA confer resistance to Cytarabine. Yamakawa *et al* also found discrepancy between culture conditions on EVI1 mediated chemo-resistance[74]. The group found that in EVI1-overexpressing AML cell lines, growth in 3-D matrigel enhanced resistance to Cytarabine when compared to growth in normal medium suspension. The group concluded that the increased resistance seen in 3-D culture was dependent on ITGA6, an integrin essential for cellular adhesion[74]. Similarly, in response to Etoposide and Daunorubicin treatment, EVI1 only conferred resistance in Rat1 fibroblasts within the 3-D Methocult culture. This is contradictory to the results seen in the human myeloid cell line U937, in which forced overexpression of *EVI1* increases the resistance to Etoposide and Daunorubicin in a 2-D assay[72]. Given that chemo-resistance to Etoposide and Daunorubicin was irrespective of culture conditions, Rommer *et al* attributed the chemo-resistance to Etoposide to EVI1-mediated upregulation of CDKN1A/p21/WAF. CDKN1A/p21/WAF is a protein involved in p53 mediated cell cycle arrest and has been shown to be induced by leukaemia associated oncogenes with a protective role in response to genotoxic stress[240]. However neither ITGA6 nor CDKN1A/p21/WAF were shown to be upregulated by EVI1 expression in the HEK293FT model when untreated or DNA damaged. The pathways proposed by these studies not seen in our data set might hinge on the differential mechanisms of actions that the chemotherapy agents engage compared to hydrogen peroxide.

EVI1 mediates the transformation of Rat1 fibroblast in response to H_2O_2 induced genotoxic stress by carboxy-terminal phosphorylation. However, in response to chemotherapy induced genotoxic stress, the lack of phosphorylation at the carboxy-terminal seems to enhance the EVI1-mediated transformation of Rat1 fibroblasts. It should be noted that the enhanced protective effect of the AQA mutation was only seen with Etoposide and Daunorubicin treatment, not Cytarabine. It is well documented that treatment with the chemotherapy compounds used within this study

result in phosphorylation and activation of ATM and the downstream kinase Chk2[216]. Therefore, it was expected that activation of ATM would result in phosphorylation of EVI1 and an enhanced protective effect whereby cells transduced with EVI1-WT formed more colonies to the EVI1-AQA mutant in response to chemotherapy treatment. It is possible that the different mechanisms by which genotoxic stress is induced might play a role. Hydrogen peroxide is a reactive oxygen species (ROS) that induces genotoxic stress by the generation of free radicals. Hydrogen peroxide reduces metal irons in the Fenton reaction, producing hydroxyl radicals (·OH). The hydroxyl radicals are highly reactive and react with the sugar residue of the DNA backbone, causing DNA damage by both single and double strand breaks[185]. In contrast Cytarabine, Etoposide and Daunorubicin are all chemotherapy agents that induce genotoxic stress by alternative mechanisms. Cytarabine is an antimetabolite that is metabolised to Cytarabine-5′-monophosphate by deoxycytidine kinase (dCK). Cytarabine-5′-monophosphate is subsequently phosphorylated to the -triphosphate form by nucleoside diphosphate kinase (NDPK). Cytarabine-5′-triphosphate competes with deoxycytidine triphosphate in the incorporation into DNA, resulting in chain termination and cell death[241,242]. Both Etoposide and Daunorubicin are topoisomerase II inhibitors that binds to both topoisomerase IIα and IIβ, stabilising the DNA-Top2 cleavage complex (Top2cc) which prevents the re-ligation of double strand breaks within the DNA during regulation of DNA topology[243,244]. Despite these differential mechanisms, it remains unclear why the EVI1-AQA mutant enhances the protective effect compared to EVI1-WT in response to chemotherapy treatment. It is possible that other SQS phosphorylation events within the EVI1 protein play a role. There is an SQS motif located just after the ZF7 at serine 336/338 and within the repressor domain at serine 516/518. It would be of interest to study these motif both in isolation and together by site-directed mutagenesis similar to serine 858/860. However, investigation into the EVI1-mediated transcriptional profile are more likely to explain the enhanced protective effect of EVI1-AQA in response to chemotherapy treatment, similar to that outlined with EVI1-WT in response to hydrogen peroxide induced genotoxic stress.

Transfection of HEK293FT cells was used as a read out to determine that transcription is differentially affected by hydrogen peroxide induced genotoxic stress and a phosphorylatable EVI1 SQS motif. This model was able to identify known

EVI1-mediated transcripts, such as *ALDOC*[85] and *TOM1L1*[245], which were amongst significantly differentially expressed transcripts within this model. The downregulation of *TOM1L1* and *MOV10*, and the upregulation of *ALDOC* and *SETX* that are maintained only by the phosphorylatable EVI1-WT in response to genotoxic stress offer insight into how EVI1-mediates genotoxic stress. Upregulation of *TOM1L1* has been shown to inhibit DNA synthesis[246], whereas upregulation of *SETX* seen in response to DNA damage by R-loops and double strand breaks[247]. MOV10 has been shown to interact with the polycomb repressive complex (PRC1) to promote gene[248], which EVI1 has been shown to interact with to regulate the repression of *PTEN*[238]. Further *ALDOC* has been shown to be a key genes in the metabolism of HSPCs in response to low oxygen conditions[249]. The transcriptomic experiment has provided further insight into the effect of carboxy-terminal phosphorylation in response to H_2O_2 induced genotoxic stress on EVI1 transcriptional profiles. A similar experiment in the transduced Kit+ HSPCs might define the different molecular mechanisms involved in the differential effect seen between H_2O_2 and chemotherapy treatment in the Rat1 fibroblasts. It would also define the effect of ATM inhibition and chemotherapy treatment on EVI1-mediated transcription. Further, a transcriptome study of Kit+ HSPCs transduced with EVI1-WT and EVI1-AQA and treated with a combination of chemotherapy and ATM inhibitor would provide insight on the enhanced resistance mediated by EVI1-AQA to Etoposide and Daunorubicin, compared to EVI1-WT.

Within this thesis the ATM inhibitor AZD1390 has shown efficacy in reducing EVI1-mediated Rat1 fibroblast transformation in response to chemotherapy treatment. The inhibition of ATM within this cellular context was shown by western blot. The reported potency of the ATM inhibitor AZD1390 (IC50 = 0.58nM) was determined by immunofluorescence of p-ATM foci in irradiated NCI-H2228 cells, a non-small cell lung cancer model[188]. Radiation therapy is not typically used in the treatment of leukaemia[250]. The common treatment strategy is usually through a combination chemotherapy regime with Cytarabine and Daunorubicin the backbone of these regimes[251]. Although this report does establish the efficacy of ATM inhibition in response to chemotherapy, it does not determine the potency and IC50 of ATM inhibition by AZD1390. It would be necessary to establish cellular potency in the context of transduced Kit+ HSPCs before establishing efficacy in mouse models. Given that EVI1-transduction of Kit+ HSPCs and subsequent transplantation of

irradiated C57/BL6 mice has been shown to be sufficient to produce EVI1-expressing leukemic mice[110], the cellular potency of AZD1390 in the transduced Kit+ HSPCs could be used to inform dosing within this model. Prior to *in vivo* studies however, it would be of interest to also establish efficacy of AZD1390 treatment in EVI1-overexpresing cell line models, such as the SB190CB cells.

The study which initially suggested ATM as a kinase that phosphorylates the carboxy-terminal SQS motif also suggests that ATM- and Rad3-Related protein kinase (ATR) can also phosphorylate the SQS motif[252]. Together with ATM, ATR is an essential kinase in the DNA damage response. ATM is primarily activated in response to DNA double strand breaks, whereas ATR responds to a broader spectrum of DNA damage including replication fork stress[216]. As both topoisomerase inhibitors Etoposide and Daunorubicin induce genotoxic stress at the replication fork by preventing negative supercoiling, ATR might mediate phosphorylation of EVI1 within this environment. Similar to the ATM inhibitor AZD0156, the ATR inhibitor AZ20 had been shown to prolong the survival of mice transplanted with AML cells[239]. The current clinical candidate AZD6738 is undergoing recruitment for a phase II trial in solid tumours when used alone as combination treatment[253]. Future studies would investigate the potential synergistic effect of the ATR inhibitor AZD6738 with the chemotherapy agents used within this study in the models previously proposed. Further it would be of interest to see whether, in response to chemotherapy treatment, ATM and/or ATR mediate the EVI1 carboxy-terminal phosphorylation.

The discovery of both phosphorylated and non-phosphorylated S858/860 and S436 in the SB1690CB AML cells indicates a dynamic process. The phosphorylation of the S858/860 motif has previously been identified by phosphoproteomic profile studies in breast cancer cell lines[132]/tumour samples[135]/patient derived xenografts[134], NSCLC cell lines[132] and HeLa cells[136,137]. The phosphorylated S436 has also been identified in colorectal[130], NSCLC[139], ovarian[134] and breast cancer[135] samples. However, the phosphorylation of S436 has yet to be reported in clinical AML samples. There have been few studies investigating the proteome in AML, some study employing mass spectrometry[254,255] and more recent study using flow-cytometric approaches to focus on traditional markers[256,257]. Therefore, further study would be needed to identify

EVI1 specific phospho-sites that are found in in EVI1-overexpressing patient samples.

In this thesis I show that the non-phosphorylatable EVI1-S436A mutation, whilst maintaining EVI1-functional readouts with respect to promotor affinity, nuclear localisation and Rat-1 transformation, confers abrogated self-renewal capacity. These data imply that the integrity of this region with the S436 available for phosphorylation is essential for EVI1-mediated haematopoietic self-renewal. Given that self-renewal has also been shown to be partially dependent on the phosphorylatable carboxy-terminal SQS motif, it is clear that dynamic phosphorylation of EVI1 has a role in haematopoietic self-renewal. In an effort to explain how the integrity of the S436 site mediates haematopoietic self-renewal, an RNA*seq* experiment was performed using Kit+ HSPCs and analysis performed by Dr Stevens and Dr Amaral. Comparative analysis of the RNA*seq* dataset generated within this study of the effect of serine 436 phosphorylatability in KIT+ HSPCs showed a significant overlap with a similar experiment performed by Kustikova *et al*[112], confirming many EVI1 target genes. Lack of complete overlap in the transcriptional regulation seen between the two studies are likely a result of differential experimental methodology. Kustikova *et al* conducted retroviral transduction with a Doxycycline inducible EVI1 construct in Lin- HSPCs from Ros a26rtTA-nls-Neo2 mice compared to the continually expressed EVI1-IRES-GFP construct in KIT+ HSPCs from C57/BL6 mice in this study. The EVI1 exposure in the Lin- negative cells was exposed for only 24 hours, whereas in this study, EVI1 exposure was for 48 hours. Additionally the type of RNA analysis differs between the studies. Kustikova *et al* uses microarray technology whereas this report used RNA*seq* which offers a wider dynamic range with regards to both expression level changes and number of transcripts identified[258]. The analysis in this study delineates transcriptional profiles that are persistently EVI1-modulated and that are partly regulated independently of S436 phosphorylation. Transcriptional profiles mediated by EVI1-WT include genes with essential roles in haematopoiesis and stem cell maintenance. It confirmed the EVI1-mediated upregulation of *ALDHA1A* and *CD36*. High expression of *ALDHA1A* in HSCs is associated with the ability to produce long-term multi-lineage haematopoietic colonies, also aberrant expression is linked with the transition to a cancer stem cell[259]. The expression of *CD36* seems to mark

cancer stem cells that are able to self-renew[260]. It also confirmed that EVI1-mediates the downregulation of *CEPBA* and *ARRB2*. Lack of expression of *CEPBA* in HSCs has been shown to block myeloid differentiation and enhance the self-renewal when expression is absent in HSCs[261]. Depletion of *ARRB2* results in an increase in cancer stem cell markers and is a marker for cancer tissue when compared to normal tissue in bladder cancer[262]. The transcriptional profiles also show that EVI1 with S436 available for phosphorylation has a more focused effect on the entire transcriptome, implying that phosphorylation of S436 directs transcriptional patterns towards self-renewal.

The more divergent transcriptional patterns engaged by the EVI1-S436A mutant could be explained by the differential protein interactions compared to EVI1-WT. Recent data from our group and others indicate that many EVI1 functions are regulated by dynamic protein interactions, such as the interaction with CtBP1[95,131,146]. Therefore, as the tertiary structure of CtBP1 is known[204,226,227], and the CtBP1 binding motifs present on the EVI1 protein are known[93], complimentary and collaborative high-end computational modelling was performed by Dr Almarzouq to determine whether the serine 436 phosphorylation affects the interaction. This analysis demonstrates that when phosphorylated, serine 436 destabilises the CtBP1 binding site α helix, increasing the binding energy needed to bind. This predicted preferential interaction of non-phosphorylatable EVI1-S436A with CtBP1 which was confirmed by immunoprecipitation. Given that CtBP1 acts as a co-repressor to a number of transcription factors, it is likely that the non-phosphorylatable EVI1-S436A mutant's higher affinity to CtBP1 explains the divergent transcriptional patterns. Detailed analysis using a similar approach to investigate other EVI1 protein interactions, such as RUVBL2 and DNMT3a, would have been of interest, however as the binding sites of these proteins with EVI1 is unknown, this was not possible.

As CtBP1 interaction is essential for EVI1 function, and only EVI1-WT with S436 available for phosphorylation confers self-renewal, it was unexpected that the phosphorylatability of S436 negatively affects affinity to CtBP1. As EVI1-CtBP1 interaction is also regulated by carboxy-terminal phosphorylation[131], these results support the concept of a dynamic kinase-governed complex that is finely regulated by EVI1 post-translational modifications. This concept also applies to other protein interactions, of which detailed analysis might provide therapeutic avenues for EVI1

overexpressing malignancies. The previously described EVI1-RUVBL2 protein interaction was used as a control for interaction with CtBP1. The preferential interaction of EVI1-WT compared with EVI1-S436 with RUVBL2 reinforces the concept of a dynamic kinase-governed complex and could provide insight into EVI1-mediated self-renewal in future studies.

This study is the first to confirm the EVI1-DNMT3a interaction by mass spectrometry. The EVI1-DNMT3a interaction had previously been seen by co-immunoprecipitation[165,175], but was not seen in the two global mass spectrometry EVI1 interactome studies[95,146]. The preferential interaction of EVI1-WT with DNMT3a was again confirmed by immunoprecipitation. It was also shown that EVI1-WT affects DNA-methylation patterns in the Kit+ HSPCs as assessed by 5mC staining. The maintenance of a population with low or absent 5mC staining only by EVI1-WT indicates an interference of EVI1 with *de-novo* methylation. Focal hypomethylation is a distinct feature of HSCs with disruption in DNMT3a, while leukemic progression of AML results in hypermethylation of CpG-islands[172]. In the Rat1 fibroblast model, there is disruption of DNMT3a with EVI1 expression leading to increased levels of DNMT3a staining. This EVI1-mediated disruption of DNMT3a levels could explain the populations devoid of 5mC staining. Further, the aberrantly high levels of EVI1 might disrupt DNMT3a by affecting the tetramer assembly of the DNMT3a complex[166]. Additionally, the RNAseq experiment revealed that only EVI1-S436A transduction resulted in an upregulation of DNMT3L, which can form part of the tertiary DNMT3a structure (*Figure 1.4*). The increased levels of DNMT3L induced exclusively by EVI1-S436A might prevent EVI1 displacement of the DNMT3a complex, resulting in the increased levels of 5mC staining seen with EVI1-S436A transduction compared to EVI1-WT. Although this study explores the role of phosphorylatable S436 EVI1 on 5mC methylation patterns, it does not provide details of the genes affected. It would be of interest to characterise the genes affected by differential methylation by pyrosequencing of transduced Kit+ HSPCs, which would provide further insight into whether the methylation patterns seen are located within the gene body and/or promoter region. Future studies could assess the relation of the methylation patterns mediated by S436 with the differentially expressed transcripts seen in the RNA*seq* analysis, linking locus and methylation status with the consequential transcriptional regulation. Recent research has

suggested that hypomethylating agents might prove successful in the treatment of relapse AML[263], and more specifically in EVI1 overexpressing paediatric AML[84]. Therefore it would be interesting to study the effect of hypomethylating agents in transformed leukemic cells in the context of S436 phosphorylation. Additionally, whether treatment with a hypomethylating agent might differentially effect gene body and/or promoter methylation, as well as the resultant dynamic effect on gene transcription.

For complete understanding of the EVI1 serine 436 phosphorylation event, future studies would investigate the mechanism by which the S436 is phosphorylated. Although the mechanism by which serine 436 is phosphorylated is not defined in this study, *in silico* analysis proposes CDK2 and CDK3 as likely candidates as they share the S436 target sequence (*Figure 3.20*). These kinases also co-immunoprecipitate with EVI1-WT in the MS interactome (*Appendix Table 7.1*). To assess whether these kinases phosphorylate serine 436, an antibody would need to be generated that is specific to the site but also discriminates between phosphorylated and non-phosphorylated forms. Initially, selective protein inhibitors for proposed kinases, such as SNX-class CDK3 inhibitors[264], would be used to treat cells and identify the phosphorylating kinase with detection of EVI1 peptides by mass spectrometry and quantitation through stable isotype labelling of modified peptides[265]. This would be of interest as CDK3 has been described to have a role in haematopoietic self-renewal in response to chemotherapy[266]. With further investigation into the mechanism of the phosphorylation of serine 436 by CKD3 might provide insight into the chemo-resistance previously seen by EVI1-AQA. Additionally EVI1 serine 436 phosphorylation has been identified in chemotherapy resistant NSCLC[132], implicating the role of this phosphorylation in chemo-resistance and highlighting additional treatment conditions to induce the phosphorylation.

Given that the serine 436 is located in both EVI1 and MDS1-EVI1 protein isoform, but not in ΔEVI1, it would also be of interest to study the effect of serine 436 available for phosphorylation in the context of these protein isoforms. MDS1-EVI1 has been proposed to play an antagonistic role to EVI1[267]. Given that the serine 436 is a promiscuous phosphorylation site for multiple kinases, and that phosphorylation is a dynamic process, phosphorylation of the site might determine the functional dominant isoform. Further, phosphorylation of MDS1-EVI1 at serine 436 is likely to

regulate function in a similar way as to EVI1. The ΔEVI1 isoform is often expressed in conjunction with *EVI1*-overexpression in AML[268], and DNA binding sites are largely overlapping between the isoforms[103]. It would be of interest to further define the role of the ΔEVI1 isoform and whether the lack of the motif harbouring serine 436 explains the inability of the isoform to transform or support normal development[104,115]. Through the proposed experimental procedures to induce the phosphorylation of the serine 436, it would be possible to study the differential function of ΔEVI1 and EVI1 in the context of serine 436 phosphorylation.

Chapter 5 Conclusion

This study has functionally investigated two dynamic phosphorylation events identified in the AML cell line SB1690CB. Site-directed mutagenesis of these phospho-sites has allowed considerable insight into their role for EVI1 function. Phosphorylation at S858/860 has been shown to be mediated by ATM in response to genotoxic stress, and the phosphorylation is essential to EVI1-mediated haematopoietic self-renewal. Transcriptomic analysis confirms EVI1-target genes modulated by carboxy-terminal phosphorylation in response to genotoxic stress. EVI1 overexpression is increasingly recognised to be associated with in the chemo-resistance seen in poor prognosis AML and other malignancies. This study offers a novel therapeutic avenue in which synergistic treatment of an ATM inhibitor with standard chemotherapy agents might be efficacious in abrogating EVI1 oncogenic potential. ATR has also been suggested to phosphorylate the S858/860 motif. An ATR inhibitor currently in the clinic has shown efficacy in AML mouse model and could be experimentally investigated in future studies in the context of EVI1-overexpression.

The availability of S436 for phosphorylation is critical to haematopoietic self-renewal, mediating transcriptional regulation of genes such as *ALDHA1A* and *CEPBA* that are essential to haematopoiesis and stem cell maintenance. Integrity of the S436 site is important for the interaction with DNMT3a and modulates 5mC methylation patterns, suggesting a role of EVI1 in *de novo* methylation, which might be relevant in the context of therapy with hypomethylating agents. Targeting of the phosphorylation of EVI1 at S436 by inhibition of the candidate phosphorylating kinases CDK2 or CDK3 might prove clinically useful. Future studies focusing on the phosphorylation of the additional EVI1 isoforms that are commonly co-expressed with EVI1 might provide further insight into the role of these isoforms.

Chapter 6 References

1. Kondo, M. *et al.* Biology of Hematopietic Stem Cells and Progenitors: Implications for Clinical Application. *Annu. Rev. Immunol.* **21**, 759–806 (2003).
2. Weissman, I. L. Stem cells: units of development, units of regeneration, and units in evolution. *Cell* **100**, 157–168 (2000).
3. Passegué, E., Jamieson, C. H. M., Ailles, L. E. & Weissman, I. L. Normal and leukemic hematopoiesis: are leukemias a stem cell disorder or a reacquisition of stem cell characteristics? *Proc. Natl. Acad. Sci. U. S. A.* **100 Suppl 1**, 11842–9 (2003).
4. Jagannathan-Bogdan, M. & Zon, L. I. Hematopoiesis. *Development* **140**, 2463–7 (2013).
5. Visvader, J. E. Cells of origin in cancer. *Nature* **469**, 314–322 (2011).
6. Seita, J. & Weissman, I. L. Hematopoietic stem cell: Self-renewal versus differentiation. *Wiley Interdisciplinary Reviews: Systems Biology and Medicine* (2010) doi:10.1002/wsbm.86.
7. Osawa, M., Hanada, K., Hamada, H. & Nakauchi, H. Long-Term Lymphohematopoietic Reconstitution by a Single CD34-Low/Negative Hematopoietic Stem Cell. *Science* vol. 273 242–245.
8. Uchida, N., Jerabek, L. & Weissman, I. L. Searching for hematopoietic stem cells. II. The heterogeneity of Thy-1.1(lo)Lin(-/lo)Sca-1+ mouse hematopoietic stem cells separated by counterflow centrifugal elutriation. *Exp. Hematol.* **24**, 649–59 (1996).
9. Ikuta, K. & Weissman, I. L. Evidence that Hematopoietic Stem Cells Express Mouse c-kit but do not Depend on Steel Factor for Their Generation. *Proceedings of the National Academy of Sciences of the United States of America* vol. 89 1502–1506.
10. Wilson, N. K. *et al.* Combinatorial transcriptional control in blood stem/progenitor cells: Genome-wide analysis of ten major transcriptional regulators. *Cell Stem Cell* (2010) doi:10.1016/j.stem.2010.07.016.
11. Rodrigues, N. P. *et al.* Haploinsufficiency of GATA-2 perturbs adult hematopoietic stem-cell homeostasis. *Blood* (2005) doi:10.1182/blood-2004-08-2989.
12. Cai, X. *et al.* Runx1 loss minimally impacts long-term hematopoietic stem cells. *PLoS One* (2011) doi:10.1371/journal.pone.0028430.
13. Goyama, S. *et al.* Evi-1 Is a Critical Regulator for Hematopoietic Stem Cells and Transformed Leukemic Cells. *Cell Stem Cell* **3**, 207–220 (2008).
14. Song, W. J. *et al.* Haploinsufficiency of CBFA2 causes familial thrombocytopenia with propensity to develop acute myelogenous leukaemia. *Nat. Genet.* (1999) doi:10.1038/13793.
15. McReynolds, L. J. *et al.* Rapid progression to AML in a patient with germline GATA2 mutation and acquired NRAS Q61K mutation. *Leuk. Res. Reports* (2019) doi:10.1016/j.lrr.2019.100176.
16. Steensma, D. P. *et al.* Clonal hematopoiesis of indeterminate potential and its distinction from myelodysplastic syndromes. *Blood* (2015) doi:10.1182/blood-2015-03-631747.
17. Bannon, S. A. & DiNardo, C. D. Hereditary Predispositions to Myelodysplastic

Syndrome. *Int. J. Mol. Sci.* **17**, (2016).

18. Arber, D. A. *et al.* The 2016 revision to the World Health Organization classification of myeloid neoplasms and acute leukemia. doi:10.1182/blood-2016-03-643544.

19. Nielsen, M. *et al.* Deletion of the 3q26 region including the EVI1 and MDS1 genes in a neonate with congenital thrombocytopenia and subsequent aplastic anaemia. *J. Med. Genet.* (2012) doi:10.1136/jmedgenet-2012-100990.

20. Bouman, A. *et al.* Congenital thrombocytopenia in a neonate with an interstitial microdeletion of 3q26.2q26.31. *Am. J. Med. Genet. Part A* (2016) doi:10.1002/ajmg.a.37451.

21. Niihori, T. *et al.* Mutations in MECOM, Encoding Oncoprotein EVI1, Cause Radioulnar Synostosis with Amegakaryocytic Thrombocytopenia. *Am. J. Hum. Genet.* (2015) doi:10.1016/j.ajhg.2015.10.010.

22. Thompson, A. A. & Nguyen, L. T. Amegakaryocytic thrombocytopenia and radio-ulnar synostosis are associated with HOXA11 mutation. *Nat. Genet.* (2000) doi:10.1038/82511.

23. Bluteau, O. *et al.* A landscape of germline mutations in a cohort of inherited bone marrow failure patients. *Blood* blood-2017-09-806489 (2017) doi:10.1182/blood-2017-09-806489.

24. Ripperger, T. *et al. MDS1* and *EVI1* complex locus (MECOM): a novel candidate gene for hereditary hematological malignancies. *Haematologica* **103**, e55–e58 (2018).

25. Germeshausen, M. *et al.* MECOM-associated syndrome: A heterogeneous inherited bone marrow failure syndrome with amegakaryocytic thrombocytopenia. *Blood Adv.* (2018) doi:10.1182/bloodadvances.2018016501.

26. Dokal, I. & Vulliamy, T. Inherited bone marrow failure syndromes. *Haematologica* **95**, 1236–40 (2010).

27. Soulier, J. Fanconi anemia. *Hematology / the Education Program of the American Society of Hematology. American Society of Hematology. Education Program* (2011) doi:10.1182/asheducation-2011.1.492.

28. Tonnies, H. *et al.* Clonal chromosomal aberrations in bone marrow cells of Fanconi anemia patients: gains of the chromosomal segment 3q26q29 as an adverse risk factor. *Blood* **101**, 3872–3874 (2003).

29. Quentin, S. *et al.* Myelodysplasia and leukemia of Fanconi anemia are associated with a specific pattern of genomic abnormalities that includes cryptic RUNX1/AML1 lesions. *Blood* **117**, e161–e170 (2011).

30. Meyer, S., Neitzel, H. & Tönnies, H. Chromosomal aberrations associated with clonal evolution and leukemic transformation in fanconi anemia: clinical and biological implications. *Anemia* **2012**, 349837 (2012).

31. Tönnies, H. *et al.* Clonal chromosomal aberrations in bone marrow cells of Fanconi anemia patients: gains of the chromosomal segment 3q26q29 as an adverse risk factor. *Blood* **101**, (2003).

32. Mehta, P. A. *et al.* Numerical chromosomal changes and risk of development of myelodysplastic syndrome–acute myeloid leukemia in patients with Fanconi anemia. *Cancer Genet. Cytogenet.* **203**, 180–186 (2010).

33. Soulier, J. Fanconi anemia. *Hematology Am. Soc. Hematol. Educ. Program* **2011**, 492–7 (2011).

34. Meyer, S. *et al.* Fanconi anemia (FA)–associated 3q gains in leukemic transformation consistently target EVI1, but do not affect low TERC expression in FA. *Blood* **117**, (2011).

35. Meyer, S. *et al.* Amplification and translocation of 3q26 with overexpression ofEVI1 in Fanconi anemia-derived childhood acute myeloid leukemia with biallelicFANCD1/BRCA2 disruption. *Genes, Chromosom. Cancer* **46**, 359–372 (2007).

36. Grimwade, D., Ivey, A. & Huntly, B. J. P. Molecular landscape of acute myeloid leukemia in younger adults and its clinical relevance. *Blood* (2016) doi:10.1182/blood-2015-07-604496.

37. Walter, M. J. *et al.* Clonal Architecture of Secondary Acute Myeloid Leukemia. *N. Engl. J. Med.* (2012) doi:10.1056/NEJMoa1106968.

38. Mardis, E. R. *et al.* Recurring mutations found by sequencing an acute myeloid leukemia genome. *N. Engl. J. Med.* (2009) doi:10.1056/NEJMoa0903840.

39. Poppe, B. *et al.* EVI1 is consistently expressed as principal transcript in common and rare recurrent 3q26 rearrangements. *Genes, Chromosom. Cancer* **45**, 349–356 (2006).

40. Stevens, a *et al.* EVI1 expression in childhood acute lymphoblastic leukaemia is not restricted to MLL and BCR/ABL rearrangements and is influenced by age. *Blood Cancer J.* **4**, e179 (2014).

41. Konantz, M. *et al.* EVI-1 modulates leukemogenic potential and apoptosis sensitivity in human acute lymphoblastic leukemia. *Leukemia* **27**, 56–65 (2013).

42. Andersson, A. *et al.* Microarray-based classification of a consecutive series of 121 childhood acute leukemias: prediction of leukemic and genetic subtype as well as of minimal residual disease status. *Leukemia* **21**, 1198–1203 (2007).

43. Cario, G. *et al.* Distinct gene expression profiles determine molecular treatment response in childhood acute lymphoblastic leukemia. *Blood* **105**, 821–826 (2005).

44. Gunnarsson, R. *et al.* Large but not small copy-number alterations correlate to high-risk genomic aberrations and survival in chronic lymphocytic leukemia: a high-resolution genomic screening of newly diagnosed patients. *Leukemia* **24**, 211–215 (2010).

45. Mrózek, K., Harper, D. P. & Aplan, P. D. Cytogenetics and Molecular Genetics of Acute Lymphoblastic Leukemia. *Hematology/Oncology Clinics of North America* (2009) doi:10.1016/j.hoc.2009.07.001.

46. Ries, L. a. G. *et al.* Cancer incidence and survival among children and adolescents: United States SEER Program 1975-1995. *NIH Pub. No. 99-4649* 179 pp. (1999).

47. Hinai, A. A. & Valk, P. J. M. Review: Aberrant *EVI1* expression in acute myeloid leukaemia. *Br. J. Haematol.* **172**, 870–878 (2016).

48. Morishita, K., Parganas, E., Matsugi, T. & Ihle, J. N. Expression of the Evi-1 zinc finger gene in 32Dc13 myeloid cells blocks granulocytic differentiation in response to granulocyte colony-stimulating factor. *Mol. Cell. Biol.* **12**, 183–9 (1992).

49. Suzukawa, K. *et al.* Identification of a breakpoint cluster region 3' of the ribophorin I gene at 3q21 associated with the transcriptional activation of the EVI1 gene in acute myelogenous leukemias with inv(3)(q21q26). *Blood* **84**, 2681–8 (1994).

50. Lugthart, S. *et al.* Clinical, molecular, and prognostic significance of WHO type inv(3)(q21q26.2)/t(3;3)(q21;q26.2) and various other 3q abnormalities in acute

myeloid leukemia. *J. Clin. Oncol.* **28**, 3890–8 (2010).

51. van Waalwijk van Doorn-Khosrovani, S. B. *et al.* Biallelic mutations in the CEBPA gene and low CEBPA expression levels as prognostic markers in intermediate-risk AML. *Hematol. J.* **4**, 31–40 (2003).

52. De Braekeleer, M. *et al.* 3q26/ *EVI1* rearrangements in myeloid hemopathies: a cytogenetic review. *Futur. Oncol.* **11**, 1675–1686 (2015).

53. Raimondi, S. C. *et al.* Chromosomal abnormalities in 478 children with acute myeloid leukemia: clinical characteristics and treatment outcome in a cooperative pediatric oncology group study-POG 8821. *Blood* **94**, 3707–16 (1999).

54. Balgobind, B. V *et al.* EVI1 overexpression in distinct subtypes of pediatric acute myeloid leukemia. *Leukemia* **24**, 942–949 (2010).

55. Ho, P. A. *et al.* High *EVI1* expression is associated with *MLL* rearrangements and predicts decreased survival in paediatric acute myeloid leukaemia: a report from the children's oncology group. *Br. J. Haematol.* **162**, 670–677 (2013).

56. Jo, A. *et al.* High expression of EVI1 and MEL1 is a compelling poor prognostic marker of pediatric AML. *Leukemia* **29**, 1076–1083 (2015).

57. Valk, P. J. M. *et al.* Prognostically Useful Gene-Expression Profiles in Acute Myeloid Leukemia. *N. Engl. J. Med.* **350**, 1617–1628 (2004).

58. Van Waalwijk van Doorn-Khosrovani, S. B. *et al.* High EVI1 expression predicts poor survival in acute myeloid leukemia: A study of 319 de novo AML patients. *Blood* **101**, 837–845 (2003).

59. Lugthart, S. *et al.* High EVI1 levels predict adverse outcome in acute myeloid leukemia: Prevalence of EVI1 overexpression and chromosome 3q26 abnormalities underestimated. *Blood* **111**, 4329–4337 (2008).

60. Gröschel, S. *et al.* High EVI1 expression predicts outcome in younger adult patients with acute myeloid leukemia and is associated with distinct cytogenetic abnormalities. *J. Clin. Oncol.* **28**, 2101–2107 (2010).

61. Matsuo, H. *et al.* EVI1 overexpression is a poor prognostic factor in pediatric patients with mixed lineage leukemia-AF9 rearranged acute myeloid leukemia. *Haematologica* **99**, e225-7 (2014).

62. Gröschel, S. *et al.* Deregulated Expression of *EVI1* Defines a Poor Prognostic Subset of *MLL* -Rearranged Acute Myeloid Leukemias: A Study of the German-Austrian Acute Myeloid Leukemia Study Group and the Dutch-Belgian-Swiss HOVON/SAKK Cooperative Group. *J. Clin. Oncol.* **31**, 95–103 (2013).

63. Langabeer, S. E. *et al.* EVI1 expression in acute myeloid leukaemia. *Br. J. Haematol.* **112**, 208–211 (2001).

64. Bindels, E. M. J. *et al.* EVI1 is critical for the pathogenesis of a subset of MLL-AF9-rearranged AMLs. *Blood* **119**, 5838–5849 (2012).

65. Haferlach, C. *et al.* ETV6 rearrangements are recurrent in myeloid malignancies and are frequently associated with other genetic events. *Genes, Chromosom. Cancer* **51**, 328–337 (2012).

66. Volkert, S. *et al.* Amplification of EVI1 on cytogenetically cryptic double minutes as new mechanism for increased expression of EVI1. *Cancer Genet.* **207**, 103–108 (2014).

67. McNeer, N. A. *et al.* Genetic mechanisms of primary chemotherapy resistance in pediatric acute myeloid leukemia. *Leukemia* (2019) doi:10.1038/s41375-019-0402-3.

68. Brown, F. C. *et al.* Genomics of primary chemoresistance and remission induction failure in paediatric and adult acute myeloid leukaemia. *Br. J. Haematol.* (2017) doi:10.1111/bjh.14413.

69. Baer, M. R. *et al.* Cytarabine, Daunorubicin and Etoposide (ADE) Chemotherapy in Acute Myeloid Leukemia (AML) Patients ≥60 Years (CALGB 9720). *Blood* **110**, 296–296 (2007).

70. Pommier, Y., Leo, E., Zhang, H. & Marchand, C. DNA topoisomerases and their poisoning by anticancer and antibacterial drugs. *Chemistry and Biology* (2010) doi:10.1016/j.chembiol.2010.04.012.

71. Emadi, A. & Karp, J. E. The clinically relevant pharmacogenomic changes in acute myelogenous leukemia. *Pharmacogenomics* (2012) doi:10.2217/pgs.12.102.

72. Rommer, A. *et al.* EVI1 Inhibits Apoptosis Induced by Antileukemic Drugs via Upregulation of CDKN1A/p21/WAF in Human Myeloid Cells. *PLoS One* (2013) doi:10.1371/journal.pone.0056308.

73. Oval, J., Jones, O. W., Montoya, M. & Taetle, R. Characterization of a factor-dependent acute leukemia cell line with translocation (3;3)(q21;q26). *Blood* (1990) doi:10.1182/blood.v76.7.1369.bloodjournal7671369.

74. Yamakawa, N., Kaneda, K., Saito, Y., Ichihara, E. & Morishita, K. The increased expression of integrin α6 (itga6) enhances drug resistance in evi1 high leukemia. *PLoS One* (2012) doi:10.1371/journal.pone.0030706.

75. Österberg, L. *et al.* Potential predictive markers of chemotherapy resistance in stage III ovarian serous carcinomas. *BMC Cancer* (2009) doi:10.1186/1471-2407-9-368.

76. Lu, Y. *et al.* EVI1 promotes epithelial-to-mesenchymal transition, cancer stem cell features and chemo-/radioresistance in nasopharyngeal carcinoma. *J. Exp. Clin. Cancer Res.* (2019) doi:10.1186/s13046-019-1077-3.

77. Paubelle, E. *et al.* Efficacy of All-Trans-Retinoic Acid in High-Risk Acute Myeloid Leukemia with Overexpression of EVI1. *Oncol. Ther.* (2019) doi:10.1007/s40487-019-0095-9.

78. Coombs, C. C., Deangelis, L. M., Feusner, J. H. & Tallman, M. S. Clinical description of acute promyelocytic leukemia (APL) patients receiving all-trans retinoic acid (ATRA) who develop pseudotumor cerebri: Incidence, diagnosis, outcomes, and recommendations for management. (2015) doi:10.1016/j.clml.2015.04.045.

79. Milligan, D. W. *et al.* Fludarabine and cytosine are less effective than standard ADE chemotherapy in high-risk acute myeloid leukemia, and addition of G-CSF and ATRA are not beneficial: results of the MRC AML-HR randomized trial. *Blood* **107**, 4614–4622 (2006).

80. Schlenk, R. F. *et al.* Phase III study of all-trans retinoic acid in previously untreated patients 61 years or older with acute myeloid leukemia. *Leukemia* **18**, 1798–1803 (2004).

81. Verhagen, H. J. M. P. *et al.* Primary acute myeloid leukemia cells with overexpression of EVI-1 are sensitive to all-trans retinoic acid. *Blood* **127**, (2016).

82. Schenk, T. *et al.* Inhibition of the LSD1 (KDM1A) demethylase reactivates the all-trans-retinoic acid differentiation pathway in acute myeloid leukemia. *Nat. Med.* **18**,

605–11 (2012).

83. Fang, Y., Liao, G. & Yu, B. LSD1/KDM1A inhibitors in clinical trials: Advances and prospects. *Journal of Hematology and Oncology* (2019) doi:10.1186/s13045-019-0811-9.

84. Mittal, N. *et al.* A critical role of epigenetic inactivation of miR-9 in EVI1 high pediatric AML. *Mol. Cancer* (2019) doi:10.1186/s12943-019-0952-z.

85. Fenouille, N. *et al.* The creatine kinase pathway is a metabolic vulnerability in EVI1-positive acute myeloid leukemia. *Nat. Med.* **23**, 301–313 (2017).

86. Alzuherri, H., McGilvray, R., Kilbey, A. & Bartholomew, C. Conservation and expression of a novel alternatively spliced Evi1 exon. *Gene* **384**, 154–162 (2006).

87. Aytekin, M., Vinatzer, U., Musteanu, M., Raynaud, S. & Wieser, R. Regulation of the expression of the oncogene EVI1 through the use of alternative mRNA 5′-ends. *Gene* **356**, 160–168 (2005).

88. Matsugi, T., Morishita, K. & Ihle, J. N. Identification, Nuclear Localization, and DNA-Binding Activity of the Zinc Finger Protein Encoded by the Evi-] Myeloid Transforming Gene. *Mol. Cell. Biol.* **10**, 1259–1264 (1990).

89. Delwel, R., Funabiki, T., Kreider, B. L., Morishita, K. & Ihle, J. N. Four of the seven zinc fingers of the Evi-1 myeloid-transforming gene are required for sequence-specific binding to GA(C/T)AAGA(T/C)AAGATAA. *Mol. Cell. Biol.* **13**, 4291–300 (1993).

90. Funabiki, T., Kreider, B. L. & Ihle, J. N. The carboxyl domain of zinc fingers of the Evi-1 myeloid transforming gene binds a consensus sequence of GAAGATGAG. *Oncogene* **9**, 1575–81 (1994).

91. Yatsula, B. *et al.* Identification of Binding Sites of EVI1 in Mammalian Cells. *J. Biol. Chem.* **280**, 30712–30722 (2005).

92. Perkins, A. S. & Kim, J. H. Zinc fingers 1-7 of EVI1 fail to bind to the GATA motif by itself but require the core site GACAAGATA for binding. *J. Biol. Chem.* **271**, 1104–10 (1996).

93. Izutsu, K. *et al.* The corepressor CtBP interacts with Evi-1 to repress transforming growth factor β signaling. *Blood* **97**, (2001).

94. Palmer, S. *et al.* Evi-1 Transforming and Repressor Activities Are Mediated by CtBP Co-repressor Proteins. *J. Biol. Chem.* **276**, 25834–25840 (2001).

95. Bard-Chapeau, E. A. *et al.* EVI1 oncoprotein interacts with a large and complex network of proteins and integrates signals through protein phosphorylation. *Proc. Natl. Acad. Sci. U. S. A.* **110**, E2885-94 (2013).

96. Dutta, P. *et al.* EVI1 splice variants modulate functional responses in ovarian cancer cells. *Mol. Oncol.* **7**, 647–668 (2013).

97. Bartholomew, C., Kilbey, A., Clark, A.-M. & Walker, M. The Evi-1 proto-oncogene encodes a transcriptional repressor activity associated with transformation. *Oncogene* **14**, 569–577 (1997).

98. Fears, S. *et al.* Intergenic splicing of MDS1 and EVI1 occurs in normal tissues as well as in myeloid leukemia and produces a new member of the PR domain family. *Proc. Natl. Acad. Sci. U. S. A.* **93**, 1642–7 (1996).

99. Pinheiro, I. *et al.* Prdm3 and Prdm16 are H3K9me1 Methyltransferases Required for Mammalian Heterochromatin Integrity. *Cell* **150**, 948–960 (2012).

100. Soderholm, J., Kobayashi, H., Mathieu, C., Rowley, J. D. & Nucifora, G. The leukemia-associated gene MDS1/EVI1 is a new type of GATA-binding transactivator. *Leukemia* **11**, 352–8 (1997).

101. Konrad, T. A. *et al.* Inducible expression of EVI1 in human myeloid cells causes phenotypes consistent with its role in myelodysplastic syndromes. *J. Leukoc. Biol.* **86**, 813–22 (2009).

102. Bordereaux, D., Fichelson, S., Tambourin, P. & Gisselbrecht, S. Alternative splicing of the Evi-1 zinc finger gene generates mRNAs which differ by the number of zinc finger motifs. *Oncogene* **5**, 925–927 (1990).

103. Sayadi, A. *et al.* Functional features of EVI1 and EVI1Δ324 isoforms of MECOM gene in genome-wide transcription regulation and oncogenicity. *Oncogene* **35**, 2311–2321 (2016).

104. Hoyt, P. R. *et al.* The Evi1 proto-oncogene is required at midgestation for neural, heart, and paraxial mesenchyme development. *Mech. Dev.* **65**, 55–70 (1997).

105. Yuasa, H. *et al.* Oncogenic transcription factor Evi1 regulates hematopoietic stem cell proliferation through GATA-2 expression. *EMBO J.* **24**, 1976–87 (2005).

106. Sato, T. *et al.* Evi-1 promotes para-aortic splanchnopleural hematopoiesis through up-regulation of GATA-2 and repression of TGF-b signaling. *Cancer Sci.* **99**, 1407–1413 (2008).

107. Sitailo, S., Sood, R., Barton, K. & Nucifora, G. Forced expression of the leukemia-associated gene EVI1 in ES cells: a model for myeloid leukemia with 3q26 rearrangements. *Leukemia* **13**, 1639–45 (1999).

108. Kataoka, K. *et al.* Evi1 is essential for hematopoietic stem cell self-renewal, and its expression marks hematopoietic cells with long-term multilineage repopulating activity. *J. Exp. Med.* **208**, 2403–2416 (2011).

109. Wang, Y. *et al.* Tracking hematopoietic precursor division ex vivo in real time. *Stem Cell Res. Ther.* (2018) doi:10.1186/s13287-017-0767-z.

110. Yoshimi, A. *et al.* Evi1 represses PTEN expression and activates PI3K/AKT/mTOR via interactions with polycomb proteins. *Blood* **117**, (2011).

111. Shimabe, M. *et al.* Pbx1 is a downstream target of Evi-1 in hematopoietic stem/progenitors and leukemic cells. *Oncogene* **28**, 4364–4374 (2009).

112. Kustikova, O. S. *et al.* Activation of Evi1 inhibits cell cycle progression and differentiation of hematopoietic progenitor cells. *Leukemia* **27**, 1127–1138 (2013).

113. Glass, C. *et al.* Global Identification of EVI1 Target Genes in Acute Myeloid Leukemia. *PLoS One* **8**, e67134 (2013).

114. Tanaka, T. *et al.* Dual functions of the AML1/Evi-1 chimeric protein in the mechanism of leukemogenesis in t(3;21) leukemias. *Mol. Cell. Biol.* **15**, 2383–92 (1995).

115. Kilbey, a & Bartholomew, C. Evi-1 ZF1 DNA binding activity and a second distinct transcriptional repressor region are both required for optimal transformation of Rat1 fibroblasts. *Oncogene* **16**, 2287–2291 (1998).

116. Kilbey, A., Stephens, V. & Bartholomew, C. Loss of cell cycle control by deregulation of cyclin-dependent kinase 2 kinase activity in Evi-1 transformed fibroblasts. *Cell Growth Differ.* **10**, 601–10 (1999).

117. Lavau, C., Szilvassy, S. J., Slany, R. & Cleary, M. L. Immortalization and leukemic

transformation of a myelomonocytic precursor by retrovirally transduced HRX-ENL. *EMBO J.* (1997) doi:10.1093/emboj/16.14.4226.

118. Senyuk, V. *et al.* The leukemia-associated transcription repressor aml1/mds1/evi1 requires ctbp to induce abnormal growth and differentiation of murine hematopoietic cells. *Oncogene* (2002) doi:10.1038/sj.onc.1205436.

119. Senyuk, V., Li, D., Zakharov, A., Mikhail, F. M. & Nucifora, G. The distal zinc finger domain of AML1/MDS1/EVI1 is an oligomerization domain involved in induction of hematopoietic differentiation defects in primary cells in vitro. *Cancer Res.* (2005) doi:10.1158/0008-5472.CAN-05-0412.

120. Takeshita, M. *et al.* AML1-Evi-1 specifically transforms hematopoietic stem cells through fusion of the entire Evi-1 sequence to AML1. *Leukemia* (2008) doi:10.1038/leu.2008.53.

121. Buonamici, S. *et al.* EVI1 induces myelodysplastic syndrome in mice. *J. Clin. Invest.* **114**, 713–9 (2004).

122. Laricchia-Robbio, L. *et al.* Point Mutations in Two EVI1 Zn Fingers Abolish EVI1-GATA1 Interaction and Allow Erythroid Differentiation of Murine Bone Marrow Cells. *Mol. Cell. Biol.* **26**, 7658–7666 (2006).

123. Maicas, M. *et al.* The MDS and EVI1 complex locus (MECOM) isoforms regulate their own transcription and have different roles in the transformation of hematopoietic stem and progenitor cells. *Biochim. Biophys. Acta - Gene Regul. Mech.* **1860**, 721–729 (2017).

124. Laricchia-Robbio, L. & Nucifora, G. Significant increase of self-renewal in hematopoietic cells after forced expression of EVI1. *Blood Cells, Mol. Dis.* **40**, 141–147 (2008).

125. White, D. J. *et al.* Phosphorylation of the Leukemic Oncoprotein EVI1 on Serine 196 Modulates DNA Binding, Transcriptional Repression and Transforming Ability. *PLoS One* **8**, (2013).

126. Zhang, Y. *et al.* Essential role of PR-domain protein MDS1-EVI1 in MLL-AF9 leukemia. *Blood* **122**, 2888–92 (2013).

127. Singh, S., Pradhan, A. K. & Chakraborty, S. SUMO1 negatively regulates the transcriptional activity of EVI1 and significantly increases its co-localization with EVI1 after treatment with arsenic trioxide. *Biochim. Biophys. Acta - Mol. Cell Res.* **1833**, 2357–2368 (2013).

128. Shackelford, D., Kenific, C., Blusztajn, A., Waxman, S. & Ren, R. Targeted degradation of the AML1/MDS1/EVI1 oncoprotein by arsenic trioxide. *Cancer Res.* **66**, 11360–9 (2006).

129. Shimahara, A., Yamakawa, N., Nishikata, I. & Morishita, K. Acetylation of Lysine 564 Adjacent to the C-terminal Binding Protein-binding Motif in EVI1 Is Crucial for Transcriptional Activation of *GATA2*. *J. Biol. Chem.* **285**, 16967–16977 (2010).

130. Shiromizu, T. *et al.* Identification of missing proteins in the neXtProt database and unregistered phosphopeptides in the phosphositeplus database as part of the chromosome-centric human proteome project. *J. Proteome Res.* (2013) doi:10.1021/pr300825v.

131. Paredes, R. *et al.* EVI1 carboxy-terminal phosphorylation is ATM-mediated and sustains transcriptional modulation and self-renewal via enhanced CtBP1 association. *Nucleic Acids Res.* (2018) doi:10.1093/nar/gky536.

132. Klammer, M. *et al.* Phosphosignature predicts dasatinib response in non-small cell lung cancer. *Mol. Cell. Proteomics* (2012) doi:10.1074/mcp.M111.016410.

133. Matsuoka, S. *et al.* ATM and ATR substrate analysis reveals extensive protein networks responsive to DNA damage. *Science (80-.).* (2007) doi:10.1126/science.1140321.

134. Mertins, P. *et al.* Ischemia in tumors induces early and sustained phosphorylation changes in stress kinase pathways but does not affect global protein levels. *Mol. Cell. Proteomics* (2014) doi:10.1074/mcp.M113.036392.

135. Mertins, P. *et al.* Proteogenomics connects somatic mutations to signalling in breast cancer. *Nature* (2016) doi:10.1038/nature18003.

136. Zhou, H. *et al.* Toward a comprehensive characterization of a human cancer cell phosphoproteome. *J. Proteome Res.* (2013) doi:10.1021/pr300630k.

137. Sharma, K. *et al.* Ultradeep Human Phosphoproteome Reveals a Distinct Regulatory Nature of Tyr and Ser/Thr-Based Signaling. *Cell Rep.* (2014) doi:10.1016/j.celrep.2014.07.036.

138. Kettenbach, A. N. *et al.* Quantitative phosphoproteomics identifies substrates and functional modules of Aurora and Polo-like kinase activities in mitotic cells. *Sci. Signal.* (2011) doi:10.1126/scisignal.2001497.

139. Schweppe, D. K., Rigas, J. R. & Gerber, S. A. Quantitative phosphoproteomic profiling of human non-small cell lung cancer tumors. *J. Proteomics* (2013) doi:10.1016/j.jprot.2013.07.023.

140. Armenteros-Monterroso, E. *et al.* The AAA+ATPase RUVBL2 is essential for the oncogenic function of c-MYB in acute myeloid leukemia. *Leukemia* (2019) doi:10.1038/s41375-019-0495-8.

141. Grigoletto, A., Lestienne, P. & Rosenbaum, J. The multifaceted proteins Reptin and Pontin as major players in cancer. *Biochimica et Biophysica Acta - Reviews on Cancer* (2011) doi:10.1016/j.bbcan.2010.11.002.

142. Basta, J. & Rauchman, M. The nucleosome remodeling and deacetylase complex in development and disease. *Translational Research* (2015) doi:10.1016/j.trsl.2014.05.003.

143. Dcona, M. M., Morris, B. L., Ellis, K. C. & Grossman, S. R. CtBP- an emerging oncogene and novel small molecule drug target: Advances in the understanding of its oncogenic action and identification of therapeutic inhibitors. *Cancer Biol. Ther.* **18**, 379–391 (2017).

144. Chakraborty, S., Senyuk, V., Sitailo, S., Chi, Y. & Nucifora, G. Interaction of EVI1 with cAMP-responsive Element-binding Protein-binding Protein (CBP) and p300/CBP-associated Factor (P/CAF) Results in Reversible Acetylation of EVI1 and in Co-localization in Nuclear Speckles. *J. Biol. Chem.* **276**, 44936–44943 (2001).

145. Hirai, H., Izutsu, K., Kurokawa, M. & Mitani, K. Oncogenic mechanisms of Evi-1 protein. *Cancer Chemother. Pharmacol.* (2001) doi:10.1007/s002800100303.

146. Ivanochko, D. *et al.* Direct interaction between the PRDM3 and PRDM16 tumor suppressors and the NuRD chromatin remodeling complex. *Nucleic Acids Res.* (2019) doi:10.1093/nar/gky1192.

147. Chinnadurai, G. Transcriptional regulation by C-terminal binding proteins. *Int. J. Biochem. Cell Biol.* **39**, 1593–1607 (2007).

148. Nitta, E. *et al.* Oligomerization of Evi-1 regulated by the PR domain contributes to recruitment of corepressor CtBP. *Oncogene* **24**, 6165–6173 (2005).

149. Turner, J. & Crossley, M. Cloning and characterization of mCtBP2, a co-repressor that associates with basic Kruppel-like factor and other mammalian transcriptional regulators. *EMBO J.* (1998) doi:10.1093/emboj/17.17.5129.

150. Chinnadurai, G. The transcriptional corepressor CtBP: A foe of multiple tumor suppressors. *Cancer Research* (2009) doi:10.1158/0008-5472.CAN-08-3349.

151. Di, L. J. *et al.* Genome-wide profiles of CtBP link metabolism with genome stability and epithelial reprogramming in breast cancer. *Nat. Commun.* (2013) doi:10.1038/ncomms2438.

152. Xia, Z. B., Anderson, M., Diaz, M. O. & Zeleznik-Le, N. J. MLL repression domain interacts with histone deacetylases, the polycomb group proteins HPC2 and BMI-1, and the corepressor C-terminal-binding protein. *Proc. Natl. Acad. Sci. U. S. A.* (2003) doi:10.1073/pnas.1436338100.

153. Hildebrand, J. D. & Soriano, P. Overlapping and Unique Roles for C-Terminal Binding Protein 1 (CtBP1) and CtBP2 during Mouse Development. *Mol. Cell. Biol.* (2002) doi:10.1128/mcb.22.15.5296-5307.2002.

154. Irigoyen, M., García-Ruiz, J. C. & Berra, E. The hypoxia signalling pathway in haematological malignancies. *Oncotarget* (2017) doi:10.18632/oncotarget.15981.

155. Korwar, S. *et al.* Design, synthesis, and biological evaluation of substrate-competitive inhibitors of C-terminal Binding Protein (CtBP). *Bioorganic Med. Chem.* (2016) doi:10.1016/j.bmc.2016.04.037.

156. Postigo, A. A. & Dean, D. C. ZEB represses transcription through interaction with the corepressor CtBP. *Proc. Natl. Acad. Sci. U. S. A.* **96**, 6683–8 (1999).

157. Cowger, J. J. M., Zhao, Q., Isovic, M. & Torchia, J. Biochemical characterization of the zinc-finger protein 217 transcriptional repressor complex: identification of a ZNF217 consensus recognition sequence. *Oncogene* **26**, 3378–3386 (2007).

158. Ballas, N. *et al.* Regulation of neuronal traits by a novel transcriptional complex. *Neuron* **31**, 353–65 (2001).

159. Caron, C. *et al.* Cdyl: a new transcriptional co-repressor. *EMBO Rep.* **4**, 877–882 (2003).

160. Fernandes, I. *et al.* Ligand-dependent nuclear receptor corepressor LCoR functions by histone deacetylase-dependent and -independent mechanisms. *Mol. Cell* **11**, 139–50 (2003).

161. Tachibana, M. *et al.* Histone methyltransferases G9a and GLP form heteromeric complexes and are both crucial for methylation of euchromatin at H3-K9. *Genes Dev.* **19**, 815–826 (2005).

162. Santos-Rosa, H. *et al.* Active genes are tri-methylated at K4 of histone H3. *Nature* **419**, 407–411 (2002).

163. Metzger, E. *et al.* LSD1 demethylates repressive histone marks to promote androgen-receptor-dependent transcription. *Nature* **437**, 436 (2005).

164. Ginder, G. D. EV(I1)olution of AML DNA methylation. *Blood* **117**, (2011).

165. Lugthart, S. *et al.* Aberrant DNA hypermethylation signature in acute myeloid leukemia directed by EVI1. *Blood* **117**, 234–41 (2011).

166. Holz-Schietinger, C., Matje, D. M., Harrison, M. F. & Reich, N. O. Oligomerization of DNMT3A controls the mechanism of de novo DNA methylation. *J. Biol. Chem.* (2011) doi:10.1074/jbc.M111.284687.

167. Challen, G. A. *et al.* Dnmt3a is essential for hematopoietic stem cell differentiation. *Nat. Genet.* (2012) doi:10.1038/ng.1009.

168. Jeong, M. *et al.* Loss of Dnmt3a Immortalizes Hematopoietic Stem Cells In Vivo. *Cell Rep.* (2018) doi:10.1016/j.celrep.2018.03.025.

169. Lu, R. *et al.* A model system for studying the DNMT3A HOTSPO mutation (DNMT3AR882) demonstrates a causal relationship between its dominant-negative effect and leukemogenesis. *Cancer Res.* (2019) doi:10.1158/0008-5472.CAN-18-3275.

170. Dai, Y. J. *et al.* Conditional knockin of Dnmt3a R878H initiates acute myeloid leukemia with mTOR pathway involvement. *Proc. Natl. Acad. Sci. U. S. A.* (2017) doi:10.1073/pnas.1703476114.

171. Russler-Germain, D. A. *et al.* The R882H DNMT3A Mutation Associated with AML Dominantly Inhibits Wild-Type DNMT3A by Blocking Its Ability to Form Active Tetramers. *Cancer Cell* (2014) doi:10.1016/j.ccr.2014.02.010.

172. Spencer, D. H. *et al.* CpG Island Hypermethylation Mediated by DNMT3A Is a Consequence of AML Progression. *Cell* (2017) doi:10.1016/j.cell.2017.01.021.

173. Jones, P. A. & Baylin, S. B. The Epigenomics of Cancer. *Cell* **128**, 683–692 (2007).

174. Figueroa, M. E. *et al.* DNA Methylation Signatures Identify Biologically Distinct Subtypes in Acute Myeloid Leukemia. *Cancer Cell* **17**, 13–27 (2010).

175. Senyuk, V., Premanand, K., Xu, P., Qian, Z. & Nucifora, G. The oncoprotein EVI1 and the DNA methyltransferase Dnmt3 co-operate in binding and De Novo methylation of target DNA. *PLoS One* (2011) doi:10.1371/journal.pone.0020793.

176. Fisser, M. C. *et al.* Induction of the proapoptotic tumor suppressor gene *Cell Adhesion Molecule 1* by chemotherapeutic agents is repressed in therapy resistant acute myeloid leukemia. *Mol. Carcinog.* **54**, 1815–1819 (2015).

177. Dickstein, J. *et al.* Methylation and silencing of miRNA-124 by EVI1 and self-renewal exhaustion of hematopoietic stem cells in murine myelodysplastic syndrome. *Proc. Natl. Acad. Sci. U. S. A.* (2010) doi:10.1073/pnas.1004297107.

178. van der Weyden, L. *et al.* Increased tumorigenesis associated with loss of the tumor suppressor gene Cadm1. *Mol. Cancer* (2012) doi:10.1186/1476-4598-11-29.

179. Hess, C. J. *et al.* Concurrent methylation of promoters from tumor associated genes predicts outcome in acute myeloid leukemia. *Leuk. Lymphoma* (2008) doi:10.1080/10428190802035990.

180. Nowek, K. *et al.* Expression of a passenger miR-9∗ predicts favorable outcome in adults with acute myeloid leukemia less than 60 years of age. *Leukemia* (2016) doi:10.1038/leu.2015.282.

181. Guo, X. *et al.* Structural insight into autoinhibition and histone H3-induced activation of DNMT3A. *Nature* (2015) doi:10.1038/nature13899.

182. Wong, K. K., Lawrie, C. H. & Green, T. M. Oncogenic Roles and Inhibitors of DNMT1, DNMT3A, and DNMT3B in Acute Myeloid Leukaemia. *Biomarker Insights* (2019) doi:10.1177/1177271919846454.

183. Meyer, S. *et al.* A cross-linker-sensitive myeloid leukemia cell line from a 2-year-old boy with severe Fanconi anemia and biallelicFANCD1/BRCA2 mutations. *Genes, Chromosom. Cancer* **42**, 404–415 (2005).

184. Yamaguchi, M. & Kashiwakura, I. Role of Reactive Oxygen Species in the Radiation Response of Human Hematopoietic Stem/Progenitor Cells. *PLoS One* (2013) doi:10.1371/journal.pone.0070503.

185. Benhusein, G. M., Mutch, E., Aburawi, S. & Williams, F. M. Genotoxic effect induced by hydrogen peroxide in human hepatoma cells using comet assay. *Libyan J. Med.* (2010) doi:10.3402/ljm.v5i0.4637.

186. Hickson, I. *et al.* Identification and characterization of a novel and specific inhibitor of the ataxia-telangiectasia mutated kinase ATM. *Cancer Res.* (2004) doi:10.1158/0008-5472.CAN-04-2727.

187. Pike, K. G. *et al.* The Identification of Potent, Selective, and Orally Available Inhibitors of Ataxia Telangiectasia Mutated (ATM) Kinase: The Discovery of AZD0156 (8-{6-[3-(Dimethylamino)propoxy]pyridin-3-yl}-3-methyl-1-(tetrahydro-2 H-pyran-4-yl)-1,3-dihydro-2 H-imidazo[4. *J. Med. Chem.* (2018) doi:10.1021/acs.jmedchem.7b01896.

188. Durant, S. T. *et al.* The brain-penetrant clinical ATM inhibitor AZD1390 radiosensitizes and improves survival of preclinical brain tumor models. *Sci. Adv.* (2018) doi:10.1126/sciadv.aat1719.

189. Gupta, D., Shah, H. P., Malu, K., Berliner, N. & Gaines, P. Differentiation and characterization of myeloid cells. *Curr. Protoc. Immunol.* (2014) doi:10.1002/0471142735.im22f05s104.

190. Barlow, J. L. *et al.* A p53-dependent mechanism underlies macrocytic anemia in a mouse model of human 5q-syndrome. *Nat. Med.* (2010) doi:10.1038/nm.2063.

191. Pillay, J., Tak, T., Kamp, V. M. & Koenderman, L. Immune suppression by neutrophils and granulocytic myeloid-derived suppressor cells: Similarities and differences. *Cellular and Molecular Life Sciences* (2013) doi:10.1007/s00018-013-1286-4.

192. Takahashi, S. & Licht, J. D. The human promyelocytic leukemia zinc finger gene is regulated by the Evi-1 oncoprotein and a novel guanine-rich site binding protein. *Leukemia* (2002) doi:10.1038/sj.leu.2402682.

193. Bard-Chapeau, E. A. *et al.* Ecotopic viral integration site 1 (EVI1) regulates multiple cellular processes important for cancer and is a synergistic partner for FOS protein in invasive tumors. *Proc. Natl. Acad. Sci.* **109**, 2168–2173 (2012).

194. Livak, K. J. & Schmittgen, T. D. Analysis of Relative Gene Expression Data Using Real-Time Quantitative PCR and the 2−ΔΔCT Method. *Methods* **25**, 402–408 (2001).

195. Aken, B. L. *et al.* Ensembl 2017. *Nucleic Acids Res.* (2017) doi:10.1093/nar/gkw1104.

196. Cunningham, F. *et al.* Ensembl 2019. *Nucleic Acids Res.* (2019) doi:10.1093/nar/gky1113.

197. Aggarwal, C. C., Hinneburg, A. & Keim, D. A. On the surprising behavior of distance metrics in high dimensional space. in *Lecture Notes in Computer Science (including subseries Lecture Notes in Artificial Intelligence and Lecture Notes in Bioinformatics)* (2001). doi:10.1007/3-540-44503-x_27.

198. Unwin, R. D. *et al.* Multiple reaction monitoring to identify sites of protein phosphorylation with high sensitivity. *Mol. Cell. Proteomics* (2005) doi:10.1074/mcp.M500113-MCP200.

199. Sievers, F. *et al.* Fast, scalable generation of high-quality protein multiple sequence alignments using Clustal Omega. *Mol. Syst. Biol.* (2011) doi:10.1038/msb.2011.75.

200. UniProt Consortium, T. UniProt: the universal protein knowledgebase. *Nucleic Acids Res.* (2018) doi:10.1093/nar/gky092.

201. Waterhouse, A. M., Procter, J. B., Martin, D. M. A., Clamp, M. & Barton, G. J. Jalview Version 2-A multiple sequence alignment editor and analysis workbench. *Bioinformatics* (2009) doi:10.1093/bioinformatics/btp033.

202. Safaei, J., Maňuch, J., Gupta, A., Stacho, L. & Pelech, S. Prediction of 492 human protein kinase substrate specificities. *Proteome Sci.* (2011) doi:10.1186/1477-5956-9-S1-S6.

203. Roy, A., Kucukural, A. & Zhang, Y. I-TASSER: A unified platform for automated protein structure and function prediction. *Nat. Protoc.* (2010) doi:10.1038/nprot.2010.5.

204. Bellesis, A. G., Jecrois, A. M., Hayes, J. A., Schiffer, C. A. & Royer, W. E. Assembly of human C-terminal binding protein (CtBP) into tetramers. *J. Biol. Chem.* (2018) doi:10.1074/jbc.RA118.002514.

205. Kozakov, D. *et al.* The ClusPro web server for protein-protein docking. *Nat. Protoc.* (2017) doi:10.1038/nprot.2016.169.

206. Schmid, N. *et al.* Definition and testing of the GROMOS force-field versions 54A7 and 54B7. *Eur. Biophys. J.* (2011) doi:10.1007/s00249-011-0700-9.

207. Zielkiewicz, J. Structural properties of water: Comparison of the SPC, SPCE, TIP4P, and TIP5P models of water. *J. Chem. Phys.* (2005) doi:10.1063/1.2018637.

208. Margreitter, C., Petrov, D. & Zagrovic, B. Vienna-PTM web server: a toolkit for MD simulations of protein post-translational modifications. *Nucleic Acids Res.* (2013) doi:10.1093/nar/gkt416.

209. Abraham, M. J. & Gready, J. E. Optimization of parameters for molecular dynamics simulation using smooth particle-mesh Ewald in GROMACS 4.5. *J. Comput. Chem.* (2011) doi:10.1002/jcc.21773.

210. Labík, S. & Smith, W. R. Scaled particle theory and the efficient calculation of the chemical potential of hard spheres in the NYT ensemble. *Mol. Simul.* (1994) doi:10.1080/08927029408022533.

211. Panagiotopoulos, A. Z. Direct determination of phase coexistence properties of fluids by monte carlo simulation in a new ensemble. *Mol. Phys.* (1987) doi:10.1080/00268978700101491.

212. Abraham, M. J. *et al.* Gromacs: High performance molecular simulations through multi-level parallelism from laptops to supercomputers. *SoftwareX* (2015) doi:10.1016/j.softx.2015.06.001.

213. Kumari, R., Kumar, R. & Lynn, A. G-mmpbsa -A GROMACS tool for high-throughput MM-PBSA calculations. *J. Chem. Inf. Model.* (2014) doi:10.1021/ci500020m.

214. Nash, A., Collier, T., Birch, H. L. & de Leeuw, N. H. ForceGen: atomic covalent bond value derivation for Gromacs. *J. Mol. Model.* (2018) doi:10.1007/s00894-017-3530-6.

215. Matsuoka, S. *et al.* ATM and ATR substrate analysis reveals extensive protein networks responsive to DNA damage. *Science* **316**, 1160–6 (2007).

216. Maréchal, A. & Zou, L. DNA damage sensing by the ATM and ATR kinases. *Cold*

Spring Harb. Perspect. Biol. (2013) doi:10.1101/cshperspect.a012716.

217. Kataoka, K. *et al.* Evi1 is essential for hematopoietic stem cell self-renewal, and its expression marks hematopoietic cells with long-term multilineage repopulating activity. *J. Exp. Med.* **208**, 2403–16 (2011).

218. Canté-Barrett, K. *et al.* Lentiviral gene transfer into human and murine hematopoietic stem cells: size matters. *BMC Res. Notes* **9**, 312 (2016).

219. Hickson, I., Pike, K. G. & Durant, S. T. Targeting ATM for Cancer Therapy: Prospects for Drugging ATM. in (2018). doi:10.1007/978-3-319-75836-7_8.

220. Goyama, S. *et al.* EVI-1 interacts with histone methyltransferases SUV39H1 and G9a for transcriptional repression and bone marrow immortalization. *Leukemia* **24**, 81–88 (2010).

221. Park, Y.-G. *et al.* Effects of Feeder Cell Types on Culture of Mouse Embryonic Stem Cell In Vitro. *Dev. Reprod.* (2015) doi:10.12717/dr.2015.19.3.119.

222. Prieto, I. *et al.* Metabolic adaptations in spontaneously immortalized PGC-1α knock-out mouse embryonic fibroblasts increase their oncogenic potential. *Redox Biol.* (2020) doi:10.1016/j.redox.2019.101396.

223. Wilson, M. *et al.* EVI1 interferes with myeloid maturation via transcriptional repression of Cebpa, via binding to two far downstream regulatory elements. *J. Biol. Chem.* (2016) doi:10.1074/jbc.M115.708156.

224. Ayoub, E. *et al.* EVI1 overexpression reprograms hematopoiesis via upregulation of Spi1 transcription. *Nat. Commun.* (2018) doi:10.1038/s41467-018-06208-y.

225. Heller, G. *et al.* EVI1 promotes tumor growth via transcriptional repression of MS4A3. *J. Hematol. Oncol.* (2015) doi:10.1186/s13045-015-0124-6.

226. Hilbert, B. J., Grossman, S. R., Schiffer, C. A. & Royer, W. E. Crystal structures of human CtBP in complex with substrate MTOB reveal active site features useful for inhibitor design. *FEBS Lett.* (2014) doi:10.1016/j.febslet.2014.03.026.

227. Hilbert, B. J. *et al.* Structure-guided design of a high affinity inhibitor to human CtBP. *ACS Chem. Biol.* (2015) doi:10.1021/cb500820b.

228. Osaki, H. *et al.* The AAA+ ATPase RUVBL2 is a critical mediator of MLL-AF9 oncogenesis. *Leukemia* (2013) doi:10.1038/leu.2013.42.

229. Mellacheruvu, D. *et al.* The CRAPome: A contaminant repository for affinity purification-mass spectrometry data. *Nat. Methods* (2013) doi:10.1038/nmeth.2557.

230. Yamaguchi, S. *et al.* Dynamics of 5-methylcytosine and 5-hydroxymethylcytosine during germ cell reprogramming. *Cell Res.* (2013) doi:10.1038/cr.2013.22.

231. Liu, H. *et al.* Phosphorylation of MLL by ATR is required for execution of mammalian S-phase checkpoint. *Nature* (2010) doi:10.1038/nature09350.

232. Guo, H. & Friedman, A. D. Phosphorylation of RUNX1 by Cyclin-Dependent Kinase Reduces Direct Interaction with HDAC1 and HDAC3 and Stimulates Marrow Progenitor Proliferation. *Blood* (2009) doi:10.1182/blood.v114.22.2508.2508.

233. Menghini, R. *et al.* Phosphorylation of GATA2 by akt increases adipose tissue differentiation and reduces adipose tissue-related inflammation: A novel pathway linking obesity to atherosclerosis. *Circulation* (2005) doi:10.1161/01.CIR.0000161814.02942.B2.

234. Wee, H. J., Voon, D. C. C., Bae, S. C. & Ito, Y. PEBP2-2/CBF-2 dependent phosphorylation of RUNX1 and p300 by HIPK2: Implications for leukemogenesis. *Blood* (2008) doi:10.1182/blood-2008-01-134122.

235. Goyama, S., Huang, G., Kurokawa, M. & Mulloy, J. C. Posttranslational modifications of RUNX1 as potential anticancer targets. *Oncogene* (2015) doi:10.1038/onc.2014.305.

236. Altomare, D. A. *et al.* AKT and mTOR phosphorylation is frequently detected in ovarian cancer and can be targeted to disrupt ovarian tumor cell growth. *Oncogene* (2004) doi:10.1038/sj.onc.1207721.

237. Chen, Z. & Cole, P. A. Synthetic approaches to protein phosphorylation. *Current Opinion in Chemical Biology* (2015) doi:10.1016/j.cbpa.2015.07.001.

238. Yoshimi, A. *et al.* Evi1 represses PTEN expression and activates PI3K/AKT/mTOR via interactions with polycomb proteins. *Blood* **117**, 3617–3628 (2011).

239. Morgado-Palacin, I. *et al.* Targeting the kinase activities of ATR and ATM exhibits antitumoral activity in mouse models of MLL-rearranged AML. *Sci. Signal.* (2016) doi:10.1126/scisignal.aad8243.

240. Forster, K. *et al.* Role of p21WAF1/CIP1 as an attenuator of both proliferative and drug-induced apoptotic signals in BCR-ABL-transformed hematopoietic cells. *Ann. Hematol.* (2008) doi:10.1007/s00277-007-0400-9.

241. Cros, E., Jordheim, L., Dumontet, C. & Galmarini, C. M. Problems related to resistance to cytarabine in acute myeloid leukemia. *Leukemia and Lymphoma* (2004) doi:10.1080/1042819032000159861.

242. Shelton, J. *et al.* Metabolism, Biochemical Actions, and Chemical Synthesis of Anticancer Nucleosides, Nucleotides, and Base Analogs. *Chemical Reviews* (2016) doi:10.1021/acs.chemrev.6b00209.

243. Lara, L. I. *et al.* Coupling the core of the anticancer drug etoposide to an oligonucleotide induces topoisomerase II-mediated cleavage at specific DNA sequences. *Nucleic Acids Res.* (2018) doi:10.1093/nar/gky072.

244. Marinello, J., Delcuratolo, M. & Capranico, G. Anthracyclines as Topoisomerase II poisons: From early studies to new perspectives. *International Journal of Molecular Sciences* (2018) doi:10.3390/ijms19113480.

245. Kellaway, S. G., Keane, P., Kennett, E. & Bonifer, C. RUNX1-EVI1 disrupts lineage determination and the cell cycle by interfering with RUNX1 and EVI1 driven gene regulatory networks. *Haematologica* (2020) doi:10.3324/haematol.2019.241885.

246. Franco, M. *et al.* The Adaptor Protein Tom1L1 Is a Negative Regulator of Src Mitogenic Signaling Induced by Growth Factors. *Mol. Cell. Biol.* (2006) doi:10.1128/mcb.26.5.1932-1947.2006.

247. Kannan, A., Bhatia, K., Branzei, D. & Gangwani, L. Combined deficiency of Senataxin and DNA-PKcs causes DNA damage accumulation and neurodegeneration in spinal muscular atrophy. *Nucleic Acids Res.* (2018) doi:10.1093/nar/gky641.

248. Messaoudi-Aubert, S. E. L. *et al.* Role for the MOV10 RNA helicase in Polycomb-mediated repression of the INK4a tumor suppressor. *Nat. Struct. Mol. Biol.* (2010) doi:10.1038/nsmb.1824.

249. Hennrich, M. L. *et al.* Cell-specific proteome analyses of human bone marrow reveal molecular features of age-dependent functional decline. *Nat. Commun.* (2018)

doi:10.1038/s41467-018-06353-4.

250. Jairam, V., Roberts, K. B. & Yu, J. B. Historical trends in the use of radiation therapy for pediatric cancers: 1973-2008. *Int. J. Radiat. Oncol. Biol. Phys.* (2013) doi:10.1016/j.ijrobp.2012.10.007.

251. Burnett, A., Wetzler, M. & Löwenberg, B. Therapeutic advances in acute myeloid leukemia. *Journal of Clinical Oncology* (2011) doi:10.1200/JCO.2010.30.1820.

252. Matsuoka, S. *et al.* Damage ATM and ATR Substrate Reveals Responsive Analysis Protein Networks to DNA Damage. *Science (80-.).* **316**, 1160–1167 (2014).

253. Foote, K. M. *et al.* Discovery and Characterization of AZD6738, a Potent Inhibitor of Ataxia Telangiectasia Mutated and Rad3 Related (ATR) Kinase with Application as an Anticancer Agent. *J. Med. Chem.* (2018) doi:10.1021/acs.jmedchem.8b01187.

254. Walters, D. K. *et al.* Phosphoproteomic analysis of AML cell lines identifies leukemic oncogenes. *Leuk. Res.* (2006) doi:10.1016/j.leukres.2006.01.001.

255. Aasebø, E., B. Forthun, R., Berven, F., Selheim, F. & Hernandez-Valladares, M. Global Cell Proteome Profiling, Phospho-signaling and Quantitative Proteomics for Identification of New Biomarkers in Acute Myeloid Leukemia Patients. *Curr. Pharm. Biotechnol.* (2015) doi:10.2174/1389201016666150826115626.

256. Lahn, M. Patient-derived acute myeloid leukemia (AML) bone marrow cells display distinct intracellular kinase phosphorylation patterns. *Cancer Manag. Res.* (2009) doi:10.2147/cmr.s5611.

257. Schumich, A. *et al.* Phospho-Profiling Linking Biology and Clinics in Pediatric Acute Myeloid Leukemia. *HemaSphere* (2020) doi:10.1097/hs9.0000000000000312.

258. Rao, M. S. *et al.* Comparison of RNA-Seq and microarray gene expression platforms for the toxicogenomic evaluation of liver from short-term rat toxicity studies. *Front. Genet.* (2019) doi:10.3389/fgene.2018.00636.

259. Tomita, H., Tanaka, K., Tanaka, T. & Hara, A. Aldehyde dehydrogenase 1A1 in stem cells and cancer. *Oncotarget* (2016) doi:10.18632/oncotarget.6920.

260. Hale, J. S. *et al.* Cancer stem cell-specific scavenger receptor 36 drives glioblastoma progression. *Stem Cells* (2014) doi:10.1002/stem.1716.

261. Somervaille, T. C. P. & Cleary, M. L. Mutant CEBPA: Priming Stem Cells for Myeloid Leukemogenesis. *Cell Stem Cell* (2009) doi:10.1016/j.stem.2009.10.008.

262. Kallifatidis, G. *et al.* B-arrestins regulate stem cell-like phenotype and response to chemotherapy in bladder cancer. *Mol. Cancer Ther.* (2019) doi:10.1158/1535-7163.MCT-18-1167.

263. Stahl, M. *et al.* Hypomethylating agents in relapsed and refractory AML: Outcomes and their predictors in a large international patient cohort. *Blood Adv.* (2018) doi:10.1182/bloodadvances.2018016121.

264. Porter, D. C. *et al.* Abstract 1820: CDK3: A novel tumor-selective drug target involved in AP1 activation and transcriptional damage response. in (2012). doi:10.1158/1538-7445.am2012-1820.

265. Bonenfant, D. *et al.* Quantitation of changes in protein phosphorylation: A simple method based on stable isotope labeling and mass spectrometry. *Proc. Natl. Acad. Sci. U. S. A.* (2003) doi:10.1073/pnas.232735599.

266. Lechman, E. R. *et al.* MiR-126 Regulates Distinct Self-Renewal Outcomes in Normal

and Malignant Hematopoietic Stem Cells. *Cancer Cell* (2016) doi:10.1016/j.ccell.2015.12.011.

267. YUAN, X., WANG, X., BI, K. & JIANG, G. The role of EVI-1 in normal hematopoiesis and myeloid malignancies (Review). *Int. J. Oncol.* **47**, 2028–2036 (2015).

268. Maicas, M. *et al.* Functional characterization of the promoter region of the human EVI1 gene in acute myeloid leukemia: RUNX1 and ELK1 directly regulate its transcription. *Oncogene* **32**, 2069–2078 (2013).

Chapter 7 Appendix

7.1 Supplemental Figures

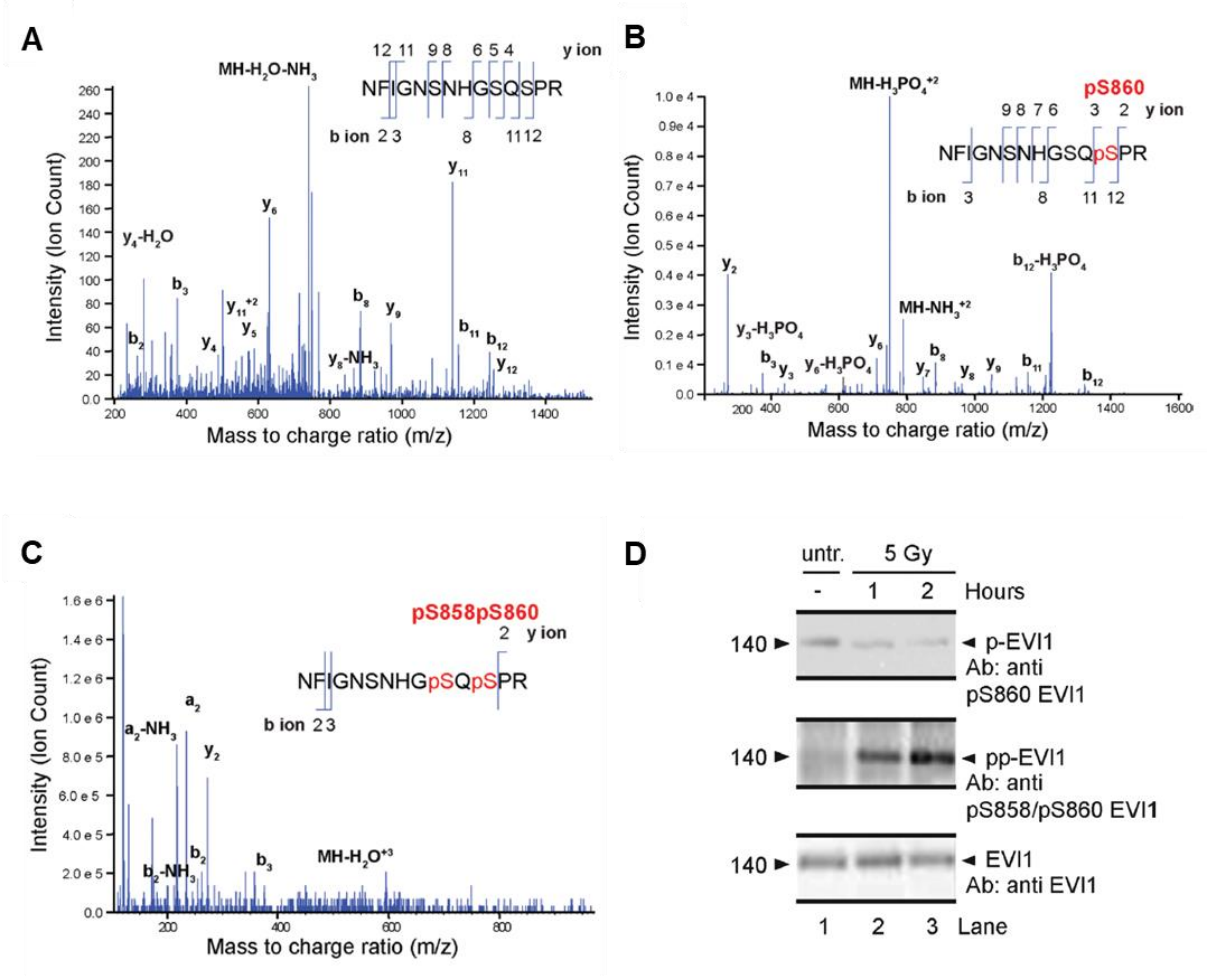

Figure 7.1: Carboxy-terminal phosphorylation. (A) *Mass spectrometry analysis of the EVI1 peptide Asn849-Arg862 from SB1690CB AML cells, demonstrating the presence of non-phosphorylated* ***(B)*** *and single Ser860 phosphorylated peptides in untreated SB1690CB cells.* ***(C)*** *The double phosphorylation of the carboxy-terminal S858/S860 SQS motif in irradiated SB1690CB cells. y- and b-type ions illustrating their position within the peptide sequence indicated. The mass/charge ratio (m/z) of the precursor ion is also shown.* ***(D)*** *Immunoprecipitated EVI1 from SB1690CB cells probed with anti-pS860-EVI1 (upper panel), and anti-pS858/pS860-EVI1 antibody, untreated (lane 1), and after 1 and 2 h (lane 2 and 3) post radiation.*

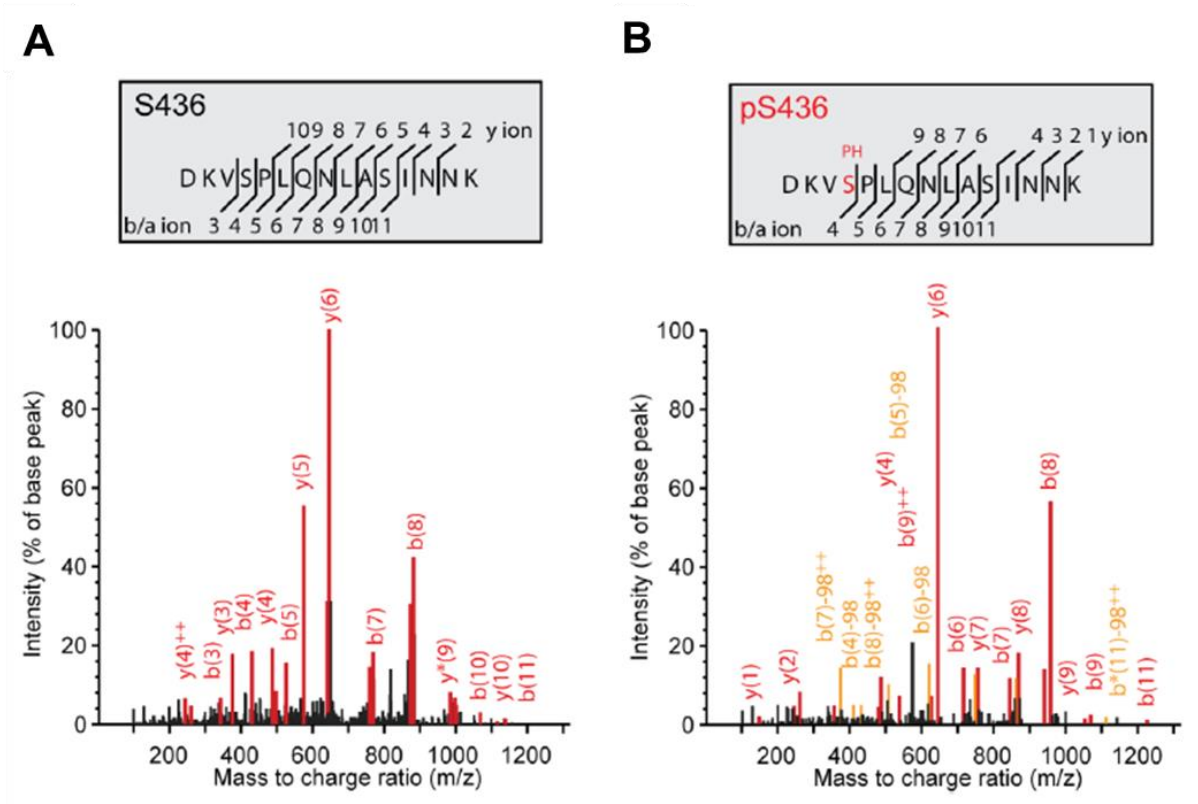

Figure 7.2: Serine 436 phosphorylation. (A and B) *Mass spectrometry analysis of the EVI1 peptide Asp433-Lys447 from SB1690CB AML cells non-phosphorylated, B, and S436 phosphorylated peptides, C.*

7.2 Supplemental Tables

Table 7.1: Previously reported EVI1 interacting proteins. *SILAC: Stable isotope labelling using amino acids in cell culture followed by mass spectrometry. Co-IP: co-immunoprecipitation. IF: immunofluorescence. Bold: proteins studied by Co-IP or IF in this report.*

Proteins	Tissue	Detection	References	Interactome
ADNP	SKOV3	SILAC	Bard-Chapeau *et al* 2013	only EVI1-WT
ARID1B	SKOV3, T74D	SILAC	Bard-Chapeau *et al* 2013, Ivanochko *et al* 2019	
AKT	293T	Co-IP	Yoshimi *et al* 2018	
B-ACTIN	293T	Co-IP	Yoshimi *et al* 2018	
CBFB	SKOV3, T74D	SILAC	Bard-Chapeau *et al* 2013, Ivanochko *et al* 20189	
CBP	Cos-7, 293T	Co-IP, IF	Chakraborty *et al* 2001	
CCT2	SKOV3	SILAC	Bard-Chapeau *et al* 2013	
CCT6A	SKOV3, T74D	SILAC	Bard-Chapeau *et al* 2013, Ivanochko *et al* 2019	
CDC42BPB	SKOV3	SILAC	Bard-Chapeau *et al* 2013	
CDY2B	SKOV3	SILAC	Bard-Chapeau *et al* 2013	
CHD4	SKOV3, T74D	SILAC	Bard-Chapeau *et al* 2013, Ivanochko *et al* 2019	
CREB1	293T	Co-IP	Chakraborty *et al* 2001	
CREM	SKOV3, K562	SILAC, Co-IP	Bard-Chapeau *et al* 2013	
CSNK2A1	SKOV3, T74D	SILAC, Co-IP	Bard-Chapeau *et al* 2013, Ivanochko *et al* 2019	EVI1-WT and EVI1-S436A
CSNK2A2	SKOV3, T74D	SILAC, Co-IP	Bard-Chapeau *et al* 2013, Ivanochko *et al* 2019	only EVI1-WT
CSNK2B	SKOV3,K562, T74D	SILAC, Co-IP	Bard-Chapeau *et al* 2013, Ivanochko *et al* 2019	
CTBP1	SKOV3, K562, 293T, Cos-7, T74D, SB1690CB	SILAC, Co-IP, IF	Paredes *et al* 2018, Bard-Chapeau *et al* 2013, Chakraborty *et al* 2001, Hirai *et al* 2001, Izutsu *et al* 2001, Ivanochko *et al* 2019	
CTBP2	SKOV3, K562, T74D	SILAC, Co-PI	Paredes *et al* 2018, Bard-Chapeau *et al* 2013, Turner and Crossley 1998, Ivanochko *et al* 2019	
DDB1	SKOV3, T74D	SILAC	Bard-Chapeau *et al* 2013, Ivanochko *et al* 2019	
DNMT3A	transfected 293T, transfected murine ES cells, SB1690CB	Co-IP, IF	Senyuk *et al* 2011, Lugthart *et al* 2011	only EVI1-WT
DNMT3B	transfected 293T	Co-IP, IF	Lugthart *et al* 2011	
DYNC1H1	SKOV3, T74D	SILAC	Bard-Chapeau *et al* 2013, Ivanochko *et al* 2019	

DYNC1I2	SKOV3, T74D	SILAC	Bard-Chapeau *et al* 2013, Ivanochko *et al* 2019	
EHMT2/ G9A	SKOV3	SILAC	Bard-Chapeau *et al* 2013, Chi *et al* 2003, Goyama *et al* 2010	
EVI1	SKOV3	SILAC	Bard-Chapeau *et al* 2013	
EZH2	293T	Co-IP	Yoshimi *et al* 2011	
FOS	SKOV3	SILAC, Co-IP	Bard-Chapeau *et al* 2013, Bard-Chapeau *et al* 2012	
FOSB	SKOV3	SILAC, Co-IP	Bard-Chapeau *et al* 2013, Bard-Chapeau *et al* 2012	
FOSL2	SKOV3	SILAC, Co-IP	Bard-Chapeau *et al* 2013, Bard-Chapeau *et al* 2012	
GATAD2B	SKOV3	SILAC	Bard-Chapeau *et al* 2013	
GCN5L2	SKOV3	SILAC, Co-IP	Bard-Chapeau *et al* 2013, Senyuk *et al* 2003,	
GTF2I	SKOV3, T74D	SILAC, Co-IP	Bard-Chapeau *et al* 2013, Ivanochko *et al* 2019	
H2AZ	SKOV3	SILAC, Co-IP	Bard-Chapeau *et al* 2013	
HADHA	SKOV3, T74D	SILAC	Bard-Chapeau *et al* 2013, Ivanochko *et al* 2019	
HCFC1	SKOV3	SILAC	Bard-Chapeau *et al* 2013	
HDAC1	SKOV3, K562, Cos-7, 293T, T74D	SILAC, Co-IP, IF	Bard-Chapeau *et al* 2013, Chakraborty *et al* 2001, Ivanochko *et al* 2018	only EVI1-WT
HDAC2	SKOV3, K562, T64D	SILAC, Co-IP, IF	Bard-Chapeau *et al* 2013, Izutsu *et al* 2001, Ivanochko *et al* 2019	
HDAC4	Cos-7, 293-T	Co-IP, IF	Chakraborty *et al* 2001	
HIC1	293-T, LoVo, COLO 205	IF	Pradhan *et al* 2014	
HIST1H4A	SKOV3	SILAC	Bard-Chapeau *et al* 2013	
HNRNPF	SKOV3, T74D	SILAC, Co-IP	Bard-Chapeau *et al* 2013, Ivanochko *et al* 2019	
HNRNPU	SKOV3, T74D	SILAC, Co-IP	Bard-Chapeau *et al* 2013, Ivanochko *et al* 2019	only EVI1-WT
IMMT	SKOV3, T74D	SILAC	Bard-Chapeau *et al* 2013, Ivanochko *et al* 2019	
JUN	SKOV3, T74D	SILAC, Co-IP	Bard-Chapeau *et al* 2013, Bard-Chapeau *et al* 2012, Ivanochko *et al* 2019	
JUNB	SKOV3	SILAC, Co-IP	Bard-Chapeau *et al* 2013, Bard-Chapeau *et al* 2012	
JNK	U937, Cos7 (transfected)	Co-IP	Kurokawa *et al* 2000	
LMNA	SKOV3, T74D	SILAC	Bard-Chapeau *et al* 2013, Ivanochko *et al* 2019	
MRE11A	SKOV3, K562	SILAC, Co-IP	Bard-Chapeau *et al* 2013	
MSH2	SKOV3, K562, T74D	SILAC, Co-IP	Bard-Chapeau *et al* 2013, Ivanochko *et al* 2019	EVI1-WT and EVI1-S436A
MSH3	SKOV3		Bard-Chapeau *et al* 2013	
MSH6	SKOV3, T74D	SILAC	Bard-Chapeau *et al* 2013, Ivanochko *et al* 2019	
NUP133	SKOV3, T74D	SILAC	Bard-Chapeau *et al* 2013, Ivanochko *et al* 2019	

NUP160	SKOV3, T74D	SILAC	Bard-Chapeau *et al* 2013, Ivanochko *et al* 2019	only EVI1-WT
NUP205	SKOV3, T74D	SILAC	Bard-Chapeau *et al* 2013, Ivanochko *et al* 2019	
NUP93	SKOV3, T74D	SILAC	Bard-Chapeau *et al* 2013, Ivanochko *et al* 2019	
p-AKT	293T	Co-IP	Yoshimi *et al* 2018	
P/CAF	COS7, 293T	Co-IP, IF	Chakraborty *et al* 2001	
PARP1	SKOV3, T74D	SILAC, Co-IP	Bard-Chapeau *et al* 2013, Ivanochko *et al* 2019	
PFKP	SKOV3, T74D	SILAC	Bard-Chapeau *et al* 2013, Ivanochko *et al* 2019	
PKP1	SKOV3	SILAC	Bard-Chapeau *et al* 2013	
PLEC1	SKOV3	SILAC, Co-IP	Bard-Chapeau *et al* 2013	
PPIA	SKOV3	SILAC, Co-IP	Bard-Chapeau *et al* 2013	
PPP1CA	SKOV3, T74D	SILAC, Co-IP	Bard-Chapeau *et al* 2013, Ivanochko *et al* 2019	only EVI1-WT
PPP1R9B	SKOV3	SILAC	Bard-Chapeau *et al* 2013	
PRDX1	SKOV3	SILAC	Bard-Chapeau *et al* 2013	only EVI1-S436A
PRKDC	SKOV3, K562, T74D	SILAC, Co-IP	Bard-Chapeau *et al* 2013, Ivanochko *et al* 2019	only EVI1-WT
PTRF	SKOV3, T74D	SILAC	Bard-Chapeau *et al* 2013, Ivanochko *et al* 2019	
PU.1	32Dcl.3	Co-IP	Laricchia-Robbio *et al*, 2009	
RAD50	SKOV3, K562	SILAC, Co-IP	Bard-Chapeau *et al* 2013	
RAN	SKOV3, T74D	SILAC, Co-IP	Bard-Chapeau *et al* 2013, Ivanochko *et al* 2019	only EVI1-WT
RBBP4	SKOV3,K562, T74D	SILAC, Co-IP	Bard-Chapeau *et al* 2013, Ivanochko *et al* 2019	only EVI1-WT
RPS19	SKOV3, T74D	SILAC, Co-IP	Bard-Chapeau *et al* 2013, Ivanochko *et al* 2019	
RRAS2	SKOV3	SILAC	Bard-Chapeau *et al* 2013	
RSU1	SKOV3	SILAC	Bard-Chapeau *et al* 2013	EVI1-WT and EVI1-S436A
RUVBL1	SKOV3	SILAC	Bard-Chapeau *et al* 2013	only EVI1-WT
RUVBL2	SKOV3, K562, T74D	SILAC, Co-IP	Bard-Chapeau *et al* 2013, Ivanochko *et al* 2019	only EVI1-WT
SMAD3	Hep-G2, COS7	Co-IP	Kurokawa *et al* 1998	
SMARCA4 / BRG1	SKOV3	SILAC, Co-IP	Bard-Chapeau *et al* 2013, Chi *et al* 2003	
SMARCA5	SKOV3, K562, T74D	SILAC, Co-IP	Bard-Chapeau *et al* 2013, Ivanochko *et al* 2019	
SMARCC2	SKOV3	SILAC, Co-IP	Bard-Chapeau *et al* 2013	
SMARCE1	SKOV3	SILAC, Co-IP	Bard-Chapeau *et al* 2013	
SMC1A	SKOV3, T74D	SILAC, Co-IP	Bard-Chapeau *et al* 2013, Ivanochko *et al* 2019	only EVI1-WT
SMC2	SKOV3, K562, T74D	SILAC, Co-IP	Bard-Chapeau *et al* 2013, Ivanochko *et al* 2019	only EVI1-WT
SMC3	SKOV3, T74D	SILAC, Co-IP	Bard-Chapeau *et al* 2013, Ivanochko *et al* 2019	only EVI1-WT
SMC4	SKOV3, T74D	SILAC	Bard-Chapeau *et al* 2013, Ivanochko *et al* 2019	only EVI1-WT

SMCHD1	SKOV3	SILAC	Bard-Chapeau *et al* 2013	
SON	SKOV3, T74D	SILAC	Bard-Chapeau *et al* 2013, Ivanochko *et al* 2019	
STAG2	SKOV3	SILAC	Bard-Chapeau *et al* 2013	
SUV39H1	Transfected HEK293, transfected COS7	SILAC, Co-IP	Spensperger *et al* 2008; Cattaneo *et al* 2008, Goyama *et al* 2010	
TBL1XR1	SKOV3	SILAC	Bard-Chapeau *et al* 2013	
TJP1	SKOV3, T74D	SILAC, Co-IP	Bard-Chapeau *et al* 2013, Ivanochko *et al* 2019	
TP53BP1	SKOV3, K562	SILAC, Co-IP	Bard-Chapeau *et al* 2013	
TRPS1	SKOV3	SILAC	Bard-Chapeau *et al* 2013	
TSPYL1	SKOV3	SILAC	Bard-Chapeau *et al* 2013	
UPF1	SKOV3, T74D	SILAC, Co-IP	Bard-Chapeau *et al* 2013, Ivanochko *et al* 2019	only EVI1-WT
USP7	SKOV3	SILAC	Bard-Chapeau *et al* 2013	
XRCC5	SKOV3, K562, T74D	SILAC, Co-IP	Bard-Chapeau *et al* 2013, Ivanochko *et al* 2019	
XRCC6	SKOV3, K562, T74D	SILAC, Co-IP	Bard-Chapeau *et al* 2013, Ivanochko *et al* 2019	
YY1	K562	SILAC, Co-IP	Bard-Chapeau *et al* 2013, Bard-Chapeau *et al* 2012	
ZNF148	SKOV3	SILAC	Bard-Chapeau *et al* 2013	
ZNF281	SKOV3, T74D	SILAC	Bard-Chapeau *et al* 2013, Ivanochko *et al* 2019	
ZNF516	SKOV3	SILAC	Bard-Chapeau *et al* 2013	